The Mechanisms of the Spindle Assembly Checkpoint and Mitotic Cell Death

Jianquan Li

Thesis submitted to Newcastle University in candidature for the degree of **Doctor of Philosophy**

Institute for Cell and Molecular Bioscience

Newcastle University

October 2018

Abstract

The spindle assembly checkpoint (SAC) monitors the chromosomes and kinetochore–microtubule attachment to prevent premature anaphase onset (Lara-Gonzalez et al., 2012), and this ensures the fidelity of cell division. The mitotic checkpoint complex (MCC), the core SAC effector, contains two sub-complexes, CDC20-MAD2 and BUBR1-BUB3 (Sudakin et al., 2001). However, the exact mechanism underlying the assembly of the MCC regarding when, where and how still is not fully addressed.

It is believed that the formation of the CDC20-MAD2 sub-complex is an initial and essential step in MCC assembly (Sudakin et al., 2001), thus the assembly of the MCC can be depicted by the observation of the formation of the CDC20-MAD2 complex (Fraschini et al., 2001, Meraldi et al., 2004, Poddar et al., 2005). Using the Duolink based in situ proximity ligation assay (PLA), the lab has previously used individual cell analysis to show the temporal and spatial *in vivo* formation of the CDC20-MAD2 complex throughout the cell cycle in HeLa cells and existence of a specific prophase form of the CDC20-MAD2 complex (Li et al., 2017). In this study, we provide evidences showing that the profile of the assembly of the CDC20-MAD2 complex revealed by using the PLA can genuinely reflect the dynamic *in vivo* interaction of these two proteins in individual cells. We also provide evidences to support the idea that the prophase specific CDC20-MAD2 complex is functional in preventing the premature degradation of cyclin B1 in prophase which ensures the proper G2/M transition.

$p31^{comet}$ (MAD2L1BP), as an important SAC silencer (Habu et al., 2002, Yang et al., 2007), which, in conjunction with TRIP13 (Thyroid hormone receptor interacting protein 13, or PCH-2 in C. elegans) promotes the disassembly of the MCC and the conversion of the

C-MAD2 back to O-MAD2 for recycling (Xia et al., 2004). It has been suggested that expression of p31^{comet} is cell cycle regulated, that there are two putative destruction motifs of D-box and KEN-box (Habu et al., 2002), and that it is an ubiquitin substrate (Udeshi et al., 2013, Wagner et al., 2011)， which implying that it is a substrate of the APC/C. However, the potential turnover property of p31^{comet} is yet to be characterized. In this study, we have examined the expression profile of p31^{comet} throughout the cell cycle using a specific anti-p31^{comet} antibody fluorescent staining and have confirmed that it is cell cycle regulated. It starts to accumulate from prophase and peaks at prometaphase and is sustained until telophase and then it declined. This is supported by the observation that the level of p31^{comet} is reduced at three hours after cells released from a mitotic block caused by nocodazole treatment and re-enters the cell cycle. The accumulation of p31^{comet} before the prometaphase and its accumulation in response to the activation of the SAC by nocodazole treatment are the results of protein synthesis. However, the potential accumulation of p31^{comet} levels in cell samples after siRNA with the components of the APC/C, especially the APC3, examined by western blot produced ambiguous inconclusive results. The preliminary data produced by depletion of Cullin-1, another E3 ligase responsible for the degradation of cell cycle substrates in G1/S, using siRNA resulted in an increase in p31^{comet}, which implies that Cullin-1 is potentially response to p31^{comet} degradation though this would require further confirmation.

The various kinds of cell death occurred during mitosis are collectively termed ‘Mitotic Catastrophe’(Vitale et al., 2011). Targeting the mitotic catastrophe signaling pathway in cancer offers a significant therapeutic advantage, and the anti-mitotic drugs such as taxanes, epothilones, and vinca alkaloids are widely used in the cancer clinic. M2I-1 (MAD2 inhibitor-1), a small molecule, has been shown to disrupt the CDC20-MAD2 interaction *in vitro* and weaken the SAC *in vivo*(Kastl et al., 2015). We report here that M2I-1 can disrupt the *in vivo* interaction of CDC20 and MAD2, and significantly increases the sensitivity of several cancer cell lines to anti-mitotic drugs, with cell death occurring after a prolonged mitotic arrest, when cell death is triggered by the premature degradation of cyclin B1 and the perturbation of the microtubule network by nocodazole or Taxol. Interestingly, the level of

MCL-1, a pro-survival protein of the Bcl-2 family is significantly elevated, but higher levels of the pro-apoptotic proteins MCL-1s, a short form of the MCL-1, act antagonistically. Taken together, our results demonstrate that M2I-1 exhibits antitumor activity in the presence of current anti-mitotic drugs such as Taxol and nocodazole and has the potential to be developed as an anticancer agent.

Declaration

I, Jianquan Li, declare that the data presented in this thesis is based on work carried out by Jianquan Li, unless stated otherwise. Moreover, neither this thesis nor any of the data within has been submitted before for any other degree or award. The contributions by others have been acknowledged, where appropriate.

Jianquan Li

Acknowledgements

Firstly, I would like to thank my supervisor Dr Jun-Yong Huang, for him giving me the opportunity to pursue this PhD programme and introducing me to the field of cell-cycle regulation. His invaluable support and patient guidance in past three year have been integral to the success of this project.

Many thanks for past and present members in Huang's lab, who have helped me over my time spent working on this project. I would like to thank Daniel Wood for helping me to adapt myself to the working of the lab at the beginning of my PhD study and set up the PLA Duolink technology, Carl Liu for sharing his experience of life and study in Newcastle University, Jonathan McLatchie for proofreading to my first and secondary year annual report, Nanmao Dang for help when it was need.

I would particularly like to thank some external members; Dr Paul A Jowsey's for collaboration in constructing plasmid DNA, Dr Git Chung for teaching me the PCR, measuring of protein and DNA concentration, Mr. Michael Aitchison for proofreading for the entire thesis, Dr Pual Dean for proofreading to the chapter one of my thesis and teaching me the identification knowledge about cell death. Dr Fei Gao for sharing her knowledge and experience and always ready to help. Dr Nuria Martinez-Lopez for sharing her experiment experience and some useful experiment tips.

I also like to thank Prof Jonathan Higgins and Dr Diana Papini for their kind provision of HeLa cell line.

Last, but by no means least, I'd like to thank all of my family members, particularly my parents, for their constant support not only during PhD study, but my entire life.

I could not have succeeded with all works without any of you!

List of Scientific Papers

1. **Jianquan Li**, Dang Nanmao, Wood DJ, Huang JY (2017). The kinetochore-dependent and -independent formation of the CDC20-MAD2 complex and its functions in HeLa cells. *Scientific reports***7:** 41072.

2. **Jianquan Li,** Nanmao Dang, Nuria Martinez Lopez, Paul A. Jowsey, Dong Huang, Robert N. Lightowlers, Fei Gao, and Jun-Yong Huang. Inducing apoptosis in cancer cell lines using a small-molecule M2I-1 that disrupted the interaction between CDC20 and MAD2. Manuscript

Table of Contents

List of Abbreviations

APAF1……. Apoptotic protease activating factor 1

APC/C……... Anaphase-promoting complex or cyclosome

ATP…….....Adenosinetriphosphate

Aurora B…… Aurora kinase B

BAK…… BCL-2 killer protein

BAX…… BCL-2 associated X protein

BCL-2…… B-cell lymphoma 2

BSA…… Bovineserumalbumin

BUB……... Budding uninhibited by benzimidazole

Cdc20…… Cell-division cycle protein 20

Cdh1……... Cadherin-1

Cdk……... Cyclin-dependent kinase

CENP-E…… Centromere Protein-E

CHX……. Cycloheximide

C-MAD2……..... Closed forms of MAD2

CRLs…….....Cullin-Ring ligases

C-terminal……...Carboxylterminal

DAPI……... 4’,6-diamidino-2-phenylindole

D-box……..Destruction box

dH_2O……..Distilledwater

DMEM…….. Dulbecco's modified Eagle's medium

DMSO..……. Dimethyl sulphoxide

DNA……..…… Deoxyribonucleic acid

Dox……...Doxacycline

EDTA……. Ethylene diamine tetra acetic acid

EGTA……...Ethyleneglycoltetra-aceticacid

EPro…….. Early prophase

GAPDH……. Glyceraldehyde 3-phosphate dehydrogenase

G1/G2phase……..... Gap1 / Gap2 phase

IF…… Immunofluorescence

I- MAD2…….. Intermediate MAD2

Int…… Interphase

Ipl1……. Ploidy 1

IP…… Immunoprecipitation

M2I-1…….. MAD2 inhibitor-1

MAD…… Mitotic arrest deficient

MCC…… Mitotic checkpoint complex

MCL-1……. Myeloid cell leukaemia-1

Met…….. Metaphase

MOMP…….Mitochondria outer membrane permeabilization

MOPS……..Morpholinopropanesulfonicacid

MPF……... Mitotic maturation-promoting factor

M phase…….. Mitotic phase

MPS1…….. Monopolar spindle-1

mRNA……... Messenger RNA

MULE…….Mcl-1 ubiquitin ligase E3

NEBD…… Nuclear envelope breakdown

N-terminal……..Amino-terminus

O-MAD2…….. Open forms of MAD2

PBS……. Phosphate buffered Saline

PCR…….PolymeraseChainReaction

PLA……...Proximity ligation assay

PP1…… Protein phosphatase 1

Pro……. Prophase

ProM……. Pro-metaphase

RZZ complex……..Rod-Zwilch-ZW10 complex

SAC…… ...Spindle assembly checkpoint

SCF…….. Skp1-Cul1-F-box-protein

SDS……..Sodiumdodecylsulphate

Sgo1……..Shugoshin 1

siRNA…… ShortinterferingRNA

S phase…… Synthesis phase

SSN…… SAC silence network

TAE……. TrisacetateEDTAbuffer

TRIP13……Thyroid hormone receptor interacting protein 13

TPR…….. Translocated promoter region Protein

Tris……..2-Amino-2-hydroxymethyl-propane-1,3-diol

TritonX-100……...4-(1,1,3,3-Tetramethylbutyl)phenyl-polyethyleneglycol

Tween20…….Polyoxyethylenesorbitanmonolaurate

Zw10……. Zeste-white10

List of figures

List of Tables

Chapter One. Introduction

Cell division is a fundamental process in the growth and proliferation of all living organisms. It is an irreversible part of the cell cycle and is strictly regulated to ensure that the daughter cells inherit a complete set of chromosomes. There are several cell cycle checkpoints which have been shown to be involved in the regulation of cell division, one of these, the spindle assembly checkpoint (SAC), monitors and regulates the mitotic events in the cell cycle through a complicated biological network system, and allows cell division progression only if all chromosomes are properly "bi-oriented" on the spindle via kinetochores. Any malposition of chromosomes on kinetochores will activate the SAC to generate diffusible anaphase "wait" signals which delay the metaphase to anaphase transition. The abnormal activities involved in turning this checkpoint "on" and "off" can produce a severe impact on cell proliferation and has severe consequences for human health and disease (Kops et al., 2005, Noatynska et al., 2012).

1.1 The Cell Cycle and Cell Cycle Checkpoints

1.1.1 *Overview of the Eukaryotic Cell Division Cycle*

In eukaryotes, there are two types of cell division: mitosis, in which each daughter cell is genetically identical to their mother cell; and meiosis, in which the number of chromosomes in the daughter cells is reduced by half to produce haploid gametes, and where the genetic information might not be identical to their mother cell after recombination.

A mitotically dividing eukaryotic cell experiences a series of consecutive stages known collectively as the cell cycle. It comprises of interphase, two growing gap phases (G1 and G2), S phase, in which the genetic material is duplicated, and a mitotic phase (M phase), in which the cell partitions the duplicated genetic material (nuclear division) followed by cytokinesis to produce two identical daughter cells. The divided cells may enter a temporary quiescent stage, called the G0 phase (Vermeulen et al., 2003, Johnson and Walker, 1999), or exit the cell cycle permanently and eventually undergoes senescence (Kuilman et al., 2010, Stanulis-Praeger, 1987).

Conventionally, a mitotic phase can be further separated into five stages: prophase, prometaphase, metaphase, anaphase, and telophase. Prophase is the longest phase occupies more than half the duration of mitosis. The sister chromatids are formed by the condensation of the homologous chromosomes and held together by a cohesin ring complex at the centromere, where the kinetochore will later form and connect the sister chromatids with the microtubules (Lodish H, 2000). At the same time, the microtubule networks are reorganized by the duplicated centrosomes, which move apart toward the cell poles. The beginning of prometaphase is marked by the nuclear envelope breakdown (NEBD) with further condensation of the chromosomes. The matured unattached kinetochores are formed at the centromere regions on bio-oriented sister-chromatids and begin sensing and binding with the microtubules radiated from the spindle poles. In metaphase, the condensed chromosomes align along the equatorial plate of the cell, and the bi-oriented kinetochores are attached with kinetochore microtubules to form the bipolar spindle with appropriate tension. Anaphase is the shortest stage in mitosis, in which the cohesin ring complex is cleaved to release and separate the sister chromatids. The segregated sister-chromatids are then pulled apart to the opposite poles of the elongated cell by the forces generated from the bipolar spindle and the astral microtubules and the cleavage furrow begins to form (FitzHarris, 2012, Maiato and Lince-Faria, 2010). During telophase, the well separated and de-condensed chromosomes begin to be encompassed by a new nuclear envelope membrane, and the majority of the spindle fibres disappear from the microtubules on the midbodies. Details are shown in Figure

1.1. Cell cycle progression is accompanied by changes in the chromosomal structure between relaxation and condensation, the chromasomes start to condense after prophase and de-condense after anaphase. As it is one of the core protein components of chromatin, the phosphorylation of histone H3 at serine 10 is closely correlated with chromosome condensation during cell division. In the late G2 phase, the phosphorylation of S-10 occurs on pericentromeric chromatin only, and as mitosis proceeds, this spreads along the chromosomes and is complete at prophase, and then at the end of mitosis, histone 3 S-10 is dephosphorylated (Gurley et al., 1978, Van Hooser et al., 1998, Paulson and Taylor, 1982). Thus the state of the S-10 phosphorylation is often used as a maker for timing mitosis (Wei et al., 1998, Shandilya et al., 2016, Dilworth et al., 2018).

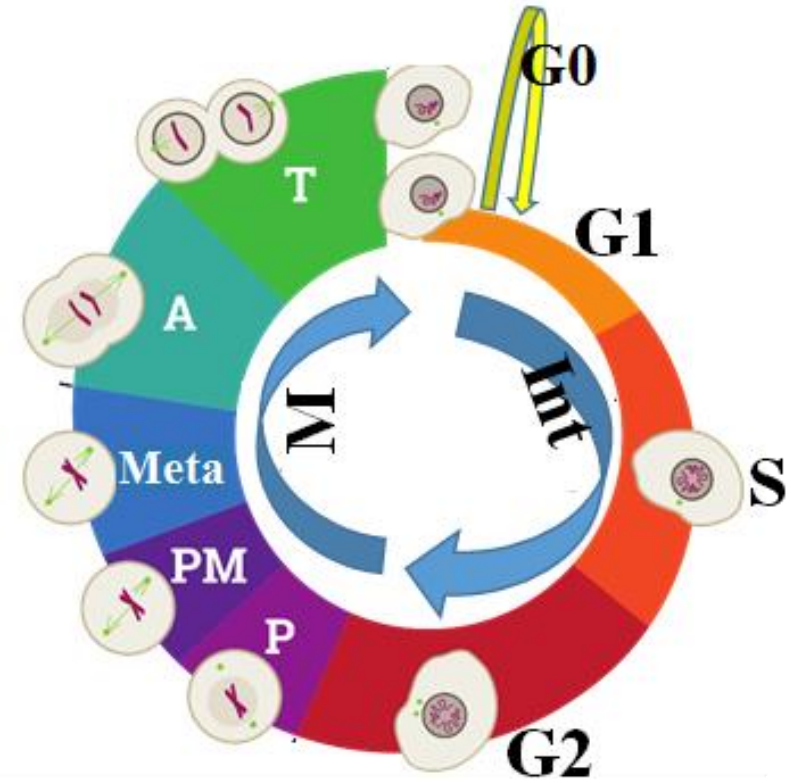

Figure 1.1: Cell cycle stages.

The cell in interphase undergoes growth and DNA replication, and then enters mitosis to complete cell division. The key phases are: G1, first gap stage in which the cell grows and prepares for DNA replication. S phase, in which most of protein synthesis and DNA is

replicated. G2 phase, the second gap stage in which the cell completes the preparation for cell division. In mitosis, cells undergo prophase, prometaphase, metaphase, anaphase and telophase and finally cytokinesis to complete the nuclear and cytoplasmic division. Int: interphase, M: Mitosis, P: prophase, PM: prometaphase, Meta: metaphase, A: anaphase, T: telophase, Source adapted from: (http://cellcycle.org.uk/).

1.1.2 *Cyclin dependent Cdks and cell cycle checkpoints*

The cell cycle is an ordered set of events, which ensures that the cell can only enter a new phase by successfully and correctly completing the previous step in the pathway, the different phases are coordinated and regulated by complex checkpoint mechanisms. The well characterised major checkpoints in mammalian cells include the G1/S (restriction/Start checkpoint), the G2/M checkpoint (DNA damage checkpoint), and the M phase checkpoint (spindle assembly checkpoint or mitotic checkpoint) (Murray, 1994).

The G1/S checkpoint is the point at which the cell commits to either enter the cell cycle or to stay in a quiescent state known as G0 depending on internal and external conditions (Bruce Alberts, 2008). The decision to drive cells into a new division cycle stage (G0-to-G1 transition) relies on the cyclin-dependent CDK kinase activity of cyclin D-CDK4 or cyclin D-CDK6 (Nurse, 2000, Sherr, 1994). Following the entry into S-phase, cyclin E-CDK2 activity promotes and initiates DNA replication (Yin et al., 1999, Koff et al., 1992). The checkpoint can also detect DNA damage and arrest the cell in G1 until the damaged DNA has been repaired (Cooper, 2000, Bertoli et al., 2013). Once completion of the DNA duplication has occurred, the cell enters a growth phase (or gap phase) known as G2 and begins to be taken over by a primary cyclin-dependent CDK activity, cyclin B1-CDK1, to synthesise the necessary proteins for undergoing mitosis. The expression and activation of cyclin B1-CDK1 is the consequence of the accumulation and coordination of a number of G2 enzyme activities such as cyclin A-CDK2, CDC25, and Wee1 (Guardavaccaro and Pagano, 2006).

The G_2/M checkpoint senses any damaged DNA or incomplete DNA replication, and generates a signal that leads to a delayed or arrested cell cycle to prevent the initiation of mitosis until damaged DNA was repaired or replication is completed (Cooper, 2000). The cyclin B1-CDK1, also called mitotic maturation-promoting factor (MPF) (Masui, 2001, Lohka et al., 1988), is the primary kinase activity that drives cell into mitosis by remodeling the microtubule network and chromosome configuration, which includes the dynamic assembly of the bipolar spindle, chromosome condensation, and the interactions between kinetochores and kinetochore microtubules (Chen et al., 2008, Crasta et al., 2006, Hagting et al., 1999).

The spindle assembly checkpoint (SAC) monitors the alignment of chromosomes on the spindles and the correct attachment of microtubules via kinetochores, thus ensuring that the identical chromosomes from parental cells are distributed into daughter cells (Cooper, 2000, Lara-Gonzalez et al., 2012). To achieve this, the SAC senses if there are any unattached kinetochores or kinetochores which are incorrectly attached to microtubules and produces inhibitory signals to prevent the activation of a mitotic-specific multi-subunit ubiquitin E3 ligase, called anaphase-promoting complex or cyclosome (APC/C), which in turn prevents the degradation of securin, an essential protein holding together the sister-chromatids (Chang and Barford, 2014, Solomon and Burton, 2008). This also maintains a high activity of cyclin B1-CDK1 to delay the metaphase-to-anaphase transition for error corrections (Lindqvist et al., 2007, Chang et al., 2003). Three checkpoints and their associated cell cycle stages are highlighted in Figure 1.2.

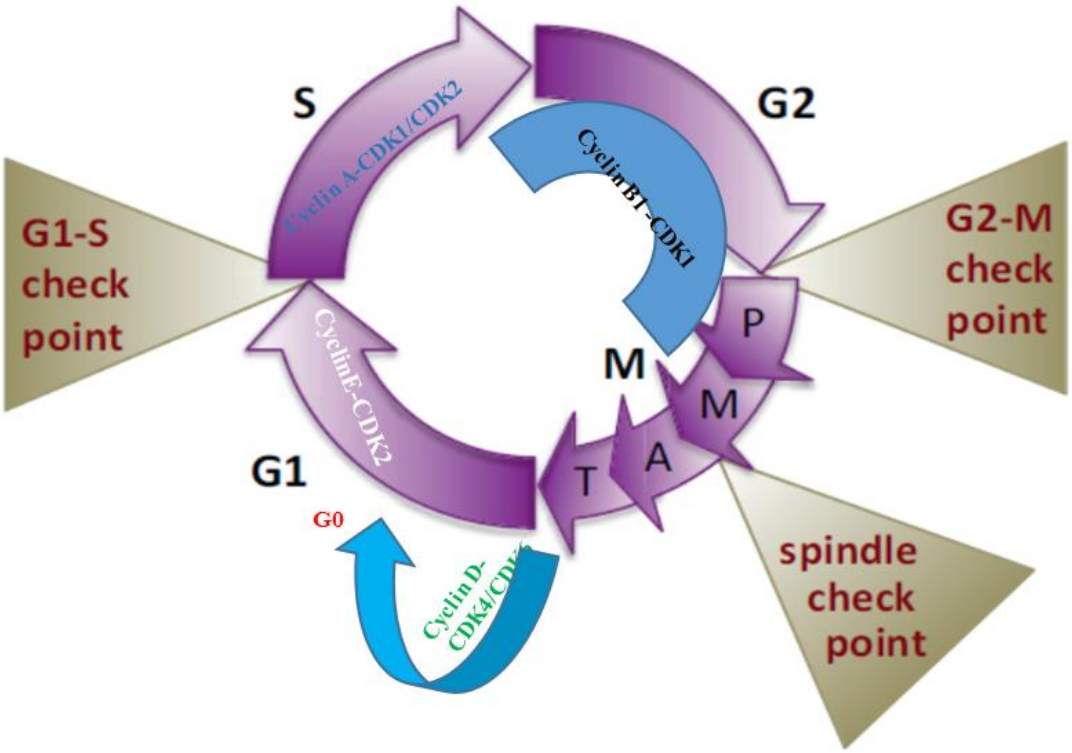

Figure 1.2: The cell cycle transitions associated with cyclin dependent Cdks activities and the cell cycle checkpoints.

The cell cycle progression is driven by the activities of cyclin dependent CDKs. Cyclin D-CDK4 or CDK6 is responsible for the G0-G1 transition. The cyclin E-CDK2 complex promotes and initiates DNA duplication, while the completion of S phase depends on the complex of cyclinA-CDK2 or cyclinA-CDK1. The cyclinB1-CDK1 complex regulates the mitosis transition. The cell cycle checkpoints monitor cell cycle progression. DNA damage activates the G1 checkpoint to arrest the cell in G1. The G2 checkpoint responds to damaged or un-replicated DNA, and only allows the repaired and replicated DNA to enter mitosis. The spindle assembly checkpoint (M checkpoint) monitors the chromosome arrangement and kinetochore-microtubule attachments and can then delay mitosis to allow for error repair. Copied from (Harashima et al., 2013).

1.2 The spindle assembly checkpoint

1.2.1 *Overview of the spindle assembly checkpoint (SAC)*

Following DNA replication, the sister chromatids are held together by cohesin, a multimeric ring structure protein complex, that has been indicated to encircle the sister chromatids during S phase and into mitosis (Nasmyth and Haering, 2009, Nasmyth, 2005). At the metaphase/anaphase transition, the cohesin ring is opened following its cleavage by separase (Uhlmann et al., 1999, Uhlmann et al., 2000), an enzyme that remains inactivated in most of the time during the cell cycle by binding with its inhibitor securin (Waizenegger et al., 2002). The release of seperase by degradation of securin is timely and strictly controlled via APC/C-ubiquitin-mediated proteolysis (Yanagida, 2005). Meanwhile, the degradation of cyclin B1 to inactivate CDK1 which leads to the mitotic exit, is also conducted by the APC/C (Lara-Gonzalez et al., 2012).The coordinated degradation of securin and cyclin B1 in mitosis is essential to segregate the genetic information correctly into the daughter cells for maintaining genome integrity (Lara-Gonzalez et al., 2012, Kops et al., 2005). To achieve this, cells have evolved a complex mitotic checkpoint surveillance mechanism, the spindle assembly checkpoint (SAC), monitoring the proper chromosome and kinetochore-microtubule attachment to prevent premature anaphase onset (Lara-Gonzalez et al., 2012). The SAC will only be satisfied when all condensed chromosomes are correct aligned on the spindle and all sister kinetochores appropriately attached with microtubules (Jia et al., 2013). Otherwise the activated SAC will produce a diffusive anaphase “wait” inhibitory signal which inhibits the APC/C to prevent the premature degradation of securin and cyclin B1, thereby preventing anaphase onset and exit from mitosis (Musacchio, 2015, Lara-Gonzalez et al., 2012). The working model is depicted in Figure 1.3.

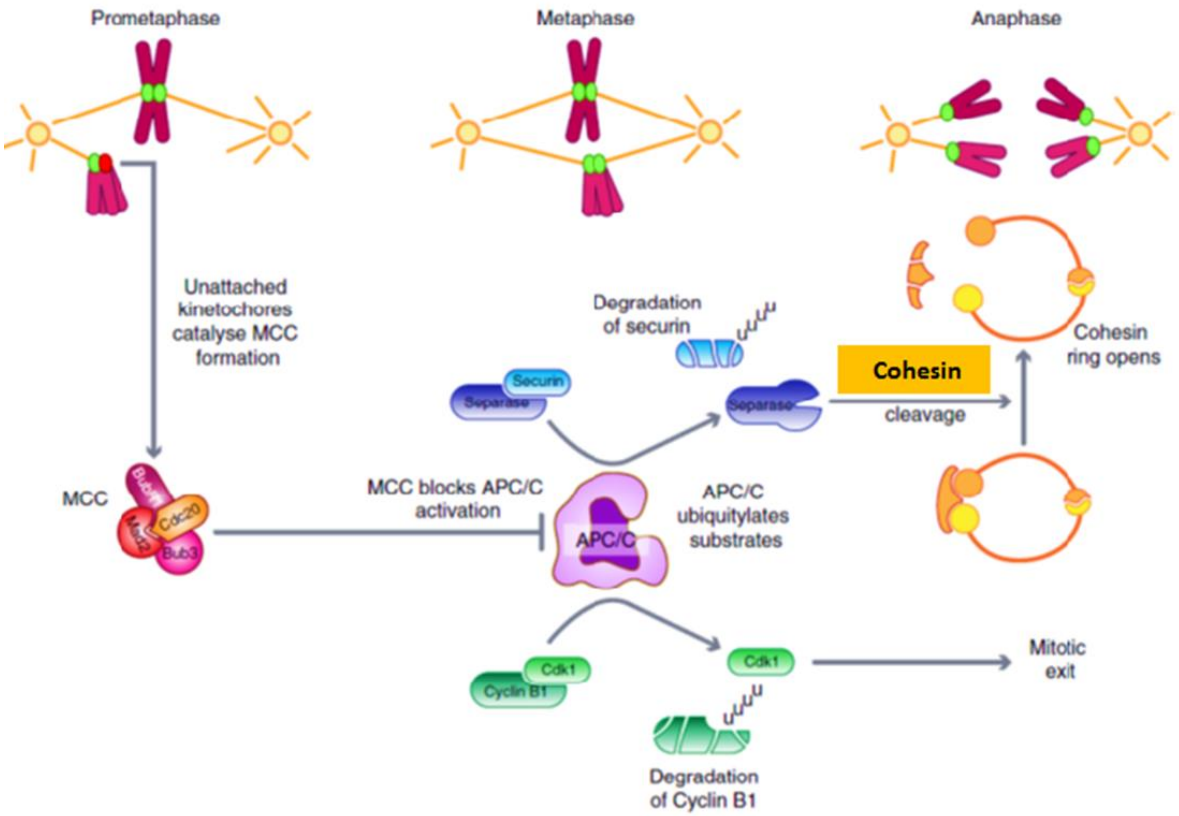

Figure 1.3: The SAC principle.

In prometaphase, the SAC surveillance mechanism senses the unattached kinetochores and facilitates the formation of an inhibitory signal. The mitotic checkpoint complex (MCC), which is composed of CDC20, MAD2, BUBR1, and BUB3, this constrains the APC/C activity so delaying the degradation of cyclin B1 and securin. Once all the chromosomes are aligned with their kinetochores attached to the spindle in metaphase, the SAC condition is satisfied, the production of MCC then ceased and the existing MCC is disassociated to silence the SAC, this in turn allows the activation of the APC/C by CDC20, the ubiquitylation and degradation of securin and cyclin B1, the liberation of separase and inactivation of CDK1. As a result, the cohesin ring structure is cleaved to allow the separation of sister chromatids (at anaphase) and mitotic exit. Adapted from (Lara-Gonzalez et al., 2012).

1.2.2 *The composition of spindle assembly checkpoint*

The SAC is also a feedback-regulating network that consists of a sensor structure (unattached kinetochores) to monitor the situations of chromosome attachments with microtubules, and to catalyse inhibitory signals, an effector system for targeting the mitotic machinery to delay cell cycle progression in mitosis or meiosis (Musacchio and Hardwick, 2002). This signal cascading pathway is shown in Figure 1.4.

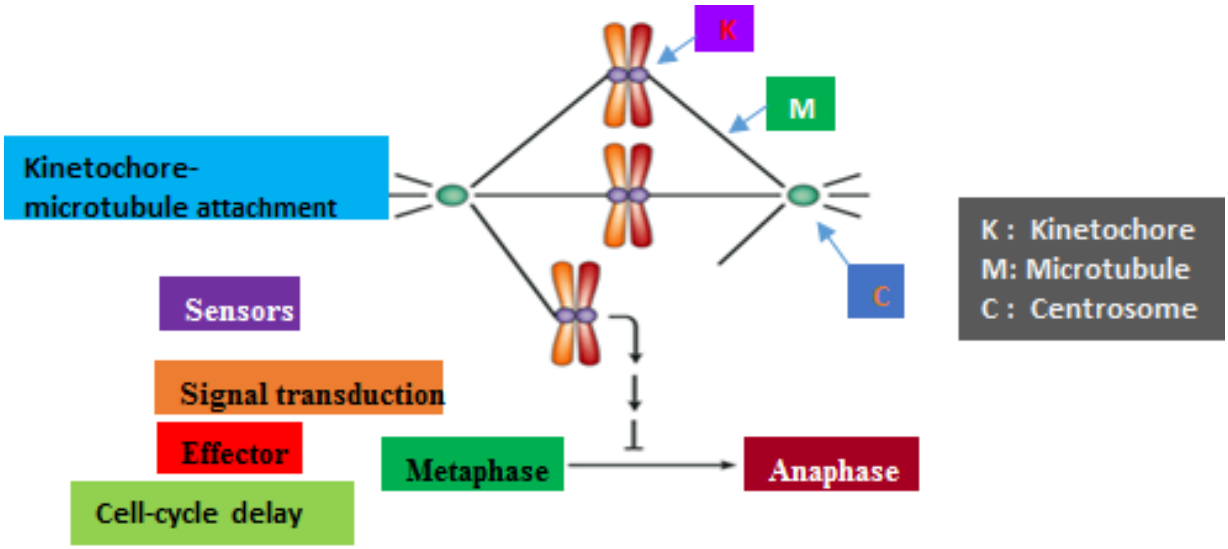

Figure 1.4: Sensing and cascading the SAC signals from unattached kinetochores.

The SAC signalling pathway consists of the sensors, receptors, and effectors of the SAC network. The sensor (unattached kinetochores or inappropriately attached kinetochores) senses the status of the attachment of kinetochores and microtubules. The inappropriate attachment will emit a signal; this signal then is transmitted to inhibit the onset of anaphase and delay the cell cycle. Modified from (Musacchio and Hardwick, 2002).

The SAC networks are composed of a few proteins, enzymes and complexes. The genes that code for the components have been identified as parts of the spindle assembly checkpoint include the MAD (mitotic arrest deficient) genes MAD1, MAD2 and MAD3 (BUBR1 in

humans) and BUB (budding uninhibited by benzimidazole) genes BUB1 and BUB3, these genes are conserved in eukaryotes (Li and Murray, 1991, Hoyt et al., 1991). Besides these core genes, SAC signalling system also involves the MPS1 (monopolar spindle-1) (Weiss and Winey, 1996, Abrieu et al., 2001, Hardwick et al., 1996), Aurora-B (Ipl1 in S. cerevisiae) (Morrow et al., 2005, Hauf et al., 2003), that are required to amplify the SAC signal or promote the mitotic checkpoint complex (MCC) formation. Additionally, kinetochore proteins, Ndc80/Hec1 (Zheng et al., 1999, Wigge and Kilmartin, 2001), CENP-E (centromere protein-E) (Mao et al., 2003, Yao et al., 2000, Abrieu et al., 2000)**,** RZZ complex (comprising of proteins Rod, ZW10 and Zwilch) (Buffin et al., 2005) and kinetochores substrates KMN (Knl1-Mis12 complex-Ndc80 complex) (Foley and Kapoor, 2013, Cheeseman et al., 2006) are also reported to be involved in checkpoint signalling.

1.2.3 *The source of spindle assembly checkpoint signaling*

To ensure that cell division does not occur before all of the chromosomes are properly attached to spindles, the SAC delays anaphase onset and prevents the premature segregation of sister chromatids with improper attachments to allow the cell to correct any defects (Lew and Burke, 2003). Existing research has indicated that either the unattached kinetochores or the defection of tension exerted by kinetochores microtubules are the source triggering the SAC signal pathway (Zhou et al., 2002).

Bipolar kinetochore-microtubule attachment is essential for correct chromosome segregation. After nuclear envelope breakdown in prometaphase, the polymerizing microtubules attempt to attach with kinetochores through a “search and capture” mechanism (Tanaka et al., 2005b, Tanaka et al., 2005a). However, this kinetochore-microtubule attachment mechanism is somewhat random, and could present several kinetochore-microtubule arrangements that would cause chromosome missegregation (Pinsky and Biggins, 2005). Several terminologies embrace the possible situations of kinetochore-microtubule attachment (Pinsky and Biggins, 2005): Amphitelic attachment, the kinetochores are attached with microtubules from its facing

poles (Figure 1.5a); Syntelic attachment, kinetochores are attached with microtubules emanating from the same pole (Figure 1.5b); Monotelic attachment, only one kinetochore is attached to the microtubules (Figure 1.5c); Merotelic attachment, a single kinetochore is attached to microtubules from both spindle poles (Figure 1.5d).

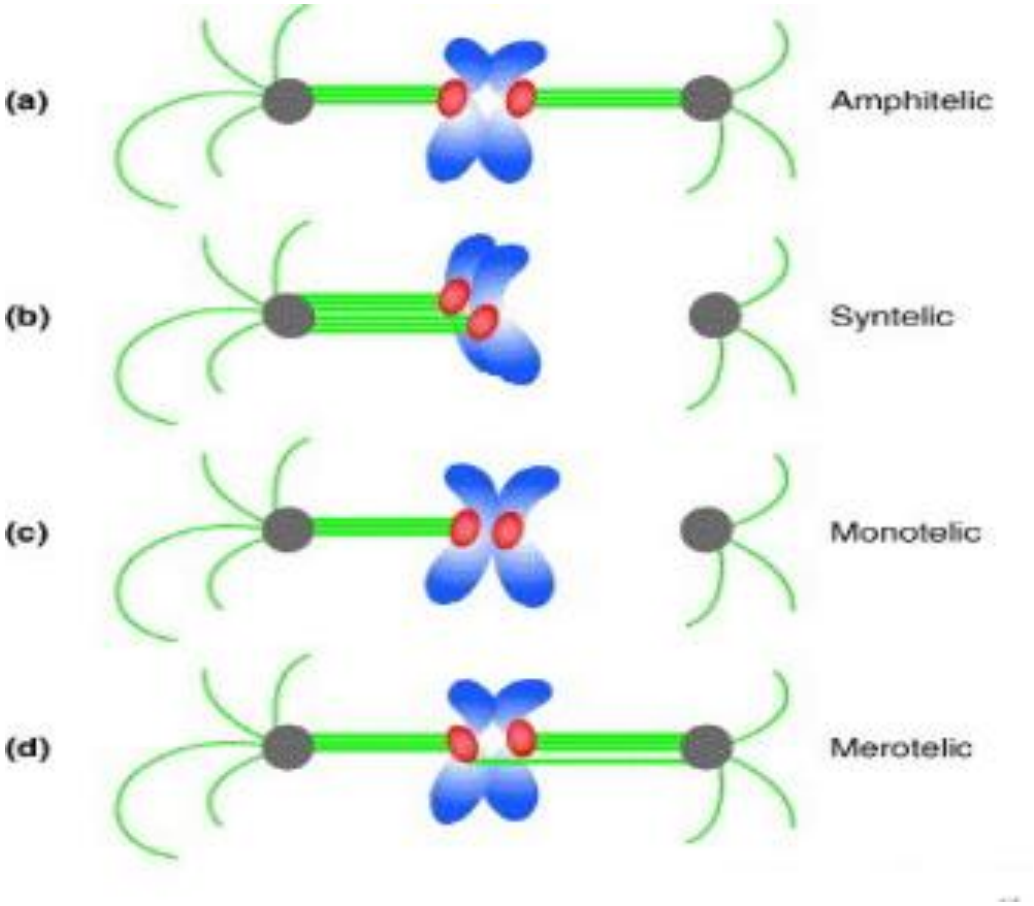

Figure 1.5: The possible situation of the attachment between kinetochores and microtubules.

a) Amphitelic: bipolar attachment. Sister kinetochores face opposite poles and bind one to one with microtubules from the facing pole. (b) Syntelic: sister kinetochores attach to microtubules from the same pole. (c) Monotelic: only one kinetochore binds to microtubules, leaving an unattached kinetochore. (d) Merotelic: besides the bipolar attachment of sister kinetochores with microtubules from facing poles, another one or both kinetochore(s) interact with microtubules from opposite poles. (Adapted from Benjamin et al., 2005).

In 1994, Rieder et al. found that in Ptk1 cells anaphase was not initiated until the last mono-oriented chromosome had formed a bi-polar attachment to the spindle, and concluded

that anaphase onset and the duration of mitosis are controlled by a metaphase-anaphase checkpoint mechanism (Rieder et al., 1994). Subsequently, using video microscopy, they found that anaphase onset would not be delayed, if a laser destroyed the centromere of the unattached kinetochore on the last mono-oriented chromosome, thus revealing that the metaphase-anaphase checkpoint monitors the situation of the sister kinetochores attachment with the spindle, and that even a single unattached kinetochore could inhibit the metaphase-anaphase transition (Rieder et al., 1995). This conclusion was supported by the observation that the impaired kinetochores by mutation of the centromeric genes activated the SAC (Pangilinan and Spencer, 1996, Wang and Burke, 1995, Spencer and Hieter, 1992), and that the SAC proteins were shown to locate only transiently on unattached kinetochores in mitosis and were removed after the occurrence of bipolar attachment (Taylor and McKeon, 1997, Taylor et al., 1998, Li and Benezra, 1996).

The cohesion of two sister chromatids opposes the force arising from sister chromatids pulled by the kinetochore microtubules towards the opposite end of the cell, which creates tensions between the two bio-oriented kinetochores (Maiato et al., 2004, Maiato and Sunkel, 2004). The separation of the chromosomes and the completion of the transition from metaphase to anaphase must overcome this tension. Under micromanipulation, Li and Nicklas observed that the attached, tensionless and syntelic chromosome pair results in spindle checkpoint signals, and cells enter anaphase when the SAC is satisfied after tension is applied across kinetochores using a force-calibrated microneedle (Li and Nicklas, 1995). Analogous observations in *Drosophila* oocytes indicated that the tension signal induces the metaphase arrest (Jang et al., 1995). Additionally, the kinetochore protein, shugoshin senses the spindle tension and participates in the activation of the SAC by a process called the “molecular spring” mechanism (Goulding and Earnshaw, 2005, Haase et al., 2012).

Although an appropriate tension is required for satisfaction of the SAC, however, it has been suggested that the unattached kinetochores and the microtubule attached kinetochores but tensionless functioned differently in the SAC mechanism (Waters et al., 1998). In

Taxol-treated cells, Magidson et al. found that it was not the tension but the unattached kinetochore activates the SAC and arrests the cell in mitosis (Magidson et al., 2016). Thus, the unattached kinetochore is thought to be a more important factor in the SAC signalling (Waters et al., 1998, Rieder et al., 1995). However, it's difficult to separate the attachment from the tension and discuss them independently (Pinsky and Biggins, 2005). Firstly, the generation of tension results from the attachment of the kinetochore-microtubules and the cohesion of the sister chromatids at the kinetochores (Zhou et al., 2002), abnormal attachments such as mono-oriented or merotelic connections could result in tensionless or defective tension. Secondly, tension affects microtubule attachments, the application of tension stabilizes and increases the number of kinetochore-microtubule attachments (Nicklas and Ward, 1994, King and Nicklas, 2000, Pinsky and Biggins, 2005). Meanwhile, the tension formation mechanism can sense the attachment of chromosome by microtubules (Zhou et al., 2002). In the SAC mechanism, different components of SAC show different roles in sensing attachment and tension (Logarinho et al., 2004). MAD2 and BUB1 localize at unattached kinetochores to detect the attachment status (Waters et al., 1998, Logarinho et al., 2004), while BUBR1 and BUB3 sense the tension (Logarinho et al., 2004, Hoffman et al., 2001). In addition, it has been suggested recently that the SAC can be activated by the proper amount of tension generated by the intra-kinetochore rather than inter-kinetochore stretching, while this stretch is distinguished from the tension across the kinetochores (Maresca and Salmon, 2010).

1.3 Spindle assembly checkpoint activation

1.3.1 *The kinetochore recruitment of the SAC proteins*

The unattached kinetochore or tensionless attachment is the condition that will trigger the SAC signaling. In responding to these conditions, the kinetochore recruitment of the SAC proteins is regarded as the first step in the pathways cascading signals (Liu and Zhang, 2016, Chen et al., 1996, Skoufias et al., 2001). It has been demonstrated that the Aurora B/INCENP complex involves the localization of MPS1, BUB1, BUB3, and centromere protein-E

(CENP-E) at the kinetochore (Vigneron et al., 2004). This localization, in turn, promotes the recruitment of the MAD1, MAD2, and CDC20 to the kinetochores (Vigneron et al., 2004). MPS1 (TKK in human) is a kinetochore-associated serine/threonine kinase and is activated through dimerization and auto-phosphorylation (Kang et al., 2007). It can directly regulate the localization of MAD1 and MAD2 at the kinetochores (Abrieu et al., 2001), also, it can partly be required for the CENP-E binding with kinetochores by phosphorylation. This kinetochore-bound CENP-E has been shown to contribute to the association of the MAD1/MAD2 complex on the unattached kinetochores (Abrieu et al., 2001). The kinetochore-bound BUB1, one of the SAC kinases, and the kinetochore-bound MAD1 are both stable (Howell et al., 2004), which initiate the recruitment of the SAC module to the outer kinetochore in early prophase (Howell et al., 2004, Johnson et al., 2004, Sharp-Baker and Chen, 2001, Taylor and McKeon, 1997). The genes rough deal (Tod), and zeste-white 10 (zw10) were first identified in *Drosophila* and conserved in eukaryotes (Williams et al., 1992, Karess and Glover, 1989, Scaerou et al., 2001), and together with another gene called zwilch (Williams et al., 2003), they form a Rod-Zw10-Zwilch complex (RZZ complex). RZZ complex is responsible for kinetochore recruitment of MAD1 and MAD2 (Buffin et al., 2005, Karess, 2005), which is regulated by Aurora B kinase activity (Kasuboski et al., 2011).

1.3.2 *The mitotic checkpoint complex (MCC)*

Although a single SAC protein such as BUBR1 and MAD2 can inhibit APC/C activity independently (Fang et al., 1998, Tang et al., 2001a, Kulukian et al., 2009), the protein complexes of BUBR1-BUB3 and CDC20-MAD2 showed a higher competency in inhibiting the APC/C (Musacchio and Salmon, 2007, Sudakin et al., 2001). The mitotic checkpoint complex (MCC) is comprised of BUB3, Mad3/BUBR1, MAD2, and CDC20, was firstly purified from mitotic extracts of HeLa cells, and its inhibitory activity is 3,000-fold greater than that of recombinant MAD2 alone (Sudakin et al., 2001). The MCC has been widely regarded as the potent APC/C inhibitor responsible for SAC activity (Lara-Gonzalez et al.,

2012), and the strength of the SAC depends on the amount of MCC formed (Collin et al., 2013).

1.3.3 *The profile of MAD2 and the 'MAD2 template' model*

Mad2 was the first gene identified in *S. cerevisiae* (Li and Murray, 1991). Subsequently, its human orthologues of MAD2 (hsMAD2, MAD2L1 or MAD2L2) were cloned (Li and Benezra, 1996). It is characterized as the primary signal transducer that links the SAC signalling events on unattached kinetochores (Tipton et al., 2011a, Luo and Yu, 2008, Mapelli and Musacchio, 2007, Ciliberto and Shah, 2009) to participate or amplify the checkpoint signal (Ciliberto and Shah, 2009, Mapelli and Musacchio, 2007, Tipton et al., 2011a).

MAD2 has two distinct native conformations, the open (O) and closed (C) forms of MAD2, O-MAD2 exists as a monomer or in the form of an O-C heterodimer, C-MAD2 can form both the O-C heterodimer and the C-C homodimer (Luo and Yu, 2008, Mapelli and Musacchio, 2007, Luo et al., 2004, Fang et al., 1998). Only dimeric MAD2 can exert the inhibitory function of the APC/C (De Antoni et al., 2005, Luo and Yu, 2008). The C-MAD2 conformation is adopted when an O-MAD2 is bound to its partners, MAD1, CDC20, BUBR1, or another MAD2 (Mapelli and Musacchio, 2007, Luo and Yu, 2008, Tipton et al., 2011b, Tipton et al., 2011a). MAD2 is expressed throughout the cell cycle. In interphase, most of the MAD2 exist as O-conformation in the cytosol and though a fraction adopts the C-conformation after binding to MAD1 and localizes on the nuclear envelope membrane (Luo et al., 2002, Campbell et al., 2001, Kitagawa, 2009). After nuclear envelope breakdown, the MAD1-C-MAD2 complex is enriched on the unattached kinetochores (Chen et al., 1996), and this kinetochore localized MAD1-C-MAD2 complex will then act as a template to recruit another O-MAD2 from the cytosol to form a MAD1-C-MAD2-O-MAD2 complex, and convert the confirmation of O-MAD2 into intermediate MAD2 (I- MAD2) (De Antoni et al., 2005). The "MAD2 template" working model is shown in Figure 1.6.

CDC20 is the primary target of I-MAD2 (Musacchio and Salmon, 2007, Yang et al., 2008). The active I-MAD2 somehow binds to CDC20 and is converted to C-MAD2, and this CDC20-bound C-MAD2 could potentially further catalyze the conversion of O-MAD2 to C-MAD2 for signal self-amplification (De Antoni et al., 2005, Simonetta et al., 2009). MAD1 is a resident of the unattached kinetochores that exchanges slowly with cytosolic pools (Howell et al., 2004), which recruits and catalyzes the activation of MAD2 as discussed above (De Antoni et al., 2005). One MAD1 molecule can bind to two molecules of MAD2: C-MAD2 and O-MAD2, only C-MAD2 is capable of being passed onto CDC20 (Luo and Yu, 2008, De Antoni et al., 2005, Shah et al., 2004).

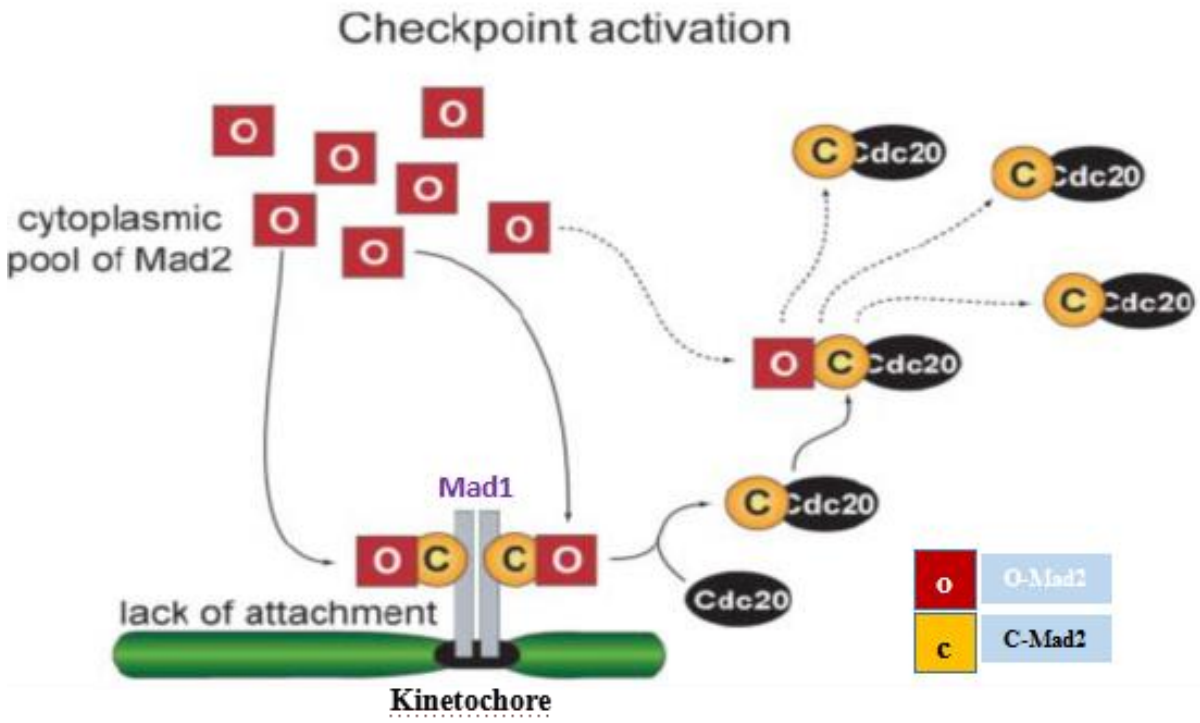

Figure 1.6: The "MAD2 template" model.

The kinetochore-bound ternary complex of MAD1-C-MAD2 binding an O-MAD2 starts the SAC. The unattached kinetochore recruits the MAD1-C-MAD2 core ternary complex, which recruits and binds to an O-MAD2 from the cytosolic pool to be converted to a C-MAD2 for binding to a CDC20. In the cytosol, the CDC20-C-MAD2 is a structural mimic of the MAD1-C-MAD2, which itself can act a template to bind and convert more O-MAD2 into CDC20-C-MAD2 for signal self-amplification. Adapted from (De Antoni et al., 2005).

1.3.4 *The profile of CDC20*

CDC20, the cell division cycle protein 20, is an essential regulator of cell division in eukaryotic cells including human cells. Its level increases at late S phase and peaks in mitosis, followed by a sharp decline (Prinz et al., 1998). It has a double life: as the co-activator of the APC/C to trigger anaphase onset, and as the key subunit of the MCC to inhibit the APC/C (Liu and Zhang, 2016, Sudakin et al., 2001, Musacchio, 2015, Kimata et al., 2008). It changes its state at multiple points in cell cycle to regulate cell division (Tang et al., 2004, Yudkovsky et al., 2000).

CDC20 is a protein related to the β subunit of trimeric G protein (Yu, 2007), which contains seven WD40 repeats, a bladed β propeller structure composed of 40 amino acids, contributing to proteins interaction (Yu, 2007, Sethi et al., 1991). Additionally, three motifs of CDC20 have been identified that can bind to the APC/C: the C-box, the IR (C-terminal isoleucine-arginine tail), and the KILR (lysine-isoleucine-leucine-arginine tetrapeptide) (Izawa and Pines, 2011). The C-box and KILR motifs of CDC20 bind to APC8 while the IR motif binds to APC3, forming the APC/C^{CDC20} complex (Qiao et al., 2016, Zhang et al., 2016). CDC20 acts as a subunit of the MCC, it utilizes the same KILR motif to bind to MAD2 (Luo et al., 2002, Izawa and Pines, 2012). CDC20 also contains a KEN box that can contribute to its ubiquitination by APC/C^{CDH1}, another co-activator of the APC/C after mitosis (Pfleger and Kirschner, 2000).

It is important for SAC signalling that MAD2 interacts with CDC20 in responding to unattached kinetochores in cell division. The mechanism of the CDC20-MAD2 interaction is complicated and not fully understood. It is thought as the first step that MAD1 at an unattached kinetochore recruits MAD2 (De Antoni et al., 2005). As MAD1 and CDC20 bind to the same MAD2 pocket, it was predicted that MAD1 and CDC20 would compete to interact with MAD2. The CDC20 interaction with MAD2 may be followed by MAD2

dissociating from MAD1 (Mapelli and Musacchio, 2007). However, the evidence shows that MAD1 is necessary for loading MAD2 onto CDC20 in living cells (Hwang et al., 1998).

1.3.5 *The mechanism of the MCC formation*

The MCC includes two sub-complexes, CDC20-MAD2 and BUBR1-BUB3, but it is unclear how the two sub-complexes join together to form the MCC. One possibility is that firstly the kinetochores facilitate the formation of MAD2-CDC20 and BUBR1-BUB3 sub-complexes respectively, and then the two sub-complexes are somehow integrated to form the MCC (De Antoni et al., 2005, Luo et al., 2000, Sironi et al., 2001, Luo et al., 2002). It has been suggested that the BUBR1-BUB3 sub-complex exists throughout the cell cycle (Hardwick et al., 2000, Larsen and Harrison, 2004, Larsen et al., 2007), so the formation of CDC20-MAD2 is an initial and essential step in the assembly of the MCC (Sudakin et al., 2001), and the mechanism of MCC assembly can be followed by the observing CDC20-MAD2 formation. Previously, researchers thought that the SAC signal works in an "on" or "off" manner, being activated after nuclear envelope breakdown in response to the unattached kinetochores, and then rapidly switched off at anaphase onset (Lara-Gonzalez et al., 2012, Musacchio and Salmon, 2007, De Antoni et al., 2005). However, this kinetochore dependent "on" or "off" mechanism has been challenged by the idea that SAC signalling acts as a "rheostat", where its strength increases and decreases gradually determined by the amount of MAD2 recruited to kinetochores and the amount of MCC formed (Collin et al., 2013). Thus, it is still a controversial area of cell cycle regulation that how does the MCC assemble.

1.3.6 *The kinetochore-dependent MCC formation*

The kinetochore dependent formation of the MCC has been widely accepted as the exclusive SAC mechanism (Musacchio, 2015, Lara-Gonzalez et al., 2012). It has been reported that the expression of BUBR1-BUB3 and CDC20-MAD2 complexes were higher in mitotic cells than that in interphase cells (Braunstein et al., 2007). The MCC components CDC20, MAD2,

BUBR1, and BUB3 are sequentially recruited and enriched on unattached kinetochores in mitosis conserved from yeast, *Drosophila* to human cells (Howell et al., 2000, Kallio et al., 2002, Shah et al., 2004, Raff et al., 2002, Li et al., 2010). The kinetochores provide the catalytic platform for the MCC assembly corresponding to the SAC signalling (Howell et al., 2000, Vink et al., 2006, Musacchio and Hardwick, 2002). Targeting MAD2 and BUBR1 to kinetochores is sufficient to maintain checkpoint arrest regulated by Aurora and Mps1 kinases (Kruse et al., 2014, Maldonado and Kapoor, 2011). The activity of BUBR1 inhibits the APC/C by blocking its binding to CDC20 (Tang et al., 2001a), while its accumulation and phosphorylation at unattached kinetochores plays an important role in association with other SAC components for maintaining the SAC function (Chen, 2002). The MCC components are released from kinetochores upon microtubule attachment after mitosis (Musacchio and Salmon, 2007, Shah et al., 2004). It has been shown that the "stripping" of MAD2, MAD1 and other SAC proteins from kinetochores is the key process of SAC inactivation (Howell et al., 2001). As a result, it has been widely accepted that the MCC is assembled in response to the unattached kinetochores (Yu, 2006, Lara-Gonzalez et al., 2012, Musacchio and Salmon, 2007), and the "MAD2 template" model partly explained how this might be done.

1.3.7 *The kinetochore-independent MCC formation*

The unattached kinetochores appear to be the primary source of C-MAD2-CDC20 (Luo et al., 2000, Sironi et al., 2001, Luo et al., 2002), and it is widely accepted that the inhibitory "on" signal of the SAC is generated exclusively by unattached kinetochores (Lara-Gonzalez et al., 2012, Musacchio and Salmon, 2007, Yu, 2006). However, evidences suggested that the MCC can form independently of unattached kinetochores (Poddar et al., 2005, Meraldi et al., 2004, Fraschini et al., 2001). The MCC can be isolated from interphase cells extracts where the kinetochore has not yet formed (Sudakin et al., 2001). The CDC20-MAD2 sub-complex is still detectable when Ndc10, an essential protein for core kinetochore assembly has been mutated (Fraschini et al., 2001, Poddar et al., 2005). The MCC component BUB3 is required for MAD2, MAD1 and BUBR1 kinetochore localization (Millband and Hardwick, 2002,

Vanoosthuyse et al., 2009), but is redundant for SAC activation (Tange and Niwa, 2008, Vanoosthuyse et al., 2009), and its kinetochore localization is not essential for SAC function (Malureanu et al., 2009). An N-terminal CDC20 binding domain of BUBR1 which lacks the BUB3-binding domain for kinetochore localization or a soluble form of the full-length BUBR1 can inhibit the APC/C in interphase (Malureanu et al., 2009). These observations indicated that the assembly of a functional MCC can take place at a cell cycle stage without appropriate kinetochores, though it's worth noting that the kinetochore independent pool of the MCC can only exert an incomplete inhibition of the APC/C (Meraldi et al., 2004, Lara-Gonzalez et al., 2011, Lara-Gonzalez et al., 2012).

1.4 Events after the SAC activation

1.4.1 *The profile of the APC/C*

As the effector of the mitotic checkpoint signalling network, the target of the MCC is the APC/C, an E3 ubiquitin ligase complex composed of 19 subunits of 14 distinct proteins including its co-activators CDC20 and CDH1 (depending on the species)(Barford, 2011, Chang et al., 2014, Chang and Barford, 2014). The APC/C stably expresses throughout the cell cycle and contributes to the ubiquitin-mediated substrate degradation (Barford, 2011). The spatial-temporal regulation of the APC/C activity is partly achieved by selectively binding to CDC20 or CDH1. At the end of mitosis, the APC/C^{CDC20} ubiquitylates two essential mitotic regulators cyclin B1 and securin which contain a consensus motif, the destruction box (D-box) (Clute and Pines, 1999, Huang and Raff, 1999, Cohen-Fix et al., 1996). The APC/$C^{CDH1,}$ on the other hand, targets substrates including CDC20 containing both a D-box and a degron called 'KEN-box' during late mitosis and G1 transition (Castro et al., 2005, Pfleger and Kirschner, 2000). The APC/C adapts a triangular bi-lobed shape linked by a scaffold structure, organized by subunits APC1, APC4, APC5 (Eme et al., 2011, Liu and Zhang, 2016) between a 'catalytic' sub-complex with subunits of APC11, APC2, and APC10 (Liu and Zhang, 2016, Thornton et al., 2006, Eme et al., 2011), and a 'TPR' (tetratricopeptide repeat) sub-complexes contains APC3, 6, 7 and 8 (Izawa and Pines, 2011). The catalytic core

of the APC/C is composed of APC2 and APC11, which are the analogues of the cullin and Rbx1 subunits of cullin-RING ligases (CRLs) of the SCF ligase superfamily (Tang et al., 2001b, Brown et al., 2014, Brown et al., 2015, Zheng et al., 2002).

Apart from the 'scaffold' structure and the 'catalytic' sub-complex, the different subunits of the 'TPR' arm of the APC/C showed different roles in its function. APC8 is responsible for the interaction with CDC20 when targeting NeK2A (Sedgwick et al., 2013, Boekhout and Wolthuis, 2015, Cohen-Fix et al., 1996), and for the degradation of cyclin A at prometaphase which is independent of the SAC (Fry and Yamano, 2006, van Zon and Wolthuis, 2010), whereas APC3 and APC8 are required for interacting with CDC20 when cyclin B1 is destroyed at the end of metaphase under SAC regulation (Izawa and Pines, 2011). Apc10 is required for the recognition and recruitment of mitotic substrates, cyclin B1 and securin, but not cyclin A, for destruction, (Izawa and Pines, 2011). This process requires that CDC20 or CDH1 interacts with APC10 and that the substrates, like cyclin B1 and securin contain degrons such as the 'D-box' and 'KEN' box (Buschhorn et al., 2011, da Fonseca et al., 2011, Chang and Barford, 2014).

1.4.2 *The inhibition of the APC/C by the MCC*

The key roles of the APC/C are controlling the fidelity of chromosome segregation in mitosis by targeting and coordinating the destruction of the mitotic regulators cyclin B1 and securin via the ubiquitin-mediated proteolysis pathway (Murray, 1994). The substrate specification and the activation of the APC/C are contributed by the binding of the APC/C to its co-activators CDC20 or CDH1 (Musacchio and Salmon, 2007, Lara-Gonzalez et al., 2012). Exactly how the SAC inhibits the active APC/C-CDC20 is not fully understood. As the main effector of the SAC, the MCC targets the APC/C, it used to be believed that by incorporated CDC20 into the MCC, it sequestered and prevented CDC20 from binding and activating the APC/C. It has been demonstrated in budding yeast that the MCC can itself act as a pseudo-substrate inhibitor of the APC/C (Burton and Solomon, 2007). The N-terminus of

Mad3p/BUBR1, the component of the MCC, contains a D-box and KEN-box, which can function together to mediate competitive binding of either CDC20 or substrate (Burton and Solomon, 2007, Sczaniecka et al., 2008). The MCC can directly bind to the APC/C and block the substrate recruitment by occupying the CDC20 binding site on the APC/C, which locks the APC/C into a "closed" state and prevents the binding and ubiquitylation of APC/C substrates (Herzog et al., 2009). This is because the MAD2-binding motif of CDC20 in the MCC mediates the interactions with the APC/C (Chang and Barford, 2014). The MCC can also directly modulate E2-ubiquitin binding to the APC/C subunits to inhibit the APC/C (Herzog et al., 2009). More recently, it has been shown that the MCC can recognize a second CDC20, which has already bound to the APC/C through two ABBA motifs in the N-terminal half of BUBR1 (Izawa and Pines, 2015).

1.5 The spindle assembly checkpoint silencing

Once all of the sister-kinetochores are bio-oriented and the tension applied to the bipolar spindle satisfies the SAC conditions, the APC/C is activated to trigger anaphase onset to allow chromatid segregation and mitotic exit (Liu and Zhang, 2016, Jia et al., 2011). Several mechanisms that contribute to this SAC silencing will be discussed.

1.5.1 *Dynein-mediated mechanism for striping kinetochore MAD1 and MAD2*

The binding of the SAC proteins, especially MAD1 and MAD2, the RZZ complex, MPS1, CENP-E and other protein components to the unattached kinetochore, is the important step of SAC signalling. So, to terminate the SAC signalling, it is equally important to remove these proteins from bio-oriented kinetochores as artificially tethering MAD1 to kinetochores delays anaphase onset (Maldonado and Kapoor, 2011, Maiato et al., 2004). This removal is mediated by a kinetochore localized minus-end-directed microtubule motor dynein mechanism (Howell et al., 2001), which can remove MAD1 and MAD2 from the kinetochore upon microtubule attachment, while the depletion of dynein blocks the removal of MAD1 and MAD2 from

attached kinetochores and arrests cell at metaphase (Howell et al., 2001, Mische et al., 2008). This is one of the important mechanisms contributing to SAC silencing (Musacchio and Salmon, 2007, Lara-Gonzalez et al., 2012). The coiled-coil domain containing protein, spindly can bind to the RZZ complex, which is required for the recruitment of cytoplasmic dynein to kinetochores in human cell (Barisic et al., 2010, Barisic and Geley, 2011). Depletion of spindly results in loss of kinetochore dynein functions, and impairs poleward chromosome movements and mitotic checkpoint inactivation (Barisic and Geley, 2011). A mutant of spindly which lacks the 'Spindly-box' persistently localized on the kinetochore but can no longer recruit dynein, and would result in a stripping defect (Barisic et al., 2010, Gassmann et al., 2010). However, other researches showed that spindly is not necessary for the removal of the checkpoint proteins from kinetochore, although where the microtubule recruitment of dynein is impaired (Chan et al., 2009). Therefore, the stripping mechanism of dynein can reduce the local kinetochore concentration of the SAC proteins and perhaps prevent MCC formation, but the details of the stripping mechanism remain elusive.

1.5.2 *Protein phosphorylation or de-phosphorylation mechanism*

Protein kinases such as BUB1 and MPS1 can promote the kinetochore localization of SAC proteins (Yamagishi et al., 2012, Hewitt et al., 2010), which results in SAC activation or maintenance of the SAC activity (London et al., 2012, Shepperd et al., 2012, Vanoosthuyse and Hardwick, 2009). In contrast, the activation of phosphatases can counteract the SAC kinases to inactivate the SAC (London et al., 2012). For instance, in budding yeast, Mps1 can directly phosphorylate the kinetochore protein Spc105 to recruit Bub1 to the kinetochore for SAC activation, while protein phosphatase 1 (PP1) can counteract this Mps1 effect (London et al., 2012). MPS1 is also required for kinetochore recruitment of MAD1 and MAD2 (Abrieu et al., 2001). Aurora B kinase activity is required to promote binding of the MCC to the APC/C (Morrow et al., 2005), while protein phosphatases 1 and 2A (PP1 and PP2A) are recruited to kinetochores to oppose these kinases activities (Manic et al., 2017). The integration of CDC20 into the MCC triggers the SAC activation, while the phosphorylation of

CDC20 stimulates its dissociation from BUBR1, and results in SAC inactivation (Miniowitz-Shemtov et al., 2012). Fengzhi et al. found that the centromere-associated protein Shugoshin (sgo1), ploidy 1(Ipl1)/Aurora B kinase, Dam1 and Mps1 form the SAC silence networks (SSN) in budding yeast, the Ip11 phosphorylates Dam1 to prevent SAC silencing before tension has been generated, while the tension-induced Dam1 de-phosphorylation by PP1 results in SAC silencing (Jin and Wang, 2013). Thus, by regulating the phosphorylation and de-phosphorylation of SAC proteins, its activity can be turned on or off (Lara-Gonzalez et al., 2012, Vanoosthuyse and Hardwick, 2009, Manic et al., 2017).

1.5.3 *The mechanism of ubiquitination in SAC silencing*

In addition to protein phosphorylation, ubiquitylation of SAC components is also considered as a pathway of SAC silencing (Reddy et al., 2007), where the APC/C ubiquitylates the SAC components for proteolysis when a proper kinetochore-microtubule attachment has been achieved (Jia et al., 2011). CDC20 is both a component of the MCC and one of the co-activators of the APC/C, its ubiquitylation and degradation at the end of mitosis influences the homeostasis of the MAD2-CDC20 interaction, and maintains the SAC silence persistently (Jia et al., 2011, Varetti et al., 2011, Uzunova et al., 2012). Similarly, BUBR1, another component of the MCC is ubiquitylated by the APC/C in metaphase, which removes the SAC inhibition (Foster and Morgan, 2012). However, the ubiquitylation of CDC20 might not be sufficient for promoting the disassembly of the MCC as it has been found that preventing the ubiquitylation of CDC20 by mutating all its possible ubiquitylation motifs does not block MCC disassembly (Nilsson et al., 2008). Moreover, the ubiquitylation of CDC20 has been shown to occur both in the process of SAC silencing but also in the process of SAC activation (Nilsson et al., 2008, Pan and Chen, 2004, Varetti et al., 2011). Therefore, the exact role of ubiquitylation in controlling SAC silencing needs to be further investigated.

1.5.4 *Silencing of the SAC by p31^{comet}*

It is a crucial step in the MCC formation and the amplification of the SAC signalling that O-MAD2 is constitutively recruited to unattached kinetochores and its conformation is converted into C-MAD2 to facilitate the production of the MCC via MAD2 template model as discussed above. Once the SAC has been satisfied, stimulating the disassembly of the existing MCC and preventing the kinetochores from recruiting more O-MAD2 to make new MCC are essential for SAC silencing.

In 2002, a screen of a cDNA library using the yeast two-hybrid system with human MAD2L1 as bait, allowed Hubu et al. to identify a novel MAD2 binding protein termed CMT2 (Caught by MAD Two). Overexpression of the protein in HeLa cells can abrogate the spindle checkpoint activation while its depletion delays anaphase onset (Habu et al., 2002). Subsequently, Xia et al. renamed it as $p31^{comet}$ because of its comet tail-like cellular localization pattern in mitosis (Xia et al., 2004), and it is also commonly known as MAD2L1BP.

The $p31^{comet}$ was found to localize to the nuclear envelope during interphase and prophase in RPE and HeLa cells (Westhorpe et al., 2011), It is unevenly distributed as speckles throughout the nucleoplasm in the early stage of mitosis (Yang et al., 2007); some of which localize near the kinetochore, and it then associates with the anaphase spindle and the microtubule midbody in telophase in HeLa cells (Habu et al., 2002). After co-staining the affinity-purified $p31^{comet}$ antibody and CREST antiserum (CREST staining the centromeres), images captured from time-lapse microscopy of $p31^{comet}$-EYFP, confirmed that it is associated with unattached kinetochores in prometaphase and at significantly lower levels as part of the kinetochore-microtubule attachment in metaphase and presents in the cytosol at all cell cycle stages, the kinetochore recruitment of $p31^{comet}$ is MAD2 dependent (Hagan et al., 2011). In nocodazole treated HeLa cells, the amount of $p31^{comet}$ bound to BUBR1-CDC20 is more than that in cells treated with Taxol, which suggests that the interaction of $p31^{comet}$ with BUBR1 and CDC20 depends on the number of unattached kinetochores (Westhorpe et al., 2011). The western blot results from highly synchronized HeLa cells released from double thymidine

block showed that the level of p31^{comet} is low at 0 hours, increased and remained constant until late mitosis, and suddenly dropped at 14 hours after release at a stage equivalent to anaphase as indicated by phospho-H3 staining (Habu et al., 2002), which suggests that p31^{comet} may be destroyed after late mitosis.

The molecular weight of full-length of p31^{comet} (CMT2) is about 31kDa. The initial sequence analysis indicated that p31^{comet} contains two putative destruction boxes (Habu et al., 2002) (Figure 1.7, marked by the black boxes). By comparison with the consensus of the destruction motifs of the D-box (R-x-x-L-x-x-x-x-N/D/E) (Glotzer et al., 1991, Burton and Solomon, 2001) and KEN box (K-E-N-x-x-x-D/N) (Pfleger and Kirschner, 2000, Burton and Solomon, 2001), we found that there is one additional potential KEN-box in the protein sequence of the human p31^{comet} (Figure 1.7, marked by the red box). The D-box and KEN-box are the signatures of mitotic proteins destroyed by the APC/C-mediated proteolysis pathway. Moreover, the results from mass spectrometry analysis indicated that p31^{comet} contains multiple potential sites of ubiquitination (Udeshi et al., 2013, Wagner et al., 2011). Bringing all these results together, it suggests that p31^{comet} could be a cell cycle regulated protein, however, the potential turnover property of p31^{comet} targeted by the APC/C or other ubiquitin ligase and its physiological functions have yet to be characterized.

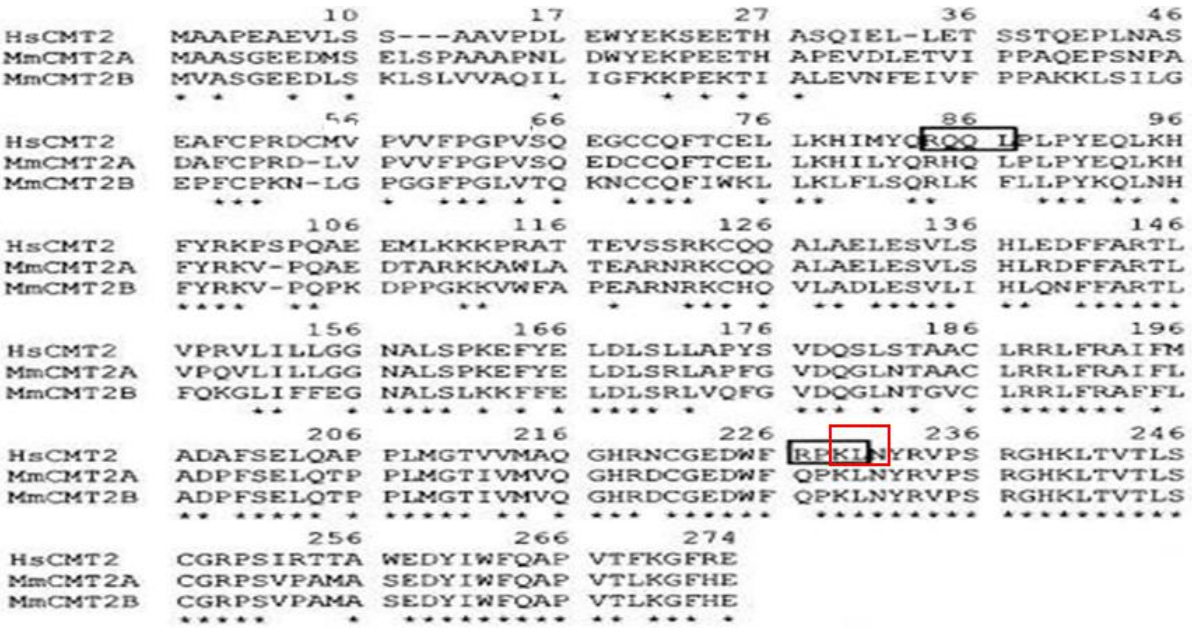

Figure 1.7: The sequence alignment of p31^{comet} (CMT2).

The sequence alignment of the human p31^{comet} (HsCMT2), two mouse homologues (MmCMT2A) and (MmCMT2B) are shown. The asterisks indicate the amino acids conserved in human and mouse. The putative D-box motifs are marked with the black boxes, and the putative KEN box motif is marked with the red box. Modified from (Habu et al., 2002).

As the MAD2 binding protein, the function of p31^{comet} has been investigated tightly in association with the SAC. It was once speculated that the mechanism of dissociation of CDC20-MAD2 by p31^{comet}, is due to p31^{comet} competing with CDC20 for binding to MAD2 to disrupt the CDC20-MAD2 interaction, but this was soon rejected as the evidence showed that CDC20 and p31^{comet} do not share the same binding site with MAD2, and binding of p31^{comet} to MAD2 does not prevent CDC20 interacting with MAD2 *in vitro* (Xia et al., 2004). p31^{comet} only binds to the close form of MAD2 (C-MAD2), and transiently interacts with MAD2 (C-MAD2) to form a CDC20-C-MAD2-p31^{comet} ternary complex *in vivo* during checkpoint inactivation (Xia et al., 2004). The structural analysis suggests that p31^{comet} binds C-MAD2 at its dimerization interface, which is required for kinetochore recruitment of O-MAD2 (Mapelli et al., 2007, Mapelli et al., 2006, Yang et al., 2007). *In vitro*, the purified p31^{comet} can restore the activity of APC/C^{CDC20} by forming the APC/C-CDC20-C-MAD2-p31^{comet} transient

complex to reverse the inhibition of the APC/C by MAD2 (Xia et al., 2004). However, it is strange to observe that p31^{comet} in fact can interact with MAD1-MAD2 throughout the cell cycle (Xia et al., 2004).

Owing to MAD2-dependent kinetochore recruitment of p31^{comet} (Hagan et al., 2011), overexpression of p31^{comet} bypassed the SAC arrest and the depletion of p31^{comet} delayed the anaphase onset (Habu et al., 2002); and the structural analysis suggests that p31^{comet} binds C-MAD2 at its dimerization interface, which is required for kinetochore recruitment of O-MAD2 (Mapelli et al., 2006, Yang et al., 2007); moreover, p31^{comet} counteracts the function of MAD2 and is required for SAC silencing (Xia et al., 2004); this led to the hypothesis that p31^{comet} by competitively binding to MAD1 bound C-MAD2 on the kinetochore, blocks the recruitment of more O-MAD2 or the capping of MAD1-C-MAD2 at the kinetochores for C-MAD2-CDC20 production (Xia et al., 2004, Yang et al., 2007, Mapelli et al., 2006). However, some more recent results suggest that this might not be the case, as p31^{comet} siRNA or overexpression does not affect the levels of kinetochore recruitment of O-MAD2 (Westhorpe et al., 2011), and the prevention of the kinetochore localization of O-MAD2 by inhibiting MPS1 activity will not increase p31^{comet} kinetochore localizations (Hewitt et al., 2010, Westhorpe et al., 2011).

p31^{comet} can promote the release of the MAD2-CDC20 complex from the MCC and disrupts the interaction of CDC20 with BUBR1, which encourages the dissociation of the MCC, a process requiring ATP hydrolysis (Teichner et al., 2011). p31^{comet} can also extract MAD2 from the free form of the MCC and cause disruption of the MCC *in vitro* (Westhorpe et al., 2011). The MCC levels increased upon the depletion of p31^{comet} by siRNA, which negatively regulates SAC activation (Westhorpe et al., 2011). These highlighted that p31^{comet} acts in MCC disassembly. However, in *vitro* observations showed that p31^{comet} is not directly involved in the disassembly of MAD2-CDC20 contained in the MCC complex but offsets the APC/C inhibition by MAD2 through forming the APC/C^{CDC20}-MAD2-p31^{comet} complex (Xia et al., 2004). The phosphorylation of SAC proteins contributes to SAC silencing, while

p31^{comet} can stimulate CDK to catalyze the phosphorylation of CDC20 in the MCC, to promote CDC20 dissociation from BUBR1, by which responses to SAC silence (Miniowitz-Shemtov et al., 2012). Moreover, p31^{comet} can promote MCC disassembly independent of CDC20 ubiquitylation (Jia et al., 2011). Interestingly, by altering its phosphorylation status, p31^{comet} can also regulate the SAC by attenuating the binding with MAD2 (Date et al., 2014).

Although exactly how p31^{comet} is involved in SAC silencing needs to be elucidated, it has repeatedly been observed that mitosis exit is delayed after the depletion of p31^{comet} (Habu et al., 2002, Xia et al., 2004, Chan et al., 2008). The overexpression of p31^{comet} in cancer cell lines caused the premature destruction of securin and led to premature sister chromatid separation and increased the resistance to antimitotic drugs (Habu and Matsumoto, 2013), while its depletion promotes sensitivity to antimitotic drugs (Ma et al., 2012). Using a genome-wide siRNA screen, Diaz-Martinez, L. A., et al. found that p31^{comet} promotes mitotic adaptation through cyclin B1 degradation and independently suppresses cancer cell death, and confirmed that its depletion in the presence of anti-cancer drugs could result in cell apoptosis. Therefore, targeting p31^{comet} is an attractive strategy for uncoupling the cell apoptosis and mitotic adaption pathways (Diaz-Martinez et al., 2014). However, other observations have shown that the overexpression of p31^{comet} can also induce cell apoptosis and senescence by interfering with MAD2 activity (Shin et al., 2015). In addition to its checkpoint functions, p31^{comet} can also regulate insulin signalling by blocking the interaction of MAD2-BUBR1 with the insulin receptor on the plasma membrane in hepatocytes, by which for the first time links chromosome stability to nutrient metabolism (Choi et al., 2016).

1.5.5 *The TRIP13 and the joint action of TRIP13 and p31^{comet} in the SAC silencing*

In recent years, a novel kinetochore protein, TRIP13 (PCH-2 in *C. elegans*) (Thyroid hormone receptor interacting protein 13), a highly conserved AAA+ATPase, has been identified as the silencer of the SAC signalling, as its depletion can delay anaphase onset

(Wang et al., 2014). It exerts the SAC inhibitory function by binding to p31^{comet}, and probably plays the predominant role in silencing the SAC (Wang et al., 2014, Eytan et al., 2014). *In vitro*, TRIP13 uses p31^{comet} as an adaptor protein to convert the conformation of C-MAD2 back to O-MAD2, which then blocks MCC formation and silences the SAC (Eytan et al., 2014, Ye et al., 2015, Ma and Poon, 2016, Brulotte et al., 2017). At the same time TRIP13 can bind to p31^{comet} to cause disassembly of the MCC, and resulting in SAC inactivation (Wang et al., 2014, Brulotte et al., 2017), this process requires ATP hydrolysis and energy input (Miniowitz-Shemtov et al., 2010). The joint action of TRIP13 and p31^{comet} in silencing the SAC and dissociating the MCC is thought to involve the following steps (Eytan et al., 2014) (Figure 1.8). Firstly, p31^{comet} releases CDC20-MAD2 from BUBR1, this process does not require TRIP13 and the conformation change of C-MAD2 but involves the CDK-dependent phosphorylation of CDC20 (Eytan et al., 2014, Miniowitz-Shemtov et al., 2012). The second step includes the release of MAD2 from the CDC20-MAD2 sub-complex or directly from the MCC, and the conversion of C-MAD2 to O-MAD2, this step requires the joint action of TRIP13 and p31^{comet} and is ATP-dependent (Eytan et al., 2014). The extraction of MAD2 from the MCC leaves a BUBR1-BUB3-CDC20 sub-complex (Westhorpe et al., 2011, Sudakin et al., 2001, Eytan et al., 2014), and exactly howCDC20 is released from BUBR1-BUB3-CDC20 sub-complex remains unknown. Very little is known about the interactions of TRIP13 with its substrates, p31^{comet} and ATP (Eytan et al., 2014), though it is critical for both the activation and inactivation of the SAC (Ma and Poon, 2016).

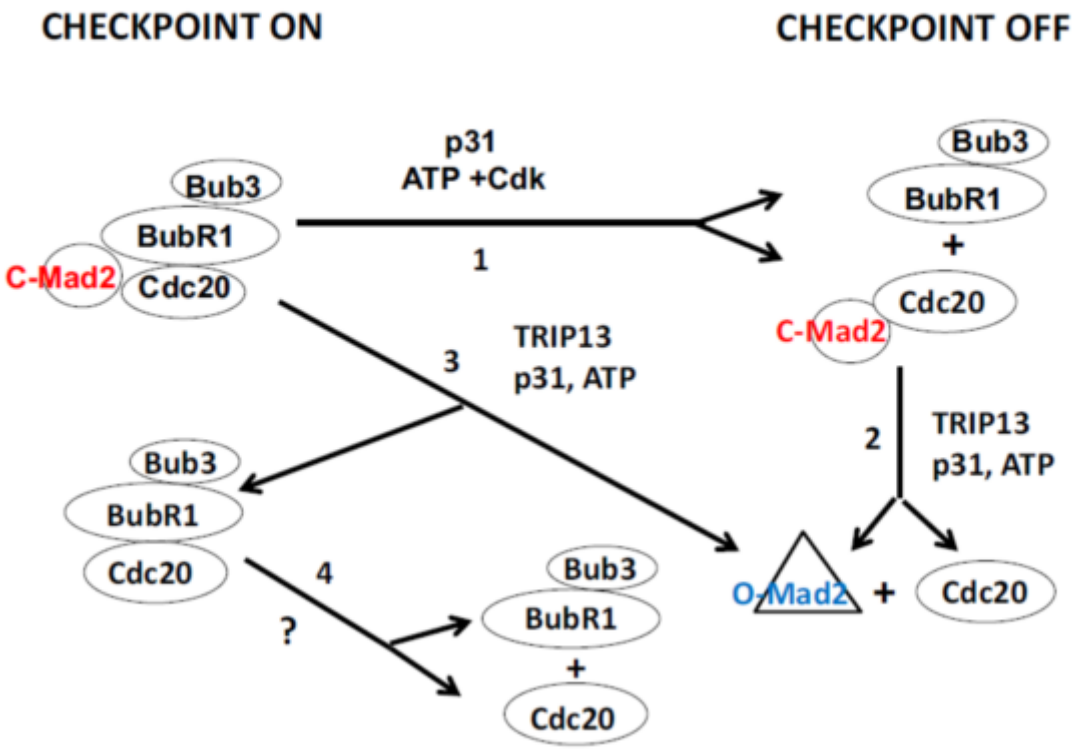

Figure 1.8: The joint actions of TRIP13 and p31^{comet} in silencing the SAC.

Step1, p31^{comet} promotes the dissociation of C-MAD2-CDC20 from BUBR1-BUB3, and CDK phosphorylates CDC20. Step 2 & 3, TRIP13 and p31^{comet} jointly cause the disassembly of the CDC20-MAD2 complex or the direct release of MAD2 from the MCC. Exactly how CDC20 is released from the BUBR1-BUB3-CDC20 complex is still unknown. Copied from (Eytan et al., 2014).

1.6 The spindle assembly checkpoint and mitotic cell death

To maintain genomic stability, the SAC produces a diffusive "wait" signal from unattached kinetochores that delays the metaphase to anaphase transition until the last of the sister-chromatids have been correctly attached to the mitotic spindle microtubules(Lara-Gonzalez et al., 2012). The activated SAC can block the APC/C to ubiquitinylate its substrates, cyclinB1 and securin for destruction, and arrest the cell in mitosis. The prolonged mitosis under sustained activation of the SAC can trigger cell death (Visconti

et al., 2016b, Janssen and Medema, 2011, Pedley and Gilmore, 2016). The exact mechanism of cell death in prolonged mitosis remains obscure, it possibly involves energy deprivation or the increased sensitivity to DNA damage during mitosis because the DNA is unprotected by the nuclear envelope (Janssen and Medema, 2011). Moreover, owing to the irreparability of damaged DNA of condensed chromosomes (Bakhoum et al., 2017, Stevens et al., 2007, Burgess et al., 2014), the silenced gene transcriptions (Gottesfeld and Forbes, 1997) and increased genome instability (Rieder and Maiato, 2004), mitosis is the most vulnerable period of the cell cycle, during which cells are more easily killed when cells suffered from irradiation, heat shock or exposed to various chemicals (Rieder and Maiato, 2004). The process of cell death in mitosis is collectively termed 'Mitotic Catastrophe' (Vitale et al., 2011). The mitotically arrested cells resulted from provoked SAC increases the incidence of being aneuploidy or genome instability in cells of offspring and often are fatal to embryos (Dobles and Sorger, 2000, Kalitsis et al., 2000). Therefore, blocking mitotic exit to induce cell death has been regarded as a promising therapeutic strategy for cancer treatment (Salmela and Kallio, 2013, Janssen et al., 2011, Visconti et al., 2016a, Gascoigne and Taylor, 2009). Indeed, some traditional anti-mitotic drugs such as taxanes, and vinca alkaloids are widely used in clinic (McGrogan et al., 2008, Jordan and Wilson, 2004). However, besides producing severe side effects, rapidly developed resistance to these anti-cancer drugs (Jordan and Wilson, 2004, Gascoigne and Taylor, 2009, McGrogan et al., 2008), most probably，the mitotic slippage undermines the efficacy of treatment (Visconti et al., 2016b). Thus we need to better understand the mechanisms underlying mitotic cell death in various circumstances (Visconti et al., 2016b).

1.6.1 ***The determination of a cell to "die "or "not die" in prolonged mitosis***

As discussed above, prolonged mitosis can lead to cell death. However, the duration of mitotic arrest is not permanent under all versions of the activated SAC and can undergo mitotic exit without sister chromatid separation and then enter the next round of the cell cycle; a process that is referred to as "adaptation" or "mitotic slippage" (Rossio et al., 2010, Rieder

and Maiato, 2004). Thus, in response to a prolonged mitotic arrest a cell could either die in mitosis or survive by exiting mitosis without dividing (Topham and Taylor, 2013). The cells that slipped from prolonged mitosis would undergo different fates (Rossio et al., 2010, Gascoigne and Taylor, 2008, Weaver and Cleveland, 2005): they might die in the next cell cycle after, being stably arrested in the G1 stage or divide unequally to produce aneuploidy daughter cells; alternatively, cells could exit mitosis with no division.

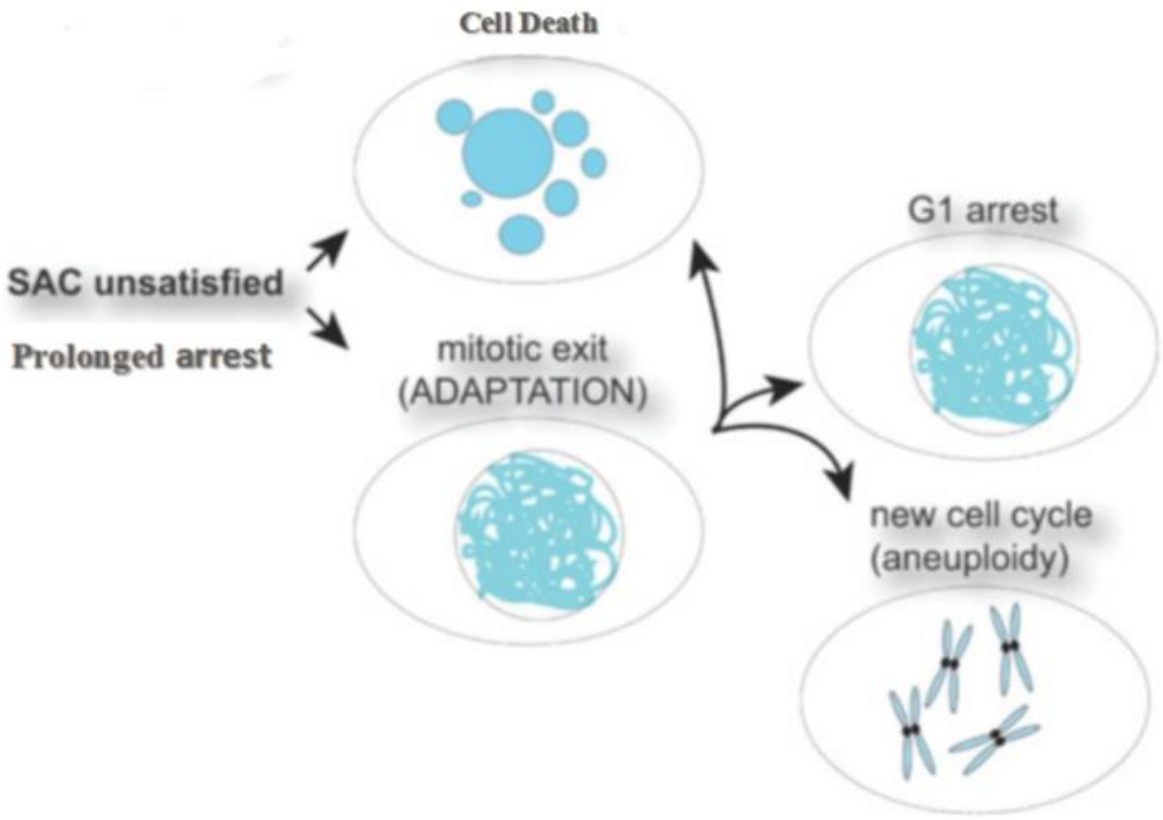

Figure 1.9: Cell fates in response to a prolonged mitotic arrest.

Cells will be arrested in mitosis in response to anti-mitotic drug treatment, such as nocodazole or taxol causing the constitutively activated spindle assembly checkpoint (SAC). As a consequence of the prolonged arrest, the cells can either die in mitosis by undergoing apoptosis or slip out of mitosis. When cells slipped out of the prolonged arrest they might die in G1 of the next cell cycle or enter a new cell cycle without cell division. (Adapted from (Rossio et al., 2010).

1.6.2 *The competing-network model*

Although prolonged mitosis can result in cell death, cell fate in prolonged mitosis does not correlate with duration of mitotic arrest (Gascoigne and Taylor, 2008, Janssen and Medema, 2011), but is influenced by caspase activation or by delaying cyclin B1 degradation (Gascoigne and Taylor, 2008, Chibazakura et al., 2004). The chronic activation of the SAC cannot completely prevent cyclinB1 degradation, which eventually results in mitotic exit (slippage) (Gascoigne and Taylor, 2008, Brito and Rieder, 2006). The overexpression of cyclin B1 can block cell cycle progression and keep the cell for longer in mitosis (Gascoigne and Taylor, 2008). A 'competing-network' model has been proposed to explain the cell destination in prolonged mitosis (Gascoigne and Taylor, 2008). According to this model, the cell fate is determined by two competing but independent networks: the strength of a yet to be defined cell death signal and the rate of cyclin B1 degradation. These two pathways show their inverse relationship determined by the thresholds of the increased cell death signal (die) and the fall of cyclin B1 levels (not die). A cell will die in mitosis if the cell death signal threshold is breached first. In contrast, the cell will slip out of mitotic arrest if the fall in cyclin B1 levels first breached the threshold (Figure 1.9) (Gascoigne and Taylor, 2008, Shi et al., 2008). For instance, the cell lines HT29 and RKO tend to die in mitosis in response to prolonged mitotic arrest due to their cyclinB1 level falling slowly to reach the mitotic exit threshold, while the DLD-1 cell line exits mitosis as its cyclin B1 level declined faster when the SAC is activated (Gascoigne and Taylor, 2008).

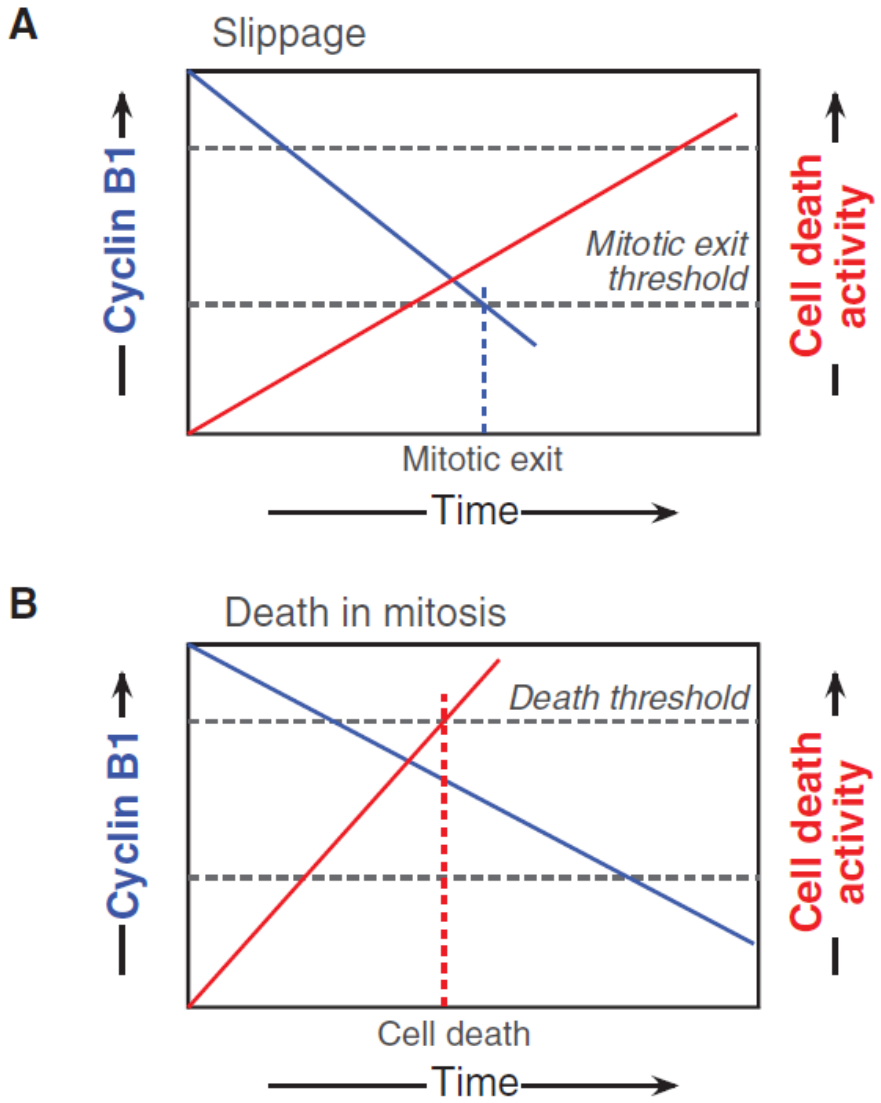

Figure 1.10: The diagram showing the 'competing-network' model for determining the cell fate in prolonged mitosis.

Under prolonged mitotic arrest, there are two competing, and independent pathways: one is a pathway giving rise to cell death signals and the other pathway controlling the degradation rate of cyclin B1. A cell will survive and undergo slippage if the fall in the cyclin B1 level breaches the 'mitotic exit threshold' first (A). Or the cell will die if the increase in the cell death signal breaches the 'Death threshold' first (B). Copied from (Gascoigne and Taylor, 2009).

1.6.3 *The mitotic cell death pathway*

Although the exact mechanism which determines the cell fate in prolonged mitosis remains unknown, a genome-wide siRNA screen revealed that no necrosis or autophagy network genes were identified as being involved in mitotic cell death and adaptation (Diaz-Martinez et al., 2014), thus the apoptotic pathway might be the only major cell death pathway determining the cell fate in response to prolonged mitotic arrest. This is supported by many observations that mitotic cell death involves the intrinsic apoptotic pathway (Diaz-Martinez et al., 2014, Topham and Taylor, 2013, Salmela and Kallio, 2013), either dependent (Allan and Clarke, 2007, Gascoigne and Taylor, 2008, Diaz-Martinez et al., 2014) or independent on caspase activities (Niikura et al., 2007).

1.6.4 *The intrinsic apoptotic pathway*

Apoptosis is a process of programmed cell death characterized by multiple changes in cell morphology including blebbing, cell shrinkage, nuclear fragmentation and extreme chromatin condensation (Kerr et al., 1972, Taylor et al., 2008), and its molecular basis includes the intrinsic (mitochondria pathway) and extrinsic apoptotic pathway (Tait and Green, 2010, Alberts, 2015).

The processes of the intrinsic apoptotic pathway include the activation or expression of pro-apoptotic proteins, the permeabilization of the mitochondrial outer membrane, to release cytochrome c and finally cell death by activation of caspase protein 3 or 7 (Slee et al., 2001). The mitochondria outer membrane permeabilization (MOMP) is the crucial process driving the cells to undergo apoptosis (Tait and Green, 2010). It is regulated by the pro-apoptotic signal mainly from the BH3 (BCL-2 homology domain) proteins including Bim, Bid, Puma, Noxa (Delannoy et al., 2018, Oda et al., 2000, Haschka et al., 2015, Yin, 2006) and the anti-apoptotic signal from the BCL-2 super-family of proteins such as BCL-xl, BCL-2 and MCL-1 (Tait and Green, 2010, Haschka et al., 2015, Pedley and Gilmore, 2016). Recently, a splicing variant of a shot-form of MCL-1 (MCL-1s) has been identified as a novel BH3 only protein, this is spliced out of the exon 2 of MCL-1 in mRNA transcription resulting in the loss

of BH1, BH2 and the transmembrane domains of MCL-1 (Bae et al., 2000). MCL-1s can dimerize with MCL-1 to antagonize the anti-apoptotic activity of MCL-1 (Bae et al., 2000, Hu et al., 2015, Lomonosova et al., 2009). In responding to a strong apoptotic stimulation signal, the increased pro-apoptotic proteins antagonize the activity of anti-apoptotic proteins to release the blocking of the homooligomerization of either BCL-2 associated X protein (BAX) or BCL-2 antagonist or killer protein (BAK) to form spanning pores on the outer membrane of mitochondria (Wei et al., 2001, Pedley and Gilmore, 2016). This allows the release of cytochrome c for binding with the apoptotic protease activating factor 1(APAF1), and then triggers the formation of the caspase activation platform-apoptosome, and subsequently the activation of caspase cascade signaling (Elmore, 2007). The active caspases (3/7) subsequently cause the cleavage of their substrate poly [ADP-ribose] polymerase-1 (PARP-1), a nuclear protein, to induce cell death. So the cleavage of PARP-1 by the active caspase is considered as the hallmark of apoptosis (Wen et al., 2012, Chaitanya et al., 2010, Fischer et al., 2003, Kaufmann et al., 1993). In contrast, the increased activities or protein levels of anti-apoptotic proteins sequester the homo oligomerization of BAX and BAK, which stops them forming the spanning pores on the mitochondrial outer membrane and so blocks the release of cytochrome c and apoptosis (Wei et al., 2001). Thus up-regulating the activities of the pro-apoptotic proteins or blocking the activities of the anti-apoptotic protein can induce apoptosis.

MCL-1 (myeloid cell leukaemia-1), a BCL-2 super-family protein has been shown to be degraded in response to prolonged mitotic arrest and this often resulted in cell death (Harley et al., 2010, Sakurikar et al., 2012, Chu et al., 2012, Kawabata et al., 2012). When MCL-1 is stabilized, it promotes the survival of mitotic cells (Topham and Taylor, 2013, Wertz et al., 2011). Thus MCL-1 plays a critical role in the determination of cell fate in response to prolonged mitosis (Harley et al., 2010, Wertz et al., 2011). The exact mechanism for MCL-1 degradation remains unclear, however, its degradation can be blocked by the proteasome inhibitor MG132 (Harley et al., 2010) suggesting that the ubiquitin-mediated E3 ligases such as the APC/C (Harley et al., 2010), SCF^{FBW7} (Inuzuka et al., 2011b), and MULE (Inuzuka et

al., 2011a, Zhong et al., 2005) are involved. As such, MCL-1 seems to possess a critical role in combination with the dynamic role of cyclin B1 in determining the cell fate in prolonged mitosis (Matson and Stukenberg, 2011).

1.7 Aims

1.7.1 *The spatial-temporal formation mechanism and function of the CDC20-MAD2 sub-complex of the MCC in the cell cycle*

The activation of the SAC is often referred to as the kinetochore-dependent assembly of the MCC. The formation of CDC20-MAD2 is an initial and essential step in assembly of the MCC (Sudakin et al., 2001). Therefore, the mechanism of MCC assembly and formation can be depicted by the observing the formation of the CDC20-MAD2 complex. However, evidence has also suggested that the MCC can form independently of unattached kinetochores (Poddar et al., 2005, Fraschini et al., 2001, Meraldi et al., 2004), and that the MCC can be isolated from interphase cell extracts where the kinetochore is not yet formed (Sudakin et al., 2001). The CDC20-MAD2 sub-complex is still biochemically detectable when Ndc10, an essential protein for core kinetochore assembly has been mutated (Fraschini et al., 2001). Some SAC proteins can exert their inhibitory functions on the APC/C independent of kinetochores in the absence of kinetochores (Tang et al., 2001a, Fang, 2002, Meraldi et al., 2004). The dynamic assembly of the CDC20-MAD2 complex has never been revealed *in vivo*. Therefore, examining the CDC20-MAD2 complex in individual cells to investigate when the MCC forms during the cell cycle will provide clues as to whether the process is kinetochore-dependent or not.

Previous work in the lab, using the Duolink based *in situ* proximity ligation assay (PLA) with specific primary antibodies against endogenous CDC20 and MAD2 in single HeLa cells, has revealed that the formation of the CDC20-MAD2 complex was cell cycle regulated and has a

"Bell" shaped profile (Figure 1.11). It starts to accumulate after late G2, increases in prophase before NEBD when the SAC has not been activated, peaks at prometaphase, and then gradually declines (Figure 1.11). This suggests that the unattached kinetochores might not be the only source for facilitating the assembly of CDC20-MAD2. Duolink PLA technology makes use of two primary antibodies raised in different animal species to target two interest proteins in fixed individual single cells. Species-specific secondary antibodies (PLA probes), each conjugated with a unique short oligonucleotide tail, bind to the primary antibodies. When the PLA probes are in close proximity (<40nm), these oligonucleotide tails can then act as a template for rolling circle amplification, and this amplification will produce a dot of fluorescent signal when labeled by complementary oligonucleotide probes (Soderberg et al., 2006). The advantage of using PLA is that it can avoid biochemical extraction or the creation of exogenous over-expressed fusion proteins and can assign signals to specific subcellular locations of the fixed individual cells under-examination. But, whether the CDC20-MAD2 fluorescent signals revealed by the PLA could reflect the genuine physical interactions between the two proteins, CDC20 and MAD2, must be tested. In this study, **1**. We would use two small chemical compounds, M2I-1 (MAD2 inhibitor-1) and reversine (MPS1 inhibitor), to test the genuine physical interaction of CDC20-MAD2 revealed by the PLA approach. M2I-1 is a small molecule that can disturb the *in vitro* interactions of CDC20 and MAD2 (Kastl et al., 2015); and reversine is a potent MPS1 kinase inhibitor, MPS1 is required for the assembly of the MCC (Maciejowski et al., 2010, Santaguida et al., 2010). **2**. After confirming the existence of a prophase CDC20-MAD2 complex formed independent of the kinetochores, we will then investigate its potential physiological function by examining if this prophase CDC20-MAD2 complex could prevent the premature degradation of cyclin B1 in early prophase.

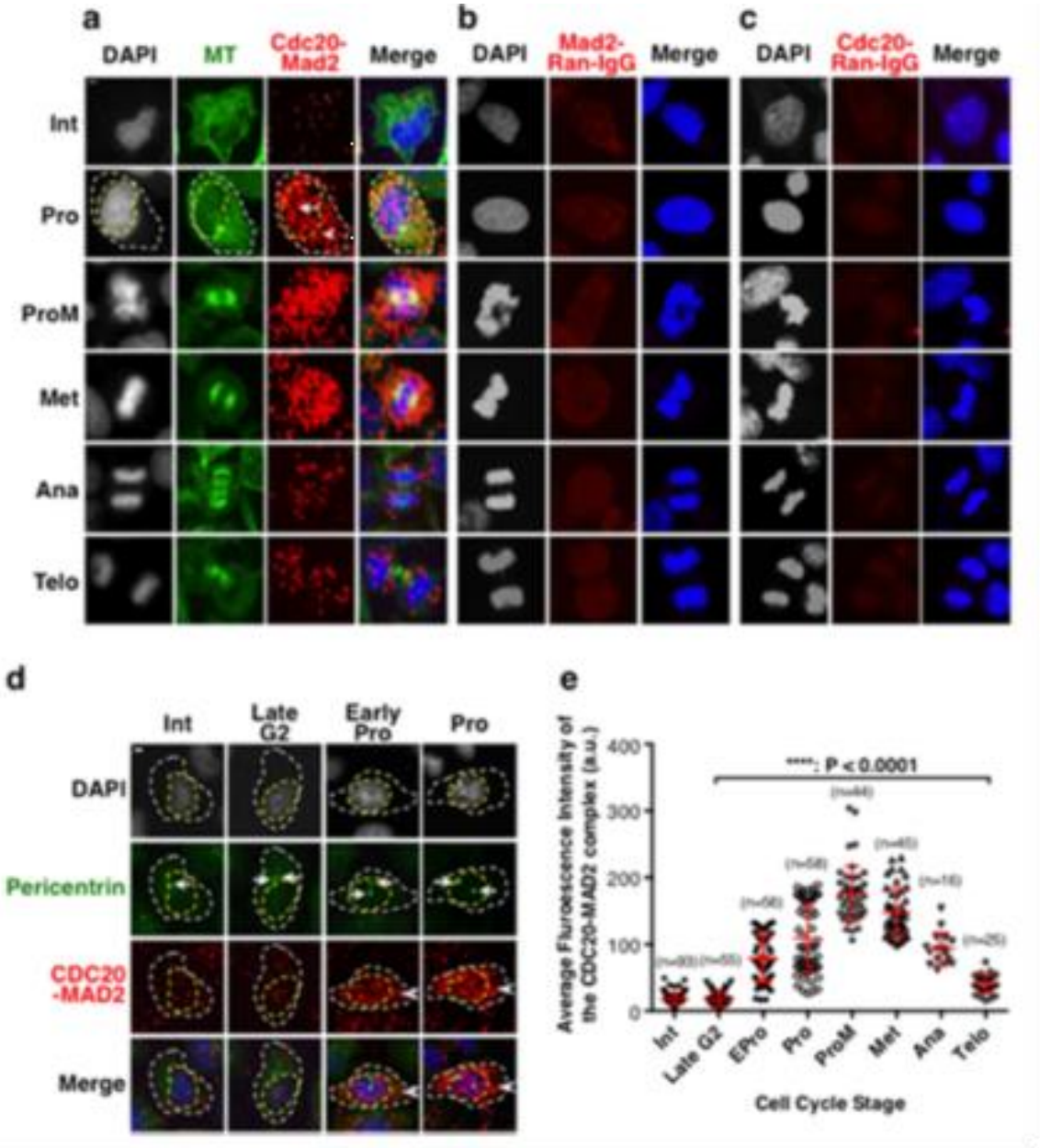
a
DAPI
MT
Cdc20-Mad2
Merge
b
DAPI
Mad2-Ran-IgG
Merge
c
DAPI
Cdc20-Ran-IgG
Merge
Int
Pro
ProM
Met
Ana
Telo
d
Int
Late G2
Early Pro
Pro
DAPI
Pericentrin
CDC20 -MAD2
Merge
e
Average Fluorescence Intensity of the CDC20-MAD2 complex (a.u.)
****: P < 0.0001
400
300
200
100
0
Int
Late G2
EPro
Pro
ProM
Met
Ana
Telo
Cell Cycle Stage

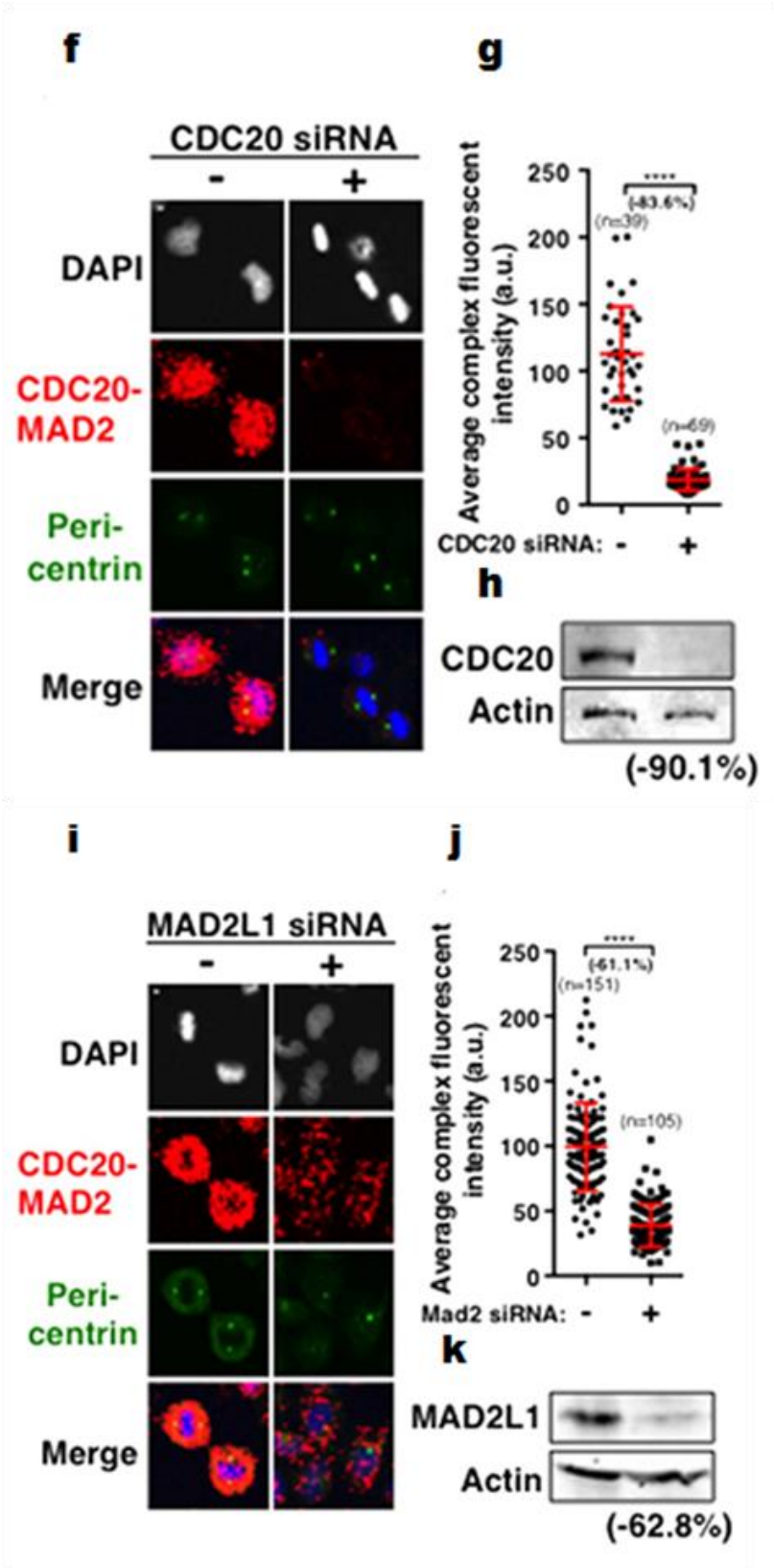

Figure 1.11: The profile of CDC20-MAD2 complex in cell cycle.

The PLA and projected Z-stack sectional confocal images were used to detect CDC20-MAD2 complex signals in fixed unperturbed HeLa cell, and image j software was used to analyse the level of CDC20-MAD2 complex in the different stages. White and yellow dash circle lines highlight the cytoplasmic and nuclear region respectively, the arrows and arrowheads highlight the fluorescent signals in the nucleus and cytoplasm respectively. DAPI (in blue) and microtubules (in green) morphologies were used to determine the cell cycle stages. (a) The interaction of CDC20-MAD2 is occurs during the cell cycle in a "bell" shaped manner, it starts to significantly increase from prophase, peak at prometaphase and decrease from metaphase, with a very low complex signal detectable in interphase. (b) & (c) The CDC20-MAD2 complex signal was not shown between pairs of MAD2-random IgG and CDC20-random IgG. (d) The staining of pericentrin antibody (in green) and DAPI (in blue) were used to further mark the cell cycle stages: interphase, late G2, early prophase and prophase, PLA detects the CDC20-MAD2 signal in these cell stages. (e) The quantitative profile in cell cycle of CDC20-MAD2 interaction illustrated by the average PLA signal from entire cellular regions (as shown with white dash line). Int: Interphase, L-G2: Late G2, Pro: Prophase, ProM: Prometaphase, Met: Metaphase, Ana: Anaphase, Telo: Telophase. Scale bar = 5μm. (f-k) showing the CDC20-MAD2 PLA signal in cells with or without the depletion of CDC20 or MAD2 using siRNA for 48 hours, the representative images were shown in (f) and (i). The quantitative results were shown in (g) and (j), the western blotting results indicated the reduction of endogenous protein of CDC20 in (h) and (k) respectively. DNA (DAPI staining) in grey and blue in merged images. Centrosomes (staining with percentrin) were shown in green. n: The number of cells used for quantification. ****P <0.0001. Standard deviation bars are in red.

1.7.2 *Characterization of the potential degradation mechanism of p31^{comet} in HeLa cells*

As discussed above, it has been shown that p31^{comet} may be destroyed in late mitosis. Initial sequence analysis indicated that p31^{comet} contains three putative destruction boxes, which are the signature for destruction of the mitotic proteins by the APC/C-mediated proteolysis pathway (Habu et al., 2002). The mass spectrometry analysis also indicated that p31^{comet} contains multiple potential ubiquitination sites (Udeshi et al., 2013, Wagner et al., 2011). However, the turnover of p31^{comet} targeted by the APC/C or any other ubiquitin-mediated E3 ligases and its relevant physiological functions have yet to be characterized. In this study, we would 1. Investigate and examine the expression profile of p31^{comet} throughout the cell cycle. 2. Try to dissect the degradation mechanism of p31^{comet} by specific antibody immuno-chemical analysis as well as by conventional biochemical approaches.

1.7.3 *The molecular basis of mitotic cell death in the case of down-regulating the SAC*

MAD2 inhibitor (M2I-1) is the first small molecule identified that disrupt the interactions between MAD2 and CDC20 or MAD2 and MAD1, which has been shown to weaken the SAC in HeLa cells (Kastl et al., 2015), and would theoretically promote cell slippage under a provoked SAC. Surprisingly, our preliminary observations show that M2I-1 can significantly increase cell death in several cancer cell lines when combined with anti-mitotic drugs such as nocodazole and Taxol. Therefore, we have systematically studied the potential mechanism that underlies the cell death induced by M2I-1 in the presence of nocodazole or Taxol.

Chapter Two. Materials and Methods

2.1. Materials

2.1.1 *Cell lines*

HeLa cell line: HeLa-Kyoto cell line (HeLa cell hereafter), a human cervical cancer cells used in my project was kindly provided by Dr. Diana Papini from Prof. Jonathan Higgins's Lab.

HT 29 cell line（originated from human Caucasian colon adenocarcinoma); **A549 cell line** (originated from human lung cancer); **MCF-7 cell line** (originated from human Caucasian breast adenocarcinoma cancer cell); **U2OS cell line** (originated from human osteosarcoma cancer) were kindly provided by Dr. Yan Zhao from the Northern Institute for Cancer Research (NICR), Newcastle University (UK).

Histone 2B-GFP HeLa cell line and a RPE1-MAD2-Venus cell line were kindly provided by Prof. Jonathan Pine's lab (CRUK).

p31^{comet} CRISPR/Cas9-KO HeLa cell line was kindly provided by Prof. Cheeseman's lab (MIT department of Biology, US).

2.1.2 *Solutions and chemicals*

Table 2.1 Solvents and detergents

Name of solution	***Code***	***Source***
Dimethyl sulfoxide (DMSO)	Sc-358801	Santa Cruz ((Dallas, Texas, USA))

Glycerol	G5516	Sigma-Aldrich (Dorset, UK)
Tween-20	Sc-2913	Santa Cruz (Dallas, Texas, USA)
Methanol	M/4000/17	Sigma-Aldrich (Dorset, UK)
Ethanol	E/06500DF/17	Sigma-Aldrich (Dorset, UK)
Triton-100	T8787	Sigma-Aldrich (Dorset, UK)

Table 2.2 Chemicals

Name of Chemicals	**Code**	**Stock concentration**	**Source**
Solid sodium chloride (NaCL)	7647-14-5	Storeas powder	Fisher-Scientific (Waltham,MA,USA)
Tris (hydroxymethyl) aminomethane	77-86-1	Store as powder	Fisher-Scientific (Waltham, MA, USA)
Nocodazole	M1404	10μg/ml in DMSO	Sigma-Aldrich (Dorset, UK)
Taxol	33069-62-4	10μM in DMSO	Sigma-Aldrich (St. Louis, MO, USA)
MAD2 inhibitor-1 (M2I-1)	GLXC-06307	10mM in DMSO	Sigma-Aldrich (St. Louis, MO, USA)
Reversine	C656820-32-5	1M in DMSO	Sigma-Aldrich (St. Louis, MO, USA)
Carbo-benzoxy-leucyl-leucyl-leucinal (MG132)	133407-82-6	10mM in DMSO	Sigma-Aldrich (St. Louis, MO, USA)
Leupetin	103476-89-7	10M in DMSO	Sigma-Aldrich, (St. Louis, MO, USA)
Thymidine	358801	2M in DMSO	Sigma-Aldrich, (St. Louis, MO, USA)
4′,6-diamidino-2-phenylindole (DAPI)	D9542	1:100 in water	Sigma-Aldrich, (St. Louis, MO, USA)
Doxycycline hyclate	D9891	1mg/ml	Sigma-Aldrich (St. Louis, MO, USA)
Cycloheximide	66-81-9	500μM in ethanol	Sigma-Aldrich, (St. Louis, MO, USA)
G418 disulfate salt	A1720	100mg/ml	Sigma-Aldrich (St. Louis, MO, USA)

Etoposide (VP-16)	E1383	10M in DMSO	Sigma-Aldrich, (St. Louis, MO, USA)
Paraformaldehyde	30525-89-4	3.7% in sterilized water	Sigma-Aldrich, (St. Louis, MO, USA)
Poly-D-lysine hydrobromide	P7405	0.1mg/ml in sterilized water	Sigma-Aldrich (St. Louis, MO, USA)
Ethylenediaminetetraacetic Acid (EDTA)	60-00-4	0.25M in sterilized water	Sigma-Aldrich (St. Louis, MO, USA)
Bovine Serum Albumin (BSA)	Sc-2323	5% (v/v) in sterilized water	Santa Cruz (Dallas, Texas, USA)
Anaphase Promoting Complex Inhibitor (APCin)	1-444	5mM in DMSO	Boston Biochem (Cambridge, MA,USA)
Tosyl-L-arginine methylester(TAME)	sc-207949	5mM in DMSO	Santa Cruz (Dallas, Texas, USA)

2.1.3 *Buffers*

1x PBS (Phosphate Buffer Saline) buffer

Prepared from 10 x PBS (Phosphate Buffer Saline，D1408, Sigma-Aldrich,UK) stock solution using steriliseddeionised water (H_2O) in 1:9 dilution accordingly.

1x PBST

1x PBS containing 0.1% Tween-20 or 0.2% triton X-100

Duolink in situ proximity ligation assay (PLA) washing Buffer A

0.01 M Tris pH 7.4, 0.15 M NaCL, 0.05% Tween 20

Filter the buffer through a 0.22 m filter and store at 4℃oC for use.

Duolink in situ PLA washing Buffer B

0.2 M Tris pH 7.5, 0.1 M NaCL

Filter the buffer through a 0.22 m filter and store at 4ºC for use.

1x protein sample loading buffer

2% SDS, 5% β-mercaptoethanol, 60 nM Tris (pH 6.8), 0.01% Bromophenol Blue, 10% glycerol

1x MOPS protein gel running buffer

50 mM MOPS, 50 mM Tris base, 0.1% SDS, 1 mM EDTA, pH 7.7

1x Western blot transfer buffer:

25 mM Tris base, 190 mM Glycine, 20% Methanol

NETN cell lysis buffer

50 mM Tris/HCL pH7.6, 150 mM NaCL, 1 mM EDTA, 0.5% NP40

1x Protease inhibitor cocktail

The original 10x Protease inhibitor cocktail was purchased from Sigma-Aldrich (p8340), and diluted in lysis buffer before prior the use.

50x TAE (Tris-Acetate-EDTA) buffer

2 M Tris base, 1 M Acetic acid, 50mM EDTA

The pH was adjusted to 8.5 with an appropriate amount of NaOH solution, and the buffer autoclaved before use.

6x DNA loading buffer

10 mM Tris-HCL (pH 7.6), 0.03% Bromophenol Blue, 0.03% xylene cyanol FF, 60% glycerol, 60 mM EDTA

LB agar medium

10g NaCL, 10g tryptone, 5g yeast extract, 20g agar

Dissolved in de-ionised H_2O and the volume adjusted to 1L.

The pH was adjusted to 7.0 with an appropriate amount NaOH solution, and the solution stored for use after being autoclaved

1x Odyssey blocking solution

Odyssey blocking solution (from LI-COR Biosciences UK) was diluted with 1xPBS in 1:1 ratio prior of the use.

2.1.4 *Antibodies*

Table 2.3 The list of primary antibodies

Antibody name	Type	Code	Dilution	Source
Anti-MAD2	Mouse monoclonal	Sc-47747	IF: 1:250 WB:1:500	Santa Cruz (Dallas, Texas, USA)
Anti-MAD2	Rabbit, Polyclonal	BL-1461	IF: 1:250 WB:1:500	Santa Cruz (Dallas, Texas, USA)
Anti-MAD2	Rabbit, Polyclonal	A310-082 A	IF: 1:250 WB:1:500	Bethyl (Dallas, Texas, USA)
Anti-full length MAD2	Rabbit, Polyclonal	PRB-452 C	IF: 1:250 WB:1:500	Convance (London,UK)
Anti-p55/CDC20 (E-7)	Mouse, monoclonal	Sc-13162 L	IF: 1:250 WB:1:500	Santa Cruz (Dallas, Texas, USA)
Anti-CDC20	Rabbit, Polyclonal	Ab26483	IF: 1:250 WB:1:500	Abcam (Cambridge, UK)
Anti-phosphohistone3 S-10	Rabbit, Polyclonal	06-570	WB:1:1000	Millipore, UK
Anti-pericentrin	Rabbit, Polyclonal	Ab 4448	IF: 1:500	Abcam (Cambridge, UK)
Anti-cyclin B1 (GNS1)	Mouse, monoclonal	SC-245	IF: 1:250 WB:1:500	Santa Cruz (Dallas, Texas, USA)
Anti-cyclin B1 (H-433)	Rabbit, Polyclonal	Sc-752	IF: 1:250 WB:1:500	Santa Cruz (Dallas, Texas, USA
Anti-p31^{comet} (Anti-MAD2L1BP)	Rabbit, Polyclonal	Ab150363	IF: 1:250 WB:1:2000	Abcam (Cambridge, UK)
Anti-β-Actin (C4)	Mouse, monoclonal	Sc-47778	WB:1:1000	Santa Cruz (Dallas, Texas, USA
Anti-MCL-1 S-19	Rabbit, Polyclonal	Sc-819	WB:1:500	Santa Cruz (Dallas, Texas, USA

Anti-GAPDH	Rabbit, Polyclonal	Ab9485	WB:1:2000	Abcam (Cambridge, UK)
Anti-GAPDH	Mouse, monoclonal	Ma5-15738	WB:1:2000	ThermoFisher Scientific (Waltham, MA, USA)
Anti- Caspase-3 (E-87)	Rabbit, Polyclonal	Ab32351	WB:1:1000	Abcam (Cambridge, UK)
Anti-GFP	Rabbit, Polyclonal	Sc-8334	WB:1:500	Santa Cruz (Dallas, Texas, USA
Anti- H2AX S-139	Rabbit, Polyclonal	Ab-2839	IF: 1:250	Abcam (Cambridge, UK)
GFP-Trap A geta-20	Rabbit, Polyclonal	70112001A	WB:1:500	ChromoTek (NY, USA)
Anti-BID FL-195	Rabbit, Polyclonal	Sc-11423	WB:1:500	Santa Cruz (Dallas, Texas, USA
Anti-BIM H-5	Rabbit, Polyclonal	Sc-374358	WB:1:500	Santa Cruz (Dallas, Texas, USA
Anti-NOXA FL-54	Rabbit, Polyclonal	Sc-30209	WB:1:500	Santa Cruz (Dallas, Texas, USA
Anti-PUMA G-3	Rabbit, Polyclonal	Sc-374223	WB:1:500	Santa Cruz (Dallas, Texas, USA

IF: Immunofluorescence staining, WB: Western blotting.

Table 2.4 The list of secondary antibodies

Antibody name	Type	Code	Dilution	Source
IgG-H+L (DyLight 488)	Goat polyclonal to rabbit	ab96899	1:1000	Abcam (Cambridge, UK)
IgG-H+L(FITC)	Goat polyclonal to mouse	ab6785	1:1000	Abcam (Cambridge, UK)
IgG-H&L (Cy5)	Goat polyclonal to rabbit	ab6564	1:1000	Abcam (Cambridge, UK)
IgG-H&L (Cy3)	Goat polyclonal to mouse	ab97035	1:1000	Abcam (Cambridge, UK)
IRDye 680	donkey anti–rabbit	926–322227	1:2000	Li-COR Biosciences (Lincoln, Nebraska, USA)
IRDye 800CW	donkey anti–mouse	926–32212	1:2000	LI-COR Biosciences (Lincoln, Nebraska, USA)

2.1.5 *PLA regents*

Duolink *in situ* PLA probe anti-rabbit PLUS (DUO92002), Duolink *in situ* PLA probe anti-mouse-MINUS (DUO92004), Duolink *in sit*u Detection regents including the blocking solution, ligation solution (5x), amplification solution (5x), ligase (A42012), polymerase (A42013) were all purchased from and distributed by Sigma-Aldrich.

2.1.6 *Plasmid DNA transfection regents*

Plasmid DNA transfection was performed using the Lipofectamine^{TM}3000 kits (TheromoFisher Scientific, UK). This kit includes p3000^{TM} regent and Lipofectamine^{TM} 3000 regent.

2.2 Methods

2.2.1 *Cell culture*

Normally, cells (besides the p31^{comet} CRISPR/Cas9-KoHeLa cell line) were grown in 75cm^2 flasks with complete medium (Dulbecco's modified Eagle's medium-DMEM) containing 1% non-essential amino-acids (Sigma-Aldrich), 1% L-glutamine (Sigma-Aldrich), 10% fetal bovine serum (Sigma-Aldrich), 1% penicillin/streptomycin (Sigma-Aldrich) at 37ºC and 5% CO_2 in a humidified incubator and maintained under standard processes. The complete DMEM medium was renewed and cells were split every 2-3 days, when the cell population reached 60-80% confluence, to maintain the appropriate cell density. The routine process includes removing the media first from the culture flask and washing the cells with 5ml pre-warmed 1xPBS briefly, then the cells were treated with 3-5ml pre-warmed trypsin (Sigma Aldrich) at 37℃, 5% CO2, for 3 minutes to detach the cells from adhering to the bottom of the flask. This is followed by the addition 6 ml complete DMEM media to terminate the trypsin activity. 5ml of this cell culture solution was then removed and replaced with 11ml fresh complete media and the cells were maintained at 37ºC, 5% CO_2 in an incubator for use.

For the culturing of the p31^{comet}CRISPR/Cas9-KoHeLa cell line, the cells were either grown in doxycycline free complete medium (Dulbecco's modified Eagle's medium-DMEM) containing 1% non-essential amino-acids, 1% L-glutamine, 10% tetracycline free fetal bovine serum, 1% penicillin/streptomycin for routine maintenance, or treated with an appropriate amount of doxycycline in complete medium as indicated to induce the knockdown/depletion of the endogenous p31^{comet} expression.

2.2.2 *Coverslips preparation*

10mm diameter round bioscillate glass coverslips (VWR. Leuven, Belgium) were sterilized by immersing in 100% ethanol for 5 minutes and left on a paper towel in a TC hood to dry, and were then Poly-lysine treated to enhance cell adherence, this was conducted by soaked these coverslips in 100µg/ml Poly-lysine (Sigma-Aldrich) for 5minutes before being allowed to dry for 2 hours on a paper towel. An individual coverslip was then placed into each well of a 24-well culture plate (Santa Cruz) before transfer of the designated cells for cell culture.

2.2.3 *Cell fixation*

For the PLA assay to detect *in vivo* protein-protein interactions in cells, the cells were grown on 10mm coverslips in wells of a culture plate as described above. The medium was gently aspirated using an appropriate pipette and the cells were washed twice with 1ml 1xPBS, and then fixed with 1ml pre-cold (-20℃) methanol fixation solution for 15minutes at room temperature before they were kept at -20℃ for use.

For conventional immunofluorescence, the cells were placed on 10 mm coverslips in the wells of a 24 or 96 well plate with a clear glass bottom under appropriate culture condition as described before. At the end of the designated time intervals, the medium was aspirated gently using an appropriate pipette and the cells were washed twice with 1ml (for each well of the

24-wells plate) or 200µl (for each well of the 96-wells plate) of 1x PBS, then replaced with 1ml (for 24-wells plate) or 200µl (for 96-wells plate) of 4% paraformaldehyde and left for 15 minutes fixation at room temperature. After this, cells were washed three times with 1xPBS, and replaced with 1ml or 200µl pre-cold (-20℃) methanol respectively and kept at -20℃ for use.

2.2.4 *Using Duolink PLA to detect in vivo CDC20-MAD2 interaction*

The cold-methanol fixed cells on coverslips were transferred into wells of a 12-wells culture plate (one coverslip per well), the cells were rehydrated and permeabilized with 0.2% PBST for 6 minutes, and washed with 1xPBS for 5 minutes, followed by steps described below.

Two steps blocking: Firstly, the cells were incubated with an appropriate amount of a blocking solution (5% BSA in 1xPBS) for anti-pericentrin antibody staining at room temperature for 15 minutes; and then the cells were treated with 20µl/per coverslip commercial PLA blocking solution (from Duolink kit) at room temperature for 10 minutes.

Primary antibodies staining: After thorough removal of the PLA blocking solution using a clean strip of waterman paper (GE Life sciences, Little Chalfont, UK), 25µl of the anti-CDC20 mouse antibody (Santa Cruz, Sc-13162L) and the anti-MAD rabbit antibody (Santa Cruz, BL-1461) in PLA diluent in 1:250 dilution was applied onto each of coverslips, and the cells were incubated at 37ºC for 120 minutes or overnight at 4ºC.

Secondary antibody staining: After incubation, the cells on the coverslips were washed with buffer A (3x5 minutes) with gentle agitation; and then the solution was removed and the coverslips dried using a strip of waterman paper before applying the secondary antibodies. The 15µl of the Duolink *in situ* PLA probe containing the anti-rabbit PLUS (DUO92002) (1:500 dilutions) and anti-mouse-MINUS (DUO92004) secondary antibodies (1:500 dilutions)

in PLA diluent were applied onto each of the coverslips to detect the primary antibodies. This was then incubated at 37ºC for a further 60 minutes.

Ligation and amplification process: After the above treatment, the cells on the coverslips were washed with buffer A (3x 5 minutes) with gentle agitation, and were then incubated with 15µl per-coverslip of the ligation solution (this is available from the commercial kit) for 30 minutes at 37ºC. The cells were then washed with buffer A (2x2 minutes) with gentle agitation before 15µl amplification solution per-coverslip was applied and the coverslips were incubated at 37ºC for 120 minutes. This was followed by washing the cells twice with buffer B (2 minutes each) with no agitation.

To determine the cell stages, the cells were additionally stained with an anti-pericentrin antibody to highlight the centrosome morphologies and DAPI to highlight the DNA morphologies. Briefly, 20µl of the pericentrin antibody (Ab4448, Abcam) diluted 1:500 dilution in PLA diluent was applied onto each coverslip. The coverslips were then incubated at 37ºC for 120 minutes. After washing with 1xPBS(3x 5 minutes), 20µlsecondary antibody (goat anti-rabbit Dylight 488nm antibody, 1:500 dilution) containing DAPI (1:3000) in PLA diluent was applied onto each of the coverslips and incubated at 37ºC for 60 minutes. The coverslips were washed with 1xPBS three times and then transferred onto a paper towel for air dry. This was followed by mounting with 50% glycerol PBS solution.

2.2.5 *Conventional immunofluorescence staining*

For testing a specific protein expression profile from individual cells, conventional immunofluorescence (IF) was used. Briefly, a sample of the permeabilized cells on a coverslip was washed with 1xPBS and blocked with 5% BSA (Bovine Serum Albumin) containing 0.2% triton X-100 for 30 minutes at room temperature. The cells were then incubated with 20µl primary antibody per coverslip (1:500 dilution in 5% BSA-PBS) at 37ºC for 120 minutes. The cells were washed with 1xPBS three times (5 minutes for each) and this was followed by

incubation with secondary antibodies (Cy5 or Cy3) at 37^{o}C for 60 minutes. After which the coverslips were washed with 1xPBS three times (5 minutes for each) and air-dried before mounted with 50% glycerol-PBS mounting solution and stored for use.

2.2.6 *Coverslips Mounting*

After the coverslip was air-dried on a piece of blue roll paper, it was mounted on a microscope slide (Academy Science, Beckenham, UK) with 5µl 50% glycerol-PBS mounting solution and sealed with nail polish. The sample in wells of a 96-wells plate was directly mounted by addition of 100µl 50% glycerol to cover the cells.

2.2.7 *Confocal microscopy*

The stained and mounted cell samples were scanned with Leica TCS SP2 confocal laser scanning microscope system using the HCX APO CS 40x 1.25 oil objective lens. Different lasers with specific wavelengths of 405nm UV laser, 488nm argon laser, 558nm laser, 594nm helium laser and 650nm laser were used to detect the DAPI, FITC (or GFP), Cy3, TexasRed (signal of the PLA complex) and Cy5 fluorescent signals respectively. Sequential scanning protocol was used to avoid bleed-through interference between channels; and a Z-stack scanning setting with the distance of 0.3µm between sections was used to cover and collect the data to represent the maximum fluorescent intensity of an entire cell volume for calculation and comparison. These Z-stack images were projected to produce a single image and used for assay.

2.2.8 *Quantification of the fluorescent signals*

The fluorescence intensity either representing an entire cell volume from the projected images or a selected region of interest from a specific section of a Z-stack image was quantified. ImageJ and photoshop software were used to measure and edit the images respectively. In this project, the average fluorescent intensities are represented by the arbitrary unit of the average of intensities of the fluorescent signals in the areas of interest.

2.2.9 *Western blotting and immunodetection of protein levels*

Sample preparation: To harvest cells from different experimental conditions, the culture medium containing any cells that have already detached from the bottom of the flask/well and are floating in the solution were collected into a 15ml Falcon tube. Those cells attached to the bottom of flasks or wells from each group were then washed with 1xPBS, followed by incubation with 1ml trypsin at 37^{o}C for 2 minutes to detach the cells. These newly suspended cells were collected and combined with the cells in the appropriate Falcon tube that had previously been collected. This suspension of cells was centrifuged at 1300 rpm and 4^{o}C for 4 minutes, and the supernatant carefully removed and discarded. The cell pellet was washed with cold 1xPBS twice and re-suspended in NETN lysis buffer on ice for 30 minutes to lyse the cells. The lysed sample was centrifuged at 15000 rpm at 4^{o}C for 15 minutes and the supernatant was transferred into a fresh 1.5ml Eppendorf tube.

The measurement of a protein concentration: The protein concentration was measured using the Bradford assay (Bio-Rad). The Bio-Rad reagent (Cat. #500-0006) was diluted in water in a ratio of 1:5. 1ml BSA protein standard solutions were prepared in the range of 0 to 50µg/ml (I used 0 µg/ml, 5 µg/ml, 10 µg/ml, 15 µg/ml, 20 µg/ml, 25 µg/ml in my experiments) diluted in 1:5 Bio-Rad regent. 5µl of an unknown concentration protein sample was mixed with 995µl diluted Bio-Rad regent (dilution factor 1:200). All the solutions were incubated at room temperature for 5 minutes respectively before their individual absorbance at 595nm was read using a calibrated Spectra Max M3. The final protein concentration of the individual samples was then calculated.

Protein sample denaturing: For preparing samples for SDS-PAGE, an appropriate amount of 5xSDS sample loading buffer was mixed with the samples so as to reduce the concentrations to that of 1xSDS loading buffer and the samples were denatured by incubation at 95^{o}C for 10 minutes.

SDS-PAGE and western blotting: 30-60µg protein samples as described above were loaded and ran on a pre-cast RunBlue Bis-Tris gel (NBT 01012, Expedeon). A 12% gel was used to detect caspase-3 (for detecting the small molecular weight fragments of cleaved caspase-3), and a 10% gel was used to detect other proteins. Proteins were separated using constant voltage at 180-200v with 1x Tris-MOPS-SDS running buffer (NXB75500, Expedeon the composition of this is described in 2.1.2) for about 1 hour. Subsequently, proteins separated from this SDS-PAGE gel were transferred onto an appropriate piece of 0.2µm reinforced nitrocellulose membrane (Schleicher & Schuell) at 80mA in 1x transfer buffer (its composition described in 2.1.2) for about 2 hours. The nitrocellulose membrane was cut to contain the region of the protein of interest and blocked with the odyssey blocking solution at room temperature for 60 minutes to reduce the non-specific background.

Immunoblotting and fluorescent detection of the protein bands: After blocking**,** the nitrocellulose membrane was incubated with specific primary antibodies in odyssey blocking solution (in 1:500-2000 dilutions depending on the individual quality of the antibody used) at 4^{o}C overnight or at room temperature for 120 minutes. Followed by washing for three times 5 minutes in 0.1% PBST. The membrane was then incubated with corresponding secondary antibodies of donkey anti-rabbit IRDye 680 or donkey anti-mouse IRDye 800CW (Invitrogen, 1:2000 dilutions in blocking solution) for 60 minutes at room temperature. After being probed with the secondary antibodies, the membrane was washed with 0.1% PBST three times again, and the fluorescent signals of protein bands of interest were detected by a CCD scanner (Odyssey, LI-COR Bioscience). ImageJ software was used to quantify the intensities of the bands. The average intensity of each band was normalized by the average intensity of the

corresponding loading controls either revealed by a β-Actin or a GAPDH band where appropriate.

2.2.10 *Co-immunoprecipitation for detecting the in vivo interaction between CDC20 and MAD2*

The RPE1-MAD2-Venus cells were grown in 60mm dishes to 80% confluence and were treated for 16 hours with either 60ng/ml nocodazole, or 60ng/ml nocodazole combined with 50μM M2I-1 respectively. The cells were then collected after trypsin treatment and centrifuged at 1300rpm and 4℃ for 4 minutes. The cell pellets were washed with an appropriate amount of cold 1xPBS and were lysed in 300μl NETN lysis buffer (10mM Tris-HCL pH7.5, 150mM NaCl; 0.5mM EDTA; 0.5% NP-40 containing 1x Protease Inhibitor Cocktail) on ice for 30 minutes. The supernatants were transferred into fresh 1.5ml tubes after being centrifuged at 15000 rpm and 4ºC for 15 minutes. The protein concentration of each sample was measured and adjusted to about 1μg/ml using the lysis buffer. 50μl of the supernatant was kept as the pre-IP sample after being mixed with an equal volume of a 2x sample-loading buffer. A slurry of GFP-Trap-A beads was washed and equilibrated with the dilution buffer (NETN buffer free of NP-40) three times. 25μl of these beads were then added to the remaining supernatant and incubated at 4ºC for one hour with end-to-end gentle rotation. After the incubation, samples were centrifuged at 2500xg for 2 minutes at 4ºC to pellet the GFP-Trap-A beads. 50μl of the supernatant was removed and mixed with an equal volume of 2x sample loading buffer and kept as the supernatant after IP (SN sample). The pellets of the GFP-Trap-A beads were washed three times with the cold dilution buffer, and then re-suspended in 100μl 2x SDS sample loading buffer used as the IP samples. All of the samples were heated at 95ºC for 10 minutes to denature the proteins before being used for western blot analysis.

2.2.11 *Nikon AIR fully automated high-speed confocal image system for live cell imaging*

The histone 2B-GFP HeLa cells were grown and treated with drugs either as described previously or in next section. Time-lapse images of the cells were recorded for 24 hours with a time interval of 5 minutes using a Nikon AIR fully automated high-speed confocal image system at 37ºC provided with 5%CO_2 and appropriate humidity. The GFP fluorescence at 488nm and DIC images were acquired throughout the time course, and the images were processed, analysed and quantified using NIS elements, ImageJ and Adobe Photoshop software.

2.3 Drug treatments

For the in vivo comparison of PLA signals of the CDC20-MAD2 complex or cyclin B1 in individual cells: HeLa cells were grown on coverslips in wells of a 24-wells plate for 24 hours to 60-80% confluence, and then each group of the cells were treated with either 0.5% (v/v) DMSO or 50μM M2I-1 in 0.5% DMSO for 16 hours. The treated cells were fixed with pre-cooled methanol for PLA analysis.

For the western blot assays the expression profiles of CDC20 and MAD2: HeLa cells were grown in 6-wells plates for 24 hours to 60-80% confluence, and then each group were treated with either 0.5% (v/v) DMSO or 50μM M2I-1 in 0.5% DMSO for 16 hours. Cells were harvested and prepared for western blot analysis as described before.

Double thymidine treatment for synchronization of cells in S phase: HeLa cells were treated with 2mM thymidine (Sigma) for 18 hours, and then released into an appropriate amount of fresh medium for 8 hours, followed by a second round of blocking with 2mM thymidine for another 16 hours. The cells were then released into an appropriate amount of fresh medium. It is generally thought that these synchronized cells would stay in S phase for 6-8 hours, and that subsequently they would enter mitosis.

For the evaluation of the PLAs of the CDC20-MAD2 complex after cell treated with MPS1 inhibitor: HeLa cells were grown on coverslips in 24-wells plate for 24 hours to 30-40% confluence. After being synchronized in S phase by double thymidine (DT) block-release treatment, the cells were released for 7 hours from the second DT blocking and were then treated with either 0.5% DMSO (v/v) or 0.5μM Reversine in 0.5% DMSO for 1.5 hours, and then by either 0.5% DMSO with 10μM MG132, or 0.5μM Revesine with 10μM MG132 in 0.5% DMSO for another 3 hours to prevent mitotic slippage. The cells were fixed by pre-colded methanol as described before for PLA analysis.

For the co-immunoprecipitation assay of the in vivo interactions between CDC20 and MAD2: The RPE1-MAD2-venus cells were grown in 60mm^2 dishes overnight to 60-80% confluence, and the cells were then treated with either nocodazole (60ng/ml) or nocodazole (60ng/ml) combined with M2I-1 (50μM) for 16 hours. The cells were harvested and lysed for the co-immunoprecipitation analysis as described before.

For assessing the expression of p31^{comet} in different cell lines after nocodazole treatment: HeLa, MCF-7, A549, HT29, and U2OS cells were placed 6-wells plate for 24 hours to 60-80% confluence, and then treated with either DMSO (0.5% in v/v) or nocodazole (60ng/ml) for 16 hours . The cells were harvested and prepared for western blotting as describe before.

For assessing the specificity of an anti-p31^{comet} antibody: The p31^{comet} CRISPR/Cas9-KO HeLa cells were grown in wells of a 6-wells plate and treated with two different concentrations of doxycycline (1μg/ml and 10μg/ml respectively) for 3 days, and a set of untreated cells was used as the control. The cells were harvested and lysed for western blotting as described before.

For assessing the molecular mechanism that underlies the accumulation of p31^{comet} in response to nocodazole treatment: HeLa cells were synchronized in S phase by double

thymidine block-release treatment. After incubation for 6-8 hours in fresh medium from the second block, the cells were treated with one of 60ng/ml nocodazole, 60ng/ml nocodazole combined with 10μM cycloheximide, or 60ng/ml nocodazole combined with 10μM MG132 and 10μM cycloheximide for 6 hours. After the treatment, the cells were harvested and lysed for western blotting as described before.

For assessing the dynamic expression profile of p31^{comet} in cells after released from mitotic arrest: HeLa cells were grown in a 75cm^2 flask and were treated with 60ng/ml nocodazole for 16 hours, and the mitotically arrested cells were shaken off the flask and briefly washed with 1xPBS and then were placed into fresh medium in 6-wells plates. The cells were harvested at 0 and 3 hours respectively and the cell lysates were prepared for western blotting as described before.

For assessing the involvement of the proteasome in the potential proteolysis of p31^{comet}: The mitotically arrested cells resulting from nocodazole treatment as described above were either placed into fresh media containing 10μM MG132, or media containing 100mM leupeptin and incubated for 3 hours. The cells were then harvested, and the cell lysates prepared for blotting as described before.

For assessing cell death in different cell lines: HeLa cells or cells from MCF-7, A549, HT29, U2OS cell lines were grown in wells of a 24-well plates for 24 hours to 60-80% confluence, and the cells treated with M2I-1 (50μM), nocodazole (60ng/ml), Taxol (30nM), nocodazole (60ng/ml) or Taxol (30nM) combined with M2I-1(50μM) in 0.5% DMSO, and 0.5% DMSO alone for 16 hours respectively. Images of the cells were taken after the treatments using a digital camera mounted on a tissue culture microscope (using a 20x objective lens) and used for analysis of cell death determined by typical apoptotic-like cell morphologies. At the same time, the cells were harvested, and cell lysates were prepared for western blot analysis to examine the expression levels of cyclinB1, MCL-1, MCL-1s, Bim, Bid, Puma, Noxa,

phosphorylated histone H3, Caspase-3 and PARP-1. Some of the cells were fixed for the analysis of the formation ofγ-H2AX foci by immunofluorescent staining.

2.4 Knocking down genes by siRNA

HeLa cells were seeded in the wells of a 6-wells plate and were grown in antibiotic free medium before they were transfected with a specific siRNAof interest using the DharmaFECT system (Dharmacon) according to the manufacture's protocol. Briefly, 10µl siRNA (5µM stock) and 5µl DharmaFECT regent were separately mixed with 190µl Opti-MEM (serum and anti-biotic free medium) respectively and incubated at room temperature for five minutes. These solutions were then mixed together and kept at room temperature for 20 minutes. After this, the siRNA mixtures were individually transferred into and mixed with 2ml antibiotic free medium and used to replace the culture medium in the wells of the plate. The cells were incubated in the presence of the specific siRNA for 72 hours. If required, the cells would be re-transfected with the same amount of siRNA as described above and the culture left for an additional 24-48 hours where appropriate. The cells were harvested, and samples were prepared accordingly for analysis.

Table 2.5 The oligo dimers used for siRNA transfections

Name of the siRNA	Company	Product code	Sequence or description
APC3	ThermoFisher Scinetific	s2759	CDC27hs validated Silencer®Select siRNA
APC3	GE Healthcare UK	M-003229-03-0005	siGENOME Human CDC27 (996) siRNA- SMARTpool
Cullin-1	ThermoFisher Scinetific	s228373	CUL1hs Silencer®Select siRNA
Cullin-1	GE Healthcare UK	L-004086-00-0005	ON-TARGETplus Human CUL1 (8454) siRNA -SMARTpool

CDC20	GE Healthcare UK	M-003225-05-0005	siGENOME Human CDC20 (991) siRNA- SMARTpool

2.5 Constructing the pCMV-6-AN-mGFP-MCL-1 and pCMV-6-AN-mGFP-MCL-1s plasmid DNA

The original pcDNA3-flag-MCL-1L and pcDNA3-flag-MCL-1s (human) were kindly provided by Professor Jeehyeon Bae's lab at Chung-Ang university of South Korea. The plasmids details are shown in figure 2.1.

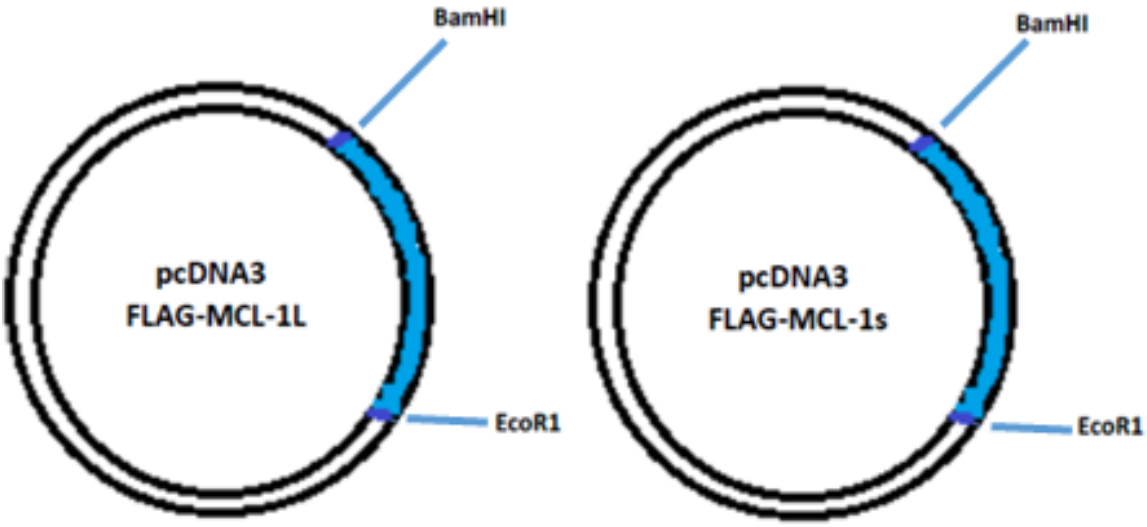

Figure2.1:The schematic of the original pcDNA3-flag-MCL-1L and pcDNA3-flag-MCL-1splasmid.

The cDNA sequence of MCL-1 or MCL-1s (highlighted in blue) is inserted into the mammalian expression vector of pcDNA3-FLAG between the BamH1 and EcoR1 restriction sites as indicated. The plasmid DNA of pcDNA3-FLAG-MCL-1(s) is ampicillin resistance.

2.5.1 *The plasmid DNA purification.*

The original pcDNA3-flag-MCL-1L and pcDNA3-flag-MCL-1s plasmid DNA were transfected and amplified in NOVA Blue competent cells. Briefly, 1µl of the original plasmid DNA was transfected into 50µl NOVA blue competent cells in a round-bottom falcon tube and left on ice for 30 minutes. The cells were then heat-shocked by placing the tube at 42ºC for 45 seconds in a water bath. The tube with the competent cells were left on ice for 2 minutes then added to 950µl of LB culture medium and left to incubate at 37ºC for 1 hour. The culture mixture was transferred into a 1.5ml Eppendorf tube and centrifuged for 1 minute at 5,000 rpm to collect the cells. The NOVA blue cells were resuspended in 250µl LB culture medium, 200µl of this cell mixture was spread onto a pre-warmed LB-agarose plate containing 100 mg/ml ampicillin, and the plates were then left upside-down at 37ºC overnight. The next day, single positive colonies were selected using sterilized tooth-picks and cultured overnight in 5ml LB medium containing 100µg/ml ampicillin with vigorous shaking at 37ºC.

After being grown overnight, the plasmid DNA was purified using a PureYield^{TM} plasmid miniprep system (A1223, Promega). Briefly, 600µl of the bacterial mixture was transferred into a 1.5ml micro-centrifuge tube, and 100µl of cell lysis buffer (blue) was added and mixed by inverting the tube 6 times. 350ml of cold (4-8ºC) neutralisation solution was added and mixed thoroughly by inverting. The lysis mixture was centrifuged at 15000 rpm for 3 minutes, and 900µl supernatant was transferred into a PureYield^{TM} minicolumn without disturbing the cell debris in the pellet. The column was centrifuged at 15000 rpm for 30 seconds. The flow-through was discarded and the minicolumn was placed into a fresh collection tube. 400µl Column Wash Solution (CWC) was applied to the column and the column was centrifuged at 15000 rpm for 30 seconds. The minicolumn was then transferred into a clean 1.5ml microcentrifuge tube, and 30µl of nuclease free water was added before the column was centrifuge at 2500xg for 30 seconds to collect the plasmid DNA. The concentration of the collected plasmid DNA was determined before it was stored for later use.

2.5.2 *The PCR amplification of MCL-1 and MCL-1s cDNA*

The purified plasmid DNA of pcDNA3-FLG-MCL-1 and pcDNA3-FLG-MCL-1s was used as the DNA template for PCR of MCL-1 and MLC-1s cDNA fragments to incorporate an Sgf1 restriction enzyme site at the 5' end of the sequence and a Mul1 restriction enzyme site at the 3' end of thesequence and the PCR fragments of the Sgf1-MCL-1(s)-Mul1 were subsequently subcloned into a mammalian expression vector, pCMV6-AN-mGFP, at Sgf1 and Mul1 sites. The processes were conducted in collaboration with and the pCMV6-AN-mGFP vector was provided by Dr. Paul Jowsey from The Medical Toxicology Centre, Institute of Cellular Medicine, NIHR Health Protection Research Unit, Newcastle University.

The primer pair used for **MCL-1 PCR:**

5'-GAATTCGCGATCGCCATGTTTGGCCTCAAAAGAAACGC

3'-GAATTCACGCGTTCATCTTATTAGATATGCCAAACC

The primer pair used for **MCL-1s PCR:**

5'-GAATTCGCGATCGCCATGTTTGGCCTCAAAAGAAACGC

3'-GAATTCACGCGTTCACAGTAAGGCTATCTTATTAGATATGC

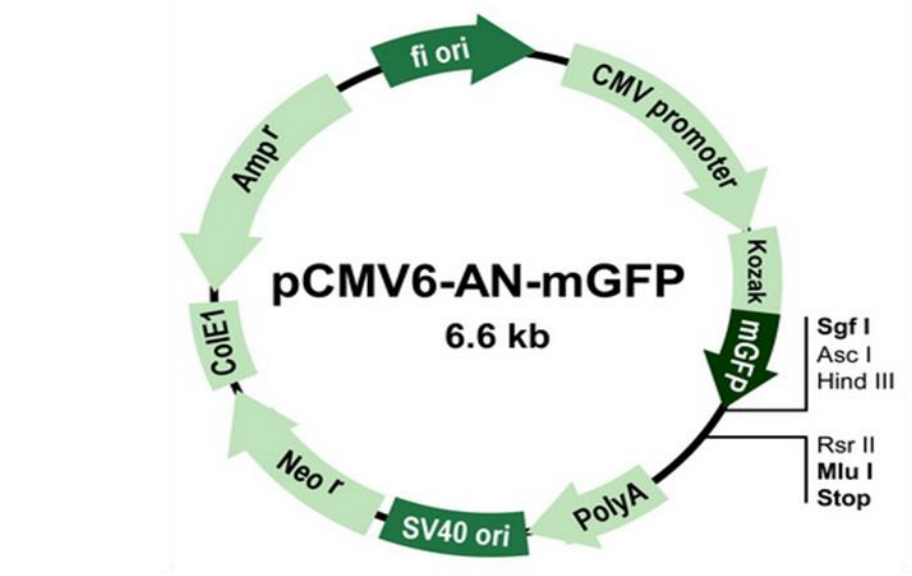

pCMV6-AN-mGFP

EcoR I BamH I Kpn I RBS Kozak Consensus mGFP Tag

CTATAGGGCGGCCGGGAATTCGTCGACTGGATCCGGTACCGAGGAGATCTGCCACC ATG AGC GGG GGC --- ---

M S G G - -

Sgf I Asc I Hind III Rsr II Mlu I

--- --- GGA CTC AGA GCG ATC GCCGGCGCGCCAGATCTCAAGCTTAACTAGTTAGCGGACCG ACG CGT TAA

- - G L R T R Stop

Not I Xho I Pme I Fse I

GCGGCCGCACTCGAGGTTTAAACGGCCGGCCGCGG

Figure 2.2: The schematic of the pCMV6-AN-mGFP expression vector and its multiple sub-cloning sites.

The pCMV6-AN-mGFP vector expresses the GFP as a tagged protein flanked with the C-terminal of the inserted protein. mGFP is an improved variant of GFP. The mGFP possesses bright green fluorescence with excitation and emission maxima at 483nm and 506nm respectively.

2.5.3 *The verification of pCMV6-AN-MCL-1-mGFP and pCMV6-AN-MCL-1s-mGFP plasmid DNA by agarose gel electrophoresis after restriction enzyme digestion*

The pCMV6-AN-MCL-1-mGFP and pCMV6-AN-MCL-1s-mGFP plasmid DNA was digested with the restriction enzyme Not1 as it has a unique restriction site in the MCL-1/MCL-1s cDNA sequence and a unique site in the multi-sub-cloning site of the vector

as shown in Figure 2.2. Briefly, 0.5-1µg (about 5µl) of the purified plasmid DNA was digested in 20µl reaction mixture containing 1µl Not1, 2µl 10x digestion buffer, and mixed with 12µl sterilized water, and incubated at 37^{o}C for 2 hours. The mixture was loaded into the wells of a 0.8% agarose gel after mixing with an appropriate amount of 5x DNA loading buffer. The digested DNA fragment was separated under a constant 200 volts along with a 1kb DNA ladder to determine the size of DNA fragments. The DNA bands were visualized using ethidium bromide under UV light and photographed with a gel documentation system (BioGene BV2040). The result is shown in Figure 2.3.

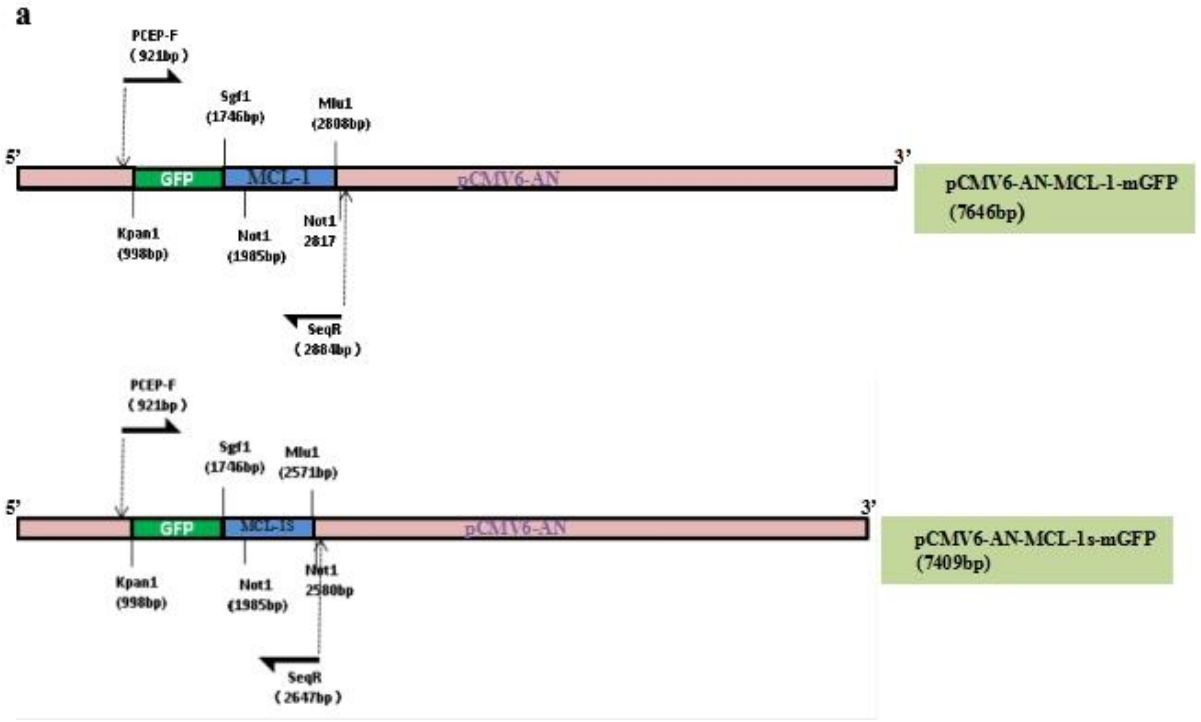

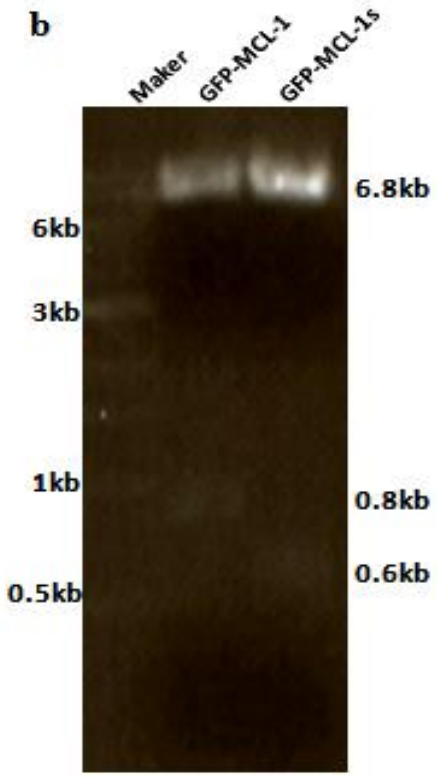

Figure 2.3: The schematic diagram of restriction enzyme sites of pCMV6-AN-Mcl-1-mGFP and pCMV6-AN-Mcl-1s-mGFP DNA, and the DNA fragments found after digestion by restriction enzyme Not1.

a. The graphic maps of pCMV6-AN-MCL-1-mGFP and pCMV6-AN-MCL-1s-mGFP with the restriction enzyme sites of Kpan1, Sgf1 and Mul1 highlighted and with the nucleotide positions in the plasmid indicated (to scale). Not1 restriction enzyme at 231bp from the 5' end of MCL-1 and the existing Not1 in the multi-sub-cloning sites of the vector behind the Mul1 at the 3' end of the MCL-1/1s were used to verify the DNA constructs. The positions of the primer of 'pCEP-F' (forward) and designed 'SeqR' (reverse, 5'ATCCCTGTGACCCCTCCCC3') for sequencing are highlighted with semi-arrows. The expected DNA fragments after the digestion with Not1 of pCMV6-AN-MCL-1-mGFP are 0.8kb and 6.8kb and for pCMV6-AN-MCL-1s-mGFP are 6.8kb and 0.6kb respectively. b. After being digested by Not1, the samples were run on a 0.8% agarose gel with 1xTAE running buffer at 200 volts for 25 minutes. There is a high molecular weight band of around 7 kb and a 0.8kb band above the 0.5kb marker associated with the pCMV6-AN-MCL-1-mGFP (GFP-MCL-1) plasmid DNA digestion, and a band of around 6.8kb and another at roughly 0.6kb associated with the pCMV-AN-MCL-1s-GFP (GFP-MCL-1s) plasmid DNA digestion. These bands are consistent with the sizes of expected with the Not1 digestion as shown in a.

2.5.4 *The plasmid DNA sequencing.*

To further verify and confirm that there are no additional point mutations introduced into the GFP-MCL-1or MCL-1s DNA sequence of pCMV6-AN-MCL-1-mGFP and pCMV6-AN-MCL-1s-mGFP plasmid DNA by the PCR process each of the plasmid DNA samples and a home designed primer 'SeqR' were sent to Source Bioscience for DNA sequencing. The plasmid DNA was sequenced using pCEP-F and SeqR which starts at 921bp and 2884bp (2647bp for GFP-MCL-1s)（as shown in Figure 2.3a）respectively of pCMV-AN-mGFP vector: GGG GAG GGG TCA CAG GGA TG).

2.6 The transfections and expression of pCMV-AN-MCL-1s-GFP plasmid DNA in MCF-7 cells.

The plasmid DNA transfections were performed using Lipofectamine^{TM}3000 (Thermo Fisher Scientific, UK) according to the commercial protocol. Briefly, MCF-7 cells were grown in wells of a 6-well plate in an antibiotic free DMEM medium to 60% confluence. 2μg of pCMV6-AN-MCL-1s-mGFP plasmid DNA was diluted in 125μl Opti-MEM medium (antibiotic free and serum free medium) containing 5μl P3000^{TM}. At the same time, 5μl Lipofectamine^{TM}3000 regent was diluted in 125μl Opti-MEM medium. After 5 minutes incubation at room temperature, the two solutions were mixed together and kept at room temperature for 15 minutes. The solution containing the DNA lipid complex was then added to MCF-7 cells for incubation at 37℃ supplied with 5% CO2 for 24 hours before being replacing with fresh complete medium. The transfected cells were examined after 24 hours.

2.7 The verification of the role of MCL-1s in inducing cell death in the presence of nocodazole combined with M2I-1.

To test the role of MCL-1s in cell death induced by M2I-1 in presence of nocodazole, MCF-7 cells were transfected with pCMV6-AN-MCL-1s-mGFP plasmid DNA as described above. After 24 hours, the transfected MCF-7 cells were collected, split and placed into two wells of a 6-wells plate, and cultured at 37ºC, 5% CO2 for another 24 hours. The cells in the two wells were treated either with 60ng/ml nocodazole or 60ng/ml nocodazole combined with 50μM M2I-1 for 16 hours. The treated cells were harvested, and cell lysates were prepared for western blotting as described before.

2.8 Statistical analysis

The data from this study were analyzed using Graph-Pad Prism 7 and reported as means ± s.d produced from for at least three independent experiments unless stated otherwise. Before the *t*-test, the data distributions were first determined by the Kolmogorov-Smirnov test using Graph-Pad Prism7, only data where the distribution gave a $p > 0.10$ to indicate a normal distribution would then be used for statistical analysis by t-testing; any non-normally distributed data was analysed by ANOVA. The statistical tests used are indicated in the corresponding text and figure legends respectively. In both cases a p-value of 0.05 was determined to be significant.

Chapter Three: The kinetochore-dependent and independent formation of the CDC20-MAD2 complex and its function in HeLa cells

3.1 Introduction

The SAC maintains genome stability by generating an anaphase "wait signal" prior to the metaphase/anaphase transition in mitosis, to ensure the accurate segregation of the sister-chromatids. It was thought that unattached kinetochores were the sole source for the SAC inhibitory signals, as a single unattached kinetochore can produce sufficient signals to delay anaphase for several hours (Rieder et al., 1995). Several proteins such as MAD2, BUBR1, BUB3, and MPS1 have been identified as the essential components of the SAC. The mitotic checkpoint complex (MCC) is the predominant APC/C inhibitory signal responsible for SAC activity and comprises MAD2, BUB3, BUBR1 and CDC20 (Sudakin et al., 2001, Lara-Gonzalez et al., 2012). The molecular basis of this kinetochore-dependent formation of the MCC is partly illustrated by the "MAD2 template model", which suggested that kinetochores bound to MAD1 can recruit an open form of MAD2 (O-MAD2) and change its conformation to a closed form of MAD2 (C-MAD2). This C-MAD2 can then recruit another O-MAD2 and change its conformation to an intermediate form MAD2 (I-MAD2). As MAD1 and CDC20 have the same binding site on C-MAD2, this intermediate form of MAD2 somehow binds to CDC20 to create the CDC20-MAD2 sub-complex (Musacchio and Salmon, 2007, De Antoni et al., 2005, Lens et al., 2003). According to this model the SAC works like an "on" and "off" switch. However, this kinetochore-dependent "on" and "off" working model has been challenged by some contradictory findings, since the MCC or its sub-complex CDC20-MAD2 can still be detected when the essential kinetochore genes have been mutated (Klebig et al., 2009, Poddar et al., 2005) or isolated from interphase cell extracts before the formation of kinetochores (Sudakin et al., 2001). Evidence also suggests that the SAC activity depends on the amount of the MCC formed and its strength is controlled like a rheostat, rather than in an "on" and "off" manner (Collin et al., 2013). It has also been shown that a nuclear

pore component, Tpr protein, can facilitate the formation of the CDC20-MAD2 complex using interphase cell extracts (Lee et al., 2008, Schweizer et al., 2013). Therefore, whether the kinetochore is the exclusive platform for cascading the SAC inhibitory signal is still questionable and when and where the MCC is formed remains elusive.

To study the spatio-temporal assembly of the CDC20-MAD2 complex *in vivo* of cells, the lab has established previously the Duolink based proximity ligation assay (PLA) to detect the interaction of CDC20 and MAD2 in individual fixed HeLa cells using specific antibodies against CDC20 and MAD2 respectively (Please see material and methods for details). Duolink PLA can directly detect the protein-protein interaction in an individual cell when two proteins of interest either form a complex or are in close proximity less than 40nm (Soderberg et al., 2006, Jarvius et al., 2007, Gullberg et al., 2004). It avoids both biochemical extraction and overexpressing an exogenous fusion protein. The preliminary results show that the interaction between CDC20 and MAD2 is cell cycle regulated and displays a "Bell" shaped profile. The CDC20-MAD2 complex formation starts before nuclear envelope breakdown (NEBD) in prophase, peaks at prometaphase and begins to decline by metaphase (Figure 1.11 a, d & e). The fluorescent signals detected by PLA are specific to the selected antibodies as there were no detectable signals when the anti-MAD2 antibody was paired with a relevant random IgG or when the anti-CDC20 antibody was paired with a relevant random IgG antibody (Figure 1.11 b & c), which also was confirmed by the results that the depletion of CDC20 or MAD2 reduced the CDC20-MAD2 PLA signal (Figure 1.11 f, g, h, I&k). Based on the observations from the single cells, these results are surprising as： 1. The assembly of the CDC20-MAD2 complex occurs not in an 'on' and 'off' manner but in a 'bell' shape; 2. The accumulation of the CDC20-MAD2 complex is not only detected in prometaphase and metaphase cells, but also in various stages of prophase cells when the SAC is not supposed to have been turned on; 3. There is very little detectable interaction between CDC20 and MAD2 in interphase cells. 4. There are still detectable signals in anaphase cells though they are at a very low level.

This might provide new insight into the SAC mechanism in terms of MCC formation in mitosis. Duolink based *in situ* PLA uses two specific primary antibodies combined with the specific secondary antibodies (PLA probes) to target two proteins complex of interest, theoretically it can detect the complex signalling from two proteins of interest within a distance of 40nm close proximity without actual physical interaction. Therefore, if these PLA signals displayed in the Figure 1.11 would reflect the genuine interactions between CDC20 and MAD2 remain to be tested.

3.2 Objectives

3.2.1. Using two small molecules, M2I-1 (MAD2 inhibitor-1) and reversine (MPS1 inhibitor), to test the genuine physical interaction of CDC20-MAD2 revealed by the PLA approach shown in Figure 1.11.

M2I-1 is a small molecule that can disturb the *in vitro* interactions of CDC20 and MAD2 (Kastl et al., 2015); and reversine is a potent MPS1 kinase inhibitor, MPS1 is required for the assembly of the MCC (Maciejowski et al., 2010, Santaguida et al., 2010). Therefore, if the PLA signals displayed in Figure 1.11 reflect the genuine interactions between CDC20 and MAD2, we would anticipate that the fluorescent signals would disappear or be significantly reduced after treatment with either M2I-1 or reversine.

3.2.2. To investigate the physiological function of the prophase specific CDC20-MAD2 complex formed independent of the kinetochores.

As we have shown previously the accumulation of the CDC20-MAD2 complex is not only detected in prometaphase and metaphase cells, but also in various stages of prophase cells where the kinetochore has not yet formed, and the SAC is not supposed to have been turned on (Sudakin et al., 2001). Therefore, we will investigate any potential physiological functions by examining if this prophase CDC20-MAD2 complex could prevent the premature

degradation of cyclin B1 in the early prophase of HeLa cells using PLA and conventional western blot analysis.

3.3 Results

3.3.1 M2I-1 can disrupt the *in vivo* interaction of CDC20 and MAD2 and significantly reduces the PLA signals of the CDC20-MAD2 complex in HeLa cells

To test if the PLA signals shown in Figure 1.11 reflect a genuine interaction between CDC20 and MAD2, we used the MAD2 inhibitor M2I-1, a small chemical that has been shown to disturb the *in vitro* interaction between a recombinant CDC20 and full length MAD2 (Kastl et al., 2015). We first checked if it could also disrupt the *in vivo* interaction between CDC20 and MAD2. Cell extracts were prepared from a MAD2-Venus RPE1 cell line after cells were treated with either 60ng/ml nocodazole or 60ng/ml nocodazole combined with 50μM M2I-1, and these extracts were used for co-immunoprecipitation conducted with an anti-GFP antibody. Nocodazole is a well-established anti-mitotic drug used in cell biology to activate the spindle assembly checkpoint (SAC) and arrest cells in mitosis. Nocodazole is known to bind with high affinity to tubulin dimers and interfere with the polymerization of microtubules (Mollinedo and Gajate, 2003, Jordan et al., 1992, Modriansky and Dvorak, 2005). The western blot results (Figure.3.1) show that the GFP antibody has precipitated almost all the MAD2-Venus fusion protein. A proportion of the CDC20 was co-precipitated with MAD2-Venus from the cell extract where the cells were only treated with nocodazole, but there was still a substantial amount of CDC20 remaining in the supernatant (sample SN) after depletion. In contrast, there was no detectable CDC20 co-precipitated with MAD2-Venus from the samples of the cells treated with nocodazole combined with M2I-1. This indicates that M2I-1 can disrupt the interaction between CDC20 and MAD2 *in vivo*.

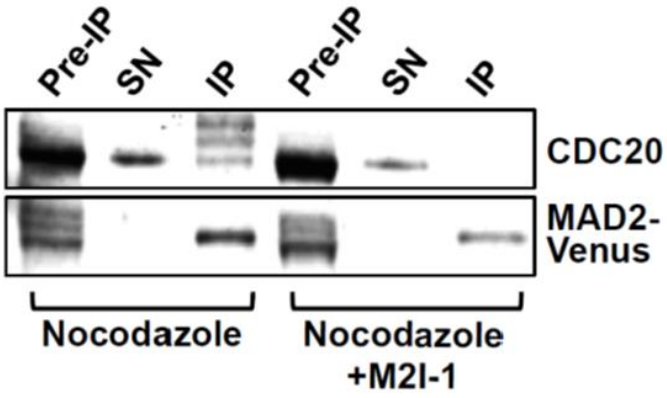

Figure 3.1: M2I-1 disrupts the interaction between CDC20 and MAD2 in vivo.

The MAD2-venus RPE1 cells were treated with nocodazole (60ng/ml) or nocodazole (60ng/ml) combined with M2I-1(50µM). A GFP-Trap kit was used to precipitate MAD2-venus from the cell extracts prepared from the treated cells. The specific anti-CDC20 and MAD2 antibodies were used to detect CDC20 and MAD2 protein bands on a western blot. Pre-IP: cell extracts before addition of GFP antibody beads, SN: supernatant after antibody depletion, IP: Samples prepared from the pellets of the immunoprecipitation.

As a result of this we anticipated that the PLA signals of the CDC20-MAD2 complex would decrease or disappear after treated with M2I-1 in HeLa cells if the PLA signals of the MAD2-CDC20 seen in Figure1.11 genuinely reflected the physical interaction of CDC20-MAD2. HeLa cells were treated with either 50µM M2I-1 or with 0.5% DMSO as a control for 16 hours (Kastl et al., 2015). The PLA was applied to detect CDC20-MAD2 interaction. The representative images at different cell cycle stages are shown in Figure 3.2a. From these, we found that the CDC20-MAD2 PLA signal decreased after M2I-1 treatment at various stages between early prophase and metaphase (Fig.3.2a). Quantitative data (Figure 3.2b) indicated that there was a 62.5% reduction in the average signal intensity of the CDC20-MAD2 complex in prophase cells, and collectively a 76.1% reduction in prometaphase and metaphase cells. This reduction in the signal seen with PLA is comparable to that shown *in vitro* by biochemical analysis where about an 86% reduction were seen using

recombinant proteins at the same concentration of M2I-1 (Kastl et al., 2015). Thus, the PLA signals are due to the interaction between CDC20 and MAD2 and the profile seen across the various stages of the cell cycle reflects its dynamic distribution.

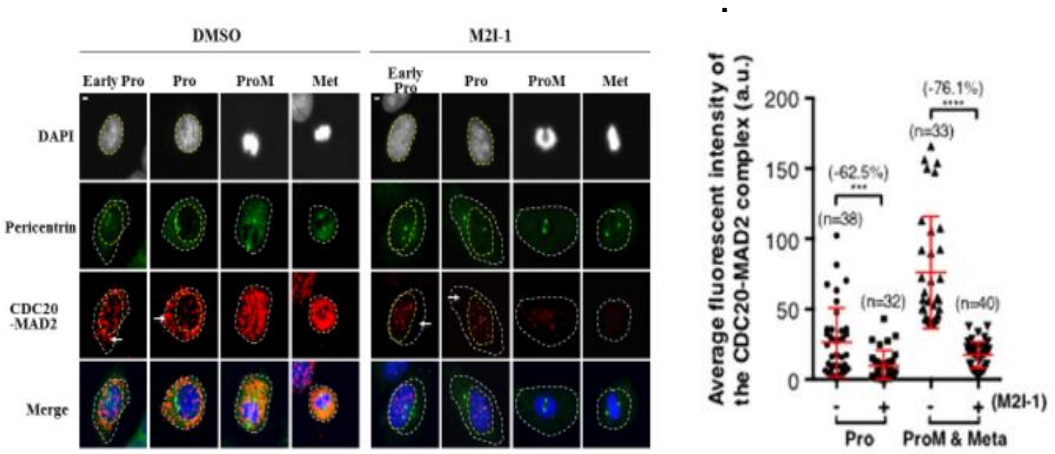

Figure 3.2: M2I-1 can significantly reduce the interaction between CDC20 and MAD2 revealed by PLA.

HeLa cells were treated with M2I-1 (50μM) in DMSO and DMSO (0.5%, v/v) respectively. The interactions of CDC20 and MAD2 were revealed by PLA in fixed cells. The projected Z-stack confocal images are displayed as indicated and ImageJ was used to quantify the average fluorescent intensities from the areas of interest. (a) Representative confocal images showing cells at early prophase (Early Pro), prophase (Pro), prometaphase (ProM), metaphase (Met), anaphase (Ana) and telophase (Telo). The cell cycle stages were determined by DNA morphology (DAPI staining in the top panel in grey and blue in the bottom panel), and the separation of the centrosomes (staining with pericentrin antibody in green on the second panel from top). The PLA fluorescent signals representing the CDC20-MAD2 complexes are displayed in red in the third panel from the top. The bottom panel shows the merged images. The white circle dash lines highlight the cell boundaries and the yellow circle dash lines highlight the nucleus. The arrows highlight the cytoplasmic or nuclear regions in cells at early prophase or prophase. The scale bar=5μm. (b) The average fluorescent intensities were quantified from cells at the indicated stages. A two-tailed unpaired t-test was used to assess the significance between two groups as indicated. Statistical significance was assigned where $p<0.05$ (**** $p< 0.0001$). Standard deviation bars are in red.

3.3.2 The M2I-1 induced reduction of the PLA signals of the CDC20-MAD2 complex is not due to decreased levels of CDC20 or MAD2 protein

Having established that M2I-1 can disrupt the interaction between CDC20 and MAD2 *in vivo*, and consequently reduce the PLA signals of CDC20-MAD2 complex in cells, we needed to determine whether the reduction in the PLA signal could result from decreased levels of either or both CDC20 and MAD2 by degradation or inhibition of the expression during M2I-1 treatment in HeLa cells. To test this, we examined the CDC20 and MAD2 levels after cells were treated by M2I-1 as described before, and the results are shown in Figure 3.3. There are no clear visible differences in the levels of CDC20 and MAD2 between the control (DMSO treated) andM2I-1 treated samples. Therefore, the observed reduction of the PLA signal of the CDC20-MAD2 complex resulted from the proteins not associating rather than reduced levels of these proteins.

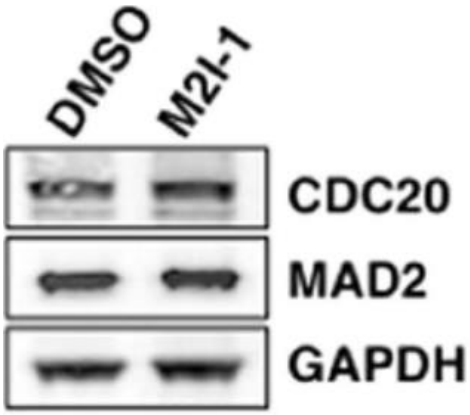

Figure 3.3: The levels of CDC20 and MAD2 remained stable after treated with M2I-1 in HeLa cells.

After HeLa cells were treated with DMSO (0.5%, v/v) and M2I-1 (50μM in 0.5% DMSO) under the same conditions as described before, the cell extracts were prepared for western blotting using a specific anti-CDC20 or MAD2 antibody, and an anti-GAPDH antibody. GAPDH bands were used as the loading control.

3.3.3 Inhibition of MPS1 kinase activity significantly reduced the PLA signals of CDC20-MAD2 complex

To further test that the PLA signals generated from the paired specific antibodies against CDC20 and MAD2 reflected the dynamic assembly of the CDC20-MAD2 complex, we have performed the PLA after the cells were treated with Reversine, a potent MPS1 kinase inhibitor (Maciejowski et al., 2010, Santaguida et al., 2010). MPS1 is also a SAC component and its kinase activity is known to be required for MCC formation, and the functions of most of the checkpoint proteins are dependent, directly or in directly on its activity (Liu and Winey, 2012). The PLA was performed after HeLa cells were treated with 0.5μM reversine together with 10Mm MG132 or MG132 alone in DMSO as the control. MG132 (carbobenzoxyl-L-leucyl-L-leucyl-L-leucinal), a known proteasome inhibitor will inhibit 20s proteasome activity to block protein degradation via ubiquitylation (Zhang et al., 2013, Kisselev and Goldberg, 2001, Genschik et al., 1998, Steinhilb et al., 2001). As a result this should prevent the degradation of CDC20 and the cell slippage, as the inhibition of MPS1 would sharply accelerate anaphase onset (Maciejowski et al., 2010, Santaguida et al., 2010). As shown in Figure 3.4a, the PLA signals of the CDC20-MAD2 complex deceased in cells treated with Reversine compared to the control cells. There was about a 50.4% reduction in the average intensity of the PLA signals (Figure 3.4b). The degree of the reduction is most likely linked to the level of the CDC20-MAD2 complex as it has been shown by co-immunoprecipitation that there was only approximately 50% reduction of MAD2 incorporated into the MCC after similar treatment in HeLa cells (Tipton et al., 2013). Thus, these results indicate that there is a direct correlation between MPS1 activity and the levels of the PLA signal, and it reflects the dynamic information about the CDC20 and MAD2 interaction *in vivo*.

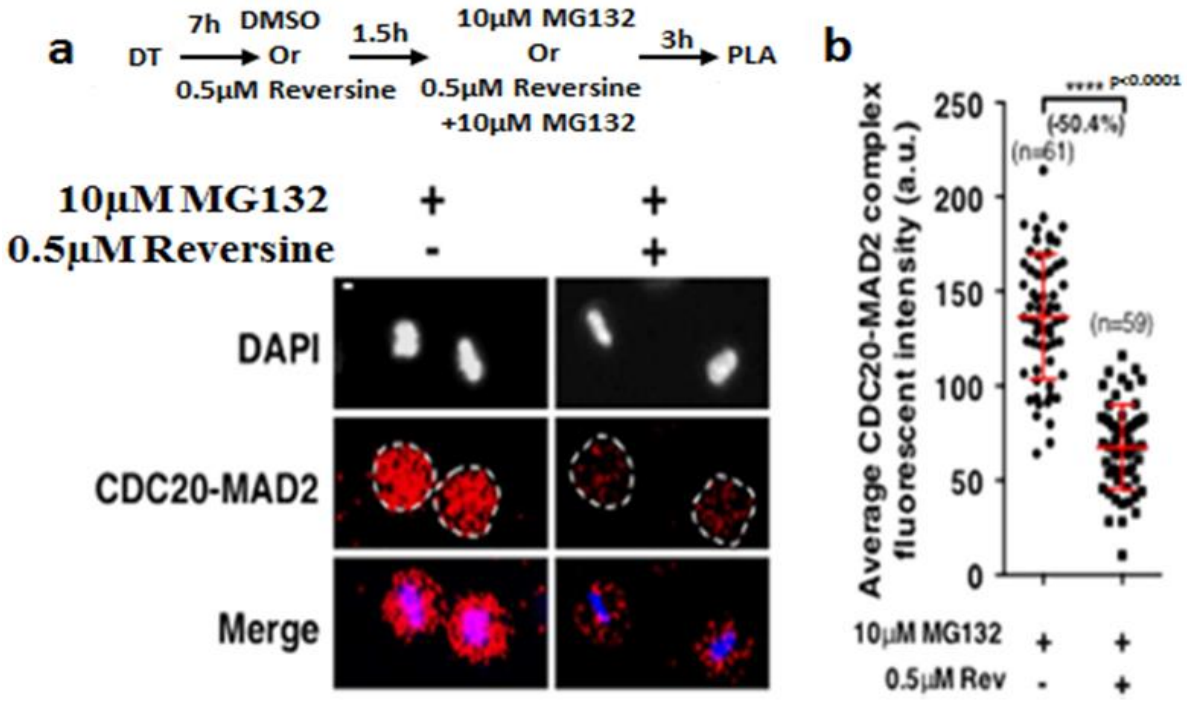

Figure 3.4: The inhibition of MPS1 activity induced reduction of PLA signals of CDC20-MAD2 complex.

After double thymidine block, cells were washed into fresh media for 7 hours before being treated with 0.1% DMSO or 0.5μM Reversine (in 0.1% DMSO) for 1.5h. This treatment was replaced by 10μM MG132 or 10μM MG132 combined with 0.5μM Reversine respectively for another 3 hours. Cells were fixed and the PLA signals of CDC20 and MAD2 complex detected using confocal system. The quantification of the average fluorescent intensities of the regions of interest was done using ImageJ software. (a) Representative confocal images showing the PLA signals under the two different experimental conditions. (b) The average PLA fluorescent intensities in arrested prometaphase and metaphase cells were quantified from the regions of interest encircled with the dash lines as shown in (a). Two-tailed uppaired t-test was used to assess the difference between the two groups as indicated, p value: ****p <0.0001. n: The total number of cells used for quantification. Scale bar = 5 μm.

3.3.4 M2I-1 induces premature degradation of cyclin B1

As these results have proved the PLA fluorescent signals detected using the specific antibodies against CDC20 and MAD2 reflect the actual dynamic assembly of the CDC20-MAD2 complex at different cell cycle stages (Figure1.11). When brought together

with other results from the lab that Tpr, one of the components of the nuclear pore complexes (NPCs), can specifically facilitate the formation of the CDC20-MAD2 complex in prophase cells independent of the SAC, and which has no effect on its formation in prometaphase and metaphase (Li et al., 2017), Our results suggested that there is a specific form of the CDC20-MAD2 complex which exists in the various stages of prophase as well as that seen in interphase cells (Sudakin et al., 2001). As it is generally believed that the SAC is activated at late prophase after nuclear envelope breakdown (NEBD) (Lara-Gonzalez et al., 2012), the assembly of this specific prophase CDC20-MAD2 complex might not be kinetochore dependent. However, whether these complexes are redundant or possess a function needs to be tested.

One of the important mitotic substrates of the APC/C is cyclin B1 regulated by the SAC (Huang and Raff, 1999, Clute and Pines, 1999). Cyclin B1 begins to express and accumulate in the cytoplasm of late G2 and early prophase cells (Fung and Poon, 2005, Ito, 2000), and the CDK1-cyclin B1 kinase activity is required for remodeling the morphologies of the chromosomes and microtubules and triggers the nuclear envelope membrane breakdown as the cell enters mitosis (Lindqvist et al., 2007, Jackman et al., 2003). Thus, cyclin B1 degradation must be prevented until late mitosis (Huang and Raff, 1999, Clute and Pines, 1999). We therefore, speculated that this prophase specific CDC20-MAD2 might also be required for protecting cyclin B1 from premature degradation in prophase.

As M2I-1 can disrupt the interaction between CDC20 and MAD2 *in vivo* (Figure.3.1& 3.2) and weakens the SAC in HeLa cells (Kastl et al., 2015), we anticipated that M2I-1 would cause the premature degradation of cyclin B1. To test this, HeLa cell were treated for 16 hours with either 0.5% DMSO, 50µM M2I-1, 60ng/ml nocodazole, and 60ng/ml nocodazole + 50µM M2I-1 (all in 0.5% DMSO) and then analyzed by western blotting. Results showed that cyclin B1 levels were significantly reduced in the samples treated with M2I-1 or M2I-1+ nocodazole (Figure. 3.5a, Lane 2 & 4) compared to the control sample (DMSO) (Figure.3.5a, lane 1) and the sample treated with nocodazole alone (Figure. 3.5a, lane 3). Cells after the

treatments with DMSO and M2I-1 were fixed with 4% paraformaldehyde and PLA stained with a pair of specific anti-cyclin B1 antibodies. Figure 3.5b shows representative confocal images allowing comparison of the levels of cyclin B1 at selected cell cycle stages. These results show that cyclin B1 was significantly decreased in all cells after treatment with M2I-1 compared to DMSO treated cells (Figure.3.5c). It can be clearly seen that the reduction in cyclin B1 not only occurred at prometaphase and metaphase but also in prophase cells (Figure. 3.5b&c). Quantitative results suggested that collectively there was a 76.5% reduction in the cyclinB1level in early prophase and prophase cells, and a 79.6% reduction from prometaphase and metaphase cells (Figure 3.5c).

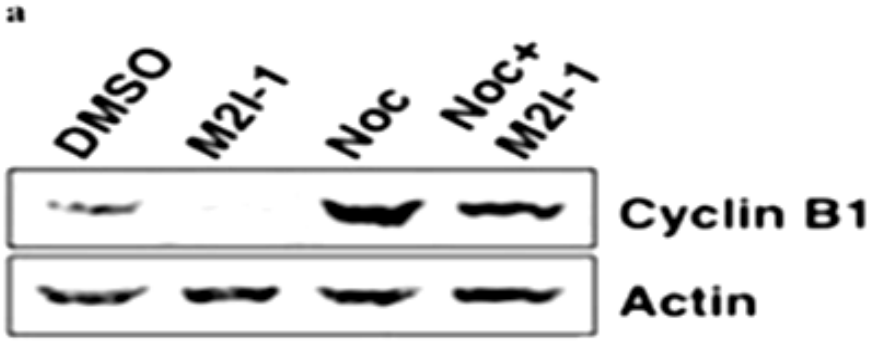

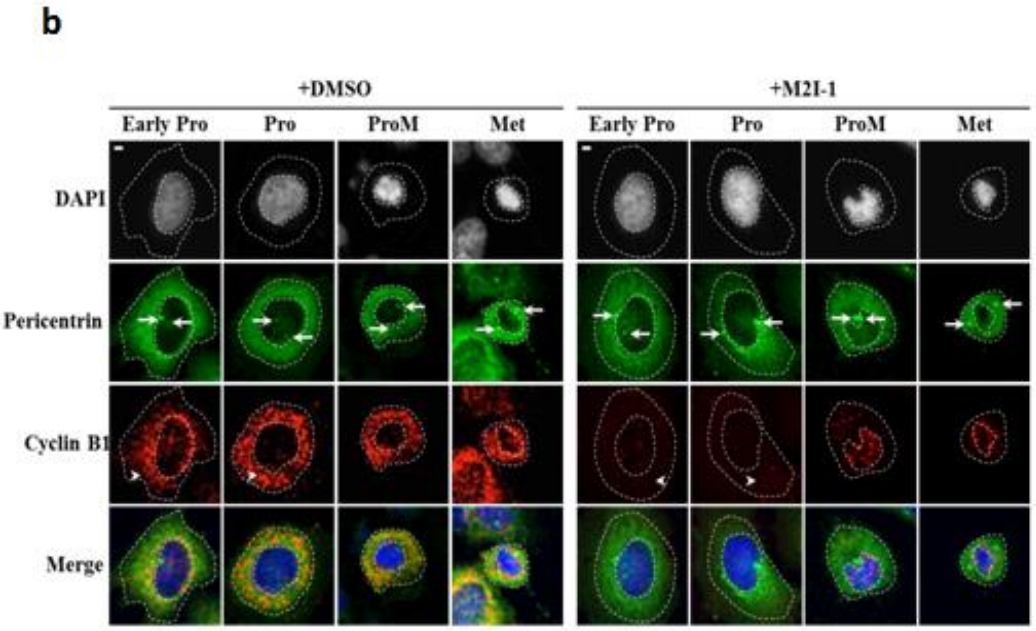

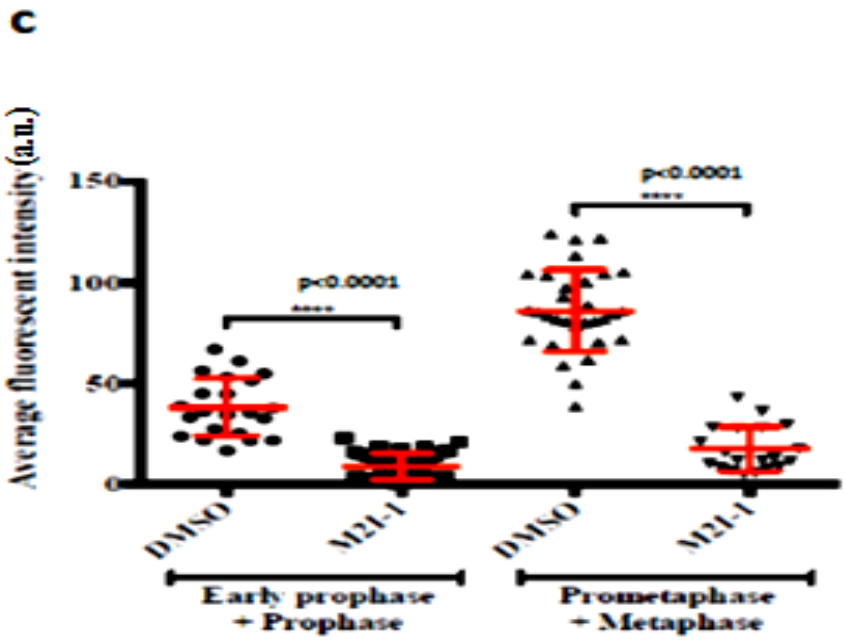

Figure 3.5: The comparison of the stability of cyclin B1 in HeLa cells after treatment with M2I-1.

(a). Cell extracts were prepared from HeLa cells after treatment with DMSO (0.5%), M2I-1 (50μM), nocodazole (60ng/ml) and nocodazole (60ng/ml) combined M2I-1(50μM) (all in 0.5% DMSO) for 16hours. Western blotting was conducted with an anti-cyclin B1 antibody (1:500 dilution). Actin bands were used as the loading control. **(**b). HeLa cells on coverslips were fixed after the treatment with 50μM M2I-1 or DMSO (0.5%, v/v) for 16 hours, and stained with a pair of cyclin B1 antibodies (anti-rabbit, H-433, Sc-752 and anti-mouse, GNS1, Sc-245) for PLA. The representative confocal images at different cell cycle stages are displayed. Cyclin B1 protein was detected in the cytoplasm of early prophase and prophase cells treated with DMSO (control, left panels), while none or very little cyclin B1 was detected in cells treated with M2I-1 at similar stages (right panels). Cell cycle stages were determined by DNA morphology (DAPI staining in grey in the top panel or in blue in the bottom panel) and centrosomes (staining with pericentrinin the second panel in green). The PLA cyclin B1 fluorescent signals were detected by TexasRed in the third panel (in red), the bottom panel shows the merged images. The white circle dash lines highlight the cell boundaries and the yellow circle dash lines highlighted the nucleus. Arrows highlighted the centrosomes. Arrowheads highlighted the cytoplasmic regions of early prophase or prophase cells. Early prophase: EPro, prophase: Pro, pro-metaphase: ProM, metaphase: Met. (c). The average intensities of fluorescent signals were quantified from cells at the indicated stages. A two-tailed unpaired t-test was used to assess the significance between two groups as indicated.

3.4 Discussion

As a surveillance control system, the spindle assembly checkpoint checks the status of chromosomal attachment at kinetochores by acting on the anaphase promoting complex/ cyclosome (APC/C). It prevents anaphase onset and premature chromosome segregation via its effector MCC (Musacchio, 2015). The MCC consists of two sub-complexes CDC20-MAD2 and BUBR1-BUB3; however, exactly how the MCC was formed is still not fully understood. The "MAD2 template" model has described the mechanism of the kinetochore-dependent dynamic recruitment of the SAC proteins and its facilitation on the formation of the CDC20-MAD2 complex. Somehow this CDC20-MAD2 subcomplex binds to the BUB3-BUBR1 complex to form the MCC (Lara-Gonzalez et al., 2012, Yu, 2006, De Antoni et al., 2005). This kinetochore-dependent MCC formation, however, might not be the only source of the MCC as it can be isolated from cell extracts of interphase HeLa cells (Sudakin and Yen, 2004, Chan et al., 1999). The CDC20-MAD2 and MCC complexes were still detectable in the absence of a functional kinetochore in the Ndc10 mutant of budding yeast (Poddar et al., 2005, Fraschini et al., 2001). However, it is equally questionable about the efficiency of the synchronization step applied for examining the interphase complex, based on the biochemical preparation (Dulla and Santamaria, 2011, Coquelle et al., 2006, Cooper, 2004, Urbani et al., 1995). Moreover, the existence of the CDC20-MAD2 or MCC complex *in vivo* has never been revealed in individual cell. Therefore, despite it playing a central role in SAC function, exactly how the MCC assembly is regulated in terms of the strength of the SAC in normal mitotic progression has yet to be determined.

PLA is one of a few widely used and commercially available methods for analyzing protein-protein interactions in their native state (http://www.olink.com/products/duolink/applications/protein-interactions). Duolink PLA technology makes use of two primary antibodies raised in different animal species to target two proteins of interest in fixed individual single cells. Species-specific secondary antibodies (PLA probes), each conjugated with a unique short oligonucleotide tail, bind to the primary antibodies. This fluorescent

signal can be detected and quantified based on microscopy images, for instance a laser scanning confocal system with appropriate excitation wavelengths. Therefore, the PLA can avoid biochemical extraction or the creation of exogenous over-expressed fusion proteins and can assign signals to specific subcellular locations. Using this technique the lab has previously demonstrated that the formation of CDC20-MAD2 complex is dynamically regulated in a bell-shaped manner in the unperturbed HeLa cell cycle. Only a basal level of the CDC20-MAD2 complex is detected in interphase and the complex accumulated from prophase onwards and peaked in prometaphase signals from the CDC20-MAD2 complex were still detectable in anaphase cells though the levels had declined significantly (Figure 1.11). However, theoretically the PLA probes can also detect two proteins of interest within a distance of 40nm of one another without actual physical interaction. Therefore, if the PLA signals displayed in Figure1.11 do reflect a genuine interaction between CDC20 and MAD2 needs to be tested.

In this study, by treating cells with two small molecules, M2I-1 and reversine, that disrupt the CDC20-MAD2 interaction (refs), we have proved that the PLA signals reflect the genuine profiles of the dynamic assembly of CDC20-MAD2 complexes at different cell cycle stages in single HeLa cells.

Chapter Four. The molecular basis of the potential degradation of p31^{comet} (MAD2L1BP) in HeLa cells

4.1 Introduction

As discussed in the introduction, p31^{comet} can delay mitosis exit by binding with MAD2 (Habu et al., 2002, Yang et al., 2007, Xia et al., 2004**).** Its overexpression increased the resistance to antimitotic drugs (Habu and Matsumoto, 2013) while depletion promotes sensitivity to antimitotic drugs (Ma et al., 2012). So studying it will improve our understanding of the molecular basis of mitotic cell death and adaption (Diaz-Martinez et al., 2014). The existing publications about the profile of p31^{comet} in the cell cycle contradict each other and are ambiguous, as some showed that expression of p31^{comet} increases in mitosis and is cell cycle regulated (Habu et al., 2002), but others showed that its levels remain constant throughout the cell cycle (Xia et al., 2004). The sequence analysis of p31^{comet} suggested that it contains several putative destruction motifs (Habu et al., 2002), which would be potentially targeted by the APC/C-dependent ubiquitin-mediated proteolysis. However, the turnover of p31^{comet} and its relevant physiological functions have yet to be characterized.

4.2 Objectives

4.2.1 To investigate and examine the expression profile of p31^{comet} throughout the cell cycle using a specific antibody and immuno-chemical analysis as well as by conventional biochemical approaches.

To achieve this, we would use immunofluorescent staining using a specific anti-p31^{comet} antibody to detect the dynamic expression and distribution patterns of p31^{comet} throughout the cell cycle of HeLa cells based on single cell analysis; and we will also use western blotting to study the dynamic stability of p31^{comet} at specific stages as well as being treated with various drugs.

4.2.2. To dissect the degradation mechanism of p31^{comet} using small interfering RNA and chemical inhibitors approaches.

It is well know that the ubiquitin-mediated degradation of the cell cycle regulators play essential roles in regulating the cell cycle transition at different stages(Choudhury et al., 2016). The Skp, Cullin, F-box containing (SCF) complex and the anaphase promoting complex or cyclosome (APC/C) are the two E3 ligases that are required for targeting specific substrates for degradation in the cell cycle with the SCF mainly targeting the substrates at G1/S and the APC/C mainly targeting the substrates in mitosis (Choudhury et al., 2016). As the sequence analysis of p31^{comet} has suggested that it contains several putative destruction motifs (Habu et al., 2002), which would be potentially targeted by the APC/C-dependent ubiquitin-mediated proteolysis. We will first look to see if p31^{comet} is a substrate of the proteasome by treating the cells with MG132, which is a potent, and cell-permeable proteasome inhibitor (Zhang et al., 2013, Kisselev and Goldberg, 2001, Genschik et al., 1998, Steinhilb et al., 2001). This will be followed by a comparison of the expression levels of p31^{comet} after transiently disrupting the functions of the APC/C or the SCF by using siRNA or chemical inhibitors.

4.3 Results

4.3.1 Testing the antibody specificity using a p31^{comet} CRISPR/Cas9-KO HeLa cell line

To verify the specificity of p31^{comet} antibody (purchased from Abcam, Ab150363) before using it for fluorescent staining and western blotting, we have tested the level of expression of p31^{comet} in a p31^{comet} CRISPR/Cas9-KO HeLa cells (a gift from Prof. Iain Cheeseman's lab), as the endogenous p31^{comet} can be knocked down by treatment with doxycycline (McKinley and Cheeseman, 2017). Cells were treated with two different concentration of doxycycline for 72 hours as indicated, and the cell extracts were prepared and subjected to western blot analysis with the antibody to p31^{comet}. The level of p31^{comet} is clearly reduced in all of the samples treated with doxycycline (Figure 4.1, lane 2 & 3) compared to the control (lane 1). The results also suggested that the effective depletion of p31^{comet} is somewhat dose dependent,

as the higher concentration of doxycycline induced a greater depletion of p31^{comet} (Figure 4.1, lane 2 & 3). Although, a complete knockdown of p31^{comet} was not achieved even using 10µg/ml of doxycycline, but the result is sufficient to prove that the Ab150363 p31^{comet} antibody specifically recognizes p31^{comet} though there is a strong non-specific band around 25KD. Therefore, there is a need to be cautious when interpreting results derived from the immunofluorescent staining.

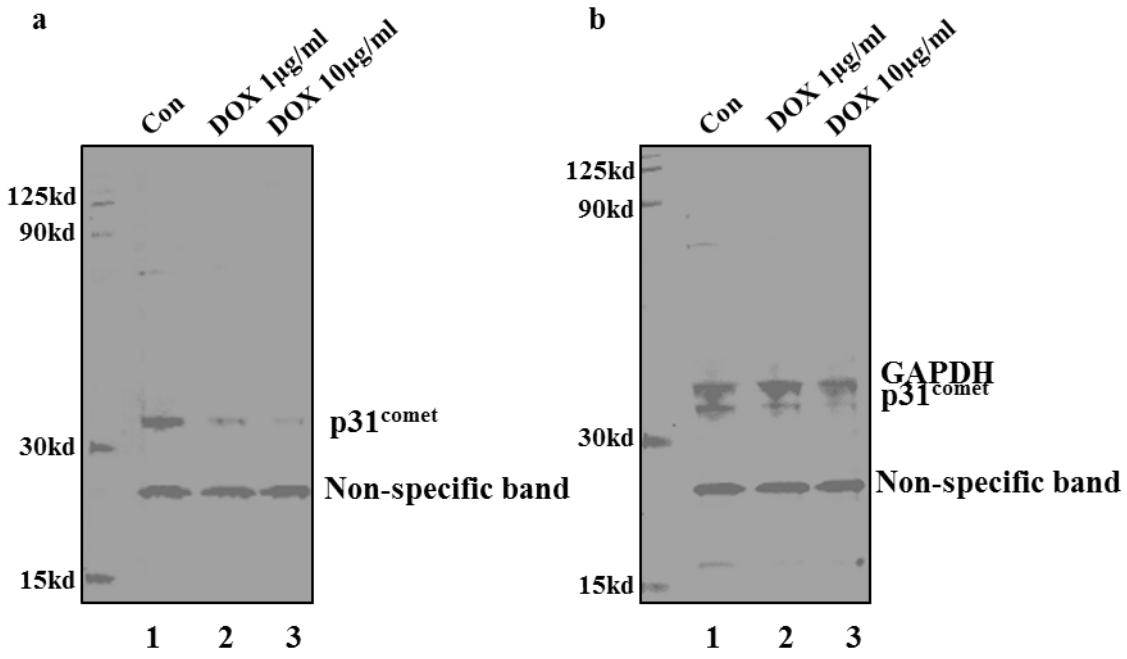

Figure 4.1: Testing the specificity of anti-p31^{comet} antibody (Ab150363) using p31^{comet} CRISPR/Cas9-KO cell line.

The p31^{comet}CRISPR/Cas9-KO line is a gift from Prof. Cheeseman's lab. Cells were treated with two concentrations of doxycycline, 1 µg/ml and 10 µg/ml for 72 hours, and a parallel-untreated cell sample was used as the control. Cell extracts were prepared for western blot analysis with the antibody to p31^{comet}. GAPDH bands were used as the loading control. Lane 1 (control); lane 2 and 3 were treated with 1µg/ml and 10 µg/ml of DOX (doxycycline) respectively.

4.3.2 The profile of p31^{comet} expression and localization in cell cycle

To examine the profile of endogenous p31^{comet} during the cell cycle, we used immunofluorescent staining to show the expression and distribution of endogenous p31^{comet} in fixed HeLa cells using the anti-p31^{comet} antibody from Abcam (Ab150363) although it also recognized a strong non-specific band at around 25KD (Figure 4.1). The results shown visually in Figure 4.2a and quantitatively in Figure 4.2b suggested that the p31^{comet} immunofluorescent signal is very low in interphase, starts to increase during prophase and peaks at pro-metaphase and metaphase and remained constantly high until telophase (Figure 4.2b). In prophase, the p31^{comet} is unevenly distributed in the nucleus and is partly localized around the nuclear envelope and is then distributed across the entire cell cytosol after prometaphase. This results partly agreed with previous reports that p31^{comet} increased as mitosis progressed (Habu et al., 2002). This preliminary result supports the idea that p31^{comet} might indeed be a cell cycle regulated turnover protein.

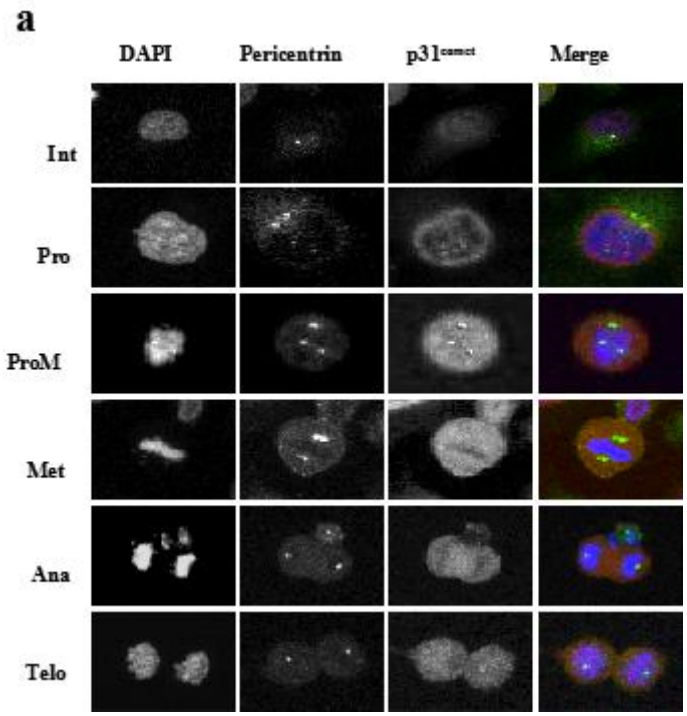

b

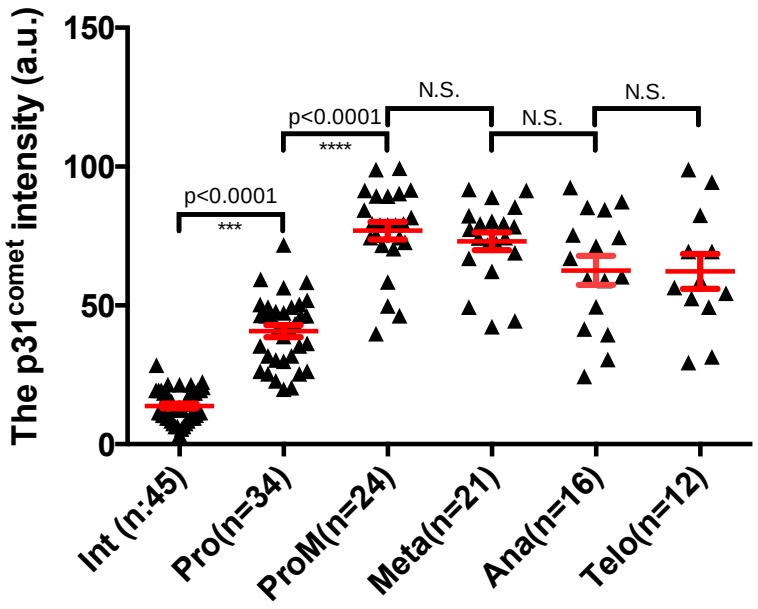

Figure 4.2: The endogenous p31^{comet} expression profile in unperturbed cell cycle of HeLa cells.

(a) Representative confocal images are shown from cells at different cell cycle stages as indicated at interphase (Int), prophase (Pro), prometaphase (ProM), metaphase (Met), anaphase (Ana) and telophase (Telo). Cell cycle phases were determined by DNA morphology shown by DAPI (in blue, and grey in the left first column) staining and the position of the centrosomes stained by pericentrin antibody in green (grey in the left second column) respectively. The p31^{comet} (Ab150363, Abcam) immunofluorescent signals are shown in red (grey in the third column), (b) The diagram showing the quantitative profile of p31^{comet} at different cell cycle stages. The average fluorescence intensity was quantified from individual cells using ImageJ software. Standard deviation bars are in red. The numbers of cell quantified in each cell cycle stage shown as n.

4.3.3 The accumulation of p31^{comet} in response to nocodazole treatment is a common phenomenon of the cancer cell lines examined in this project

p31^{comet} has been thought to cause the disruption or dissociation of the MCC thus silencing the SAC activity (Yang et al., 2007, Habu et al., 2002), and the overexpression of p31^{comet} can result in premature exit from mitosis (Habu et al., 2002). However, our preliminary results showed that p31^{comet} increased from prophase and peaked at prometaphase and metaphase,

and this temporal profile of p31^{comet} is inconsistent with its known functions. To confirm the increase of p31^{comet} during mitosis, we examined the level of p31^{comet} in nocodazole arrested HeLa cells, an anti-mitotic drug that can activate the SAC by depolymerising microtubules and arrest cell at prometaphase (Haraguchi et al., 1997, Rieder and Maiato, 2004). Results show that the level of p31^{comet} clearly increased after nocodazole treatment compared to the control (Figure 4.3a). The quantitative data indicated that cells treated with nocodazole had a p31^{comet} level of 108% compared to the control sample where the cells were only treated with DMSO (Figure 4.3b).

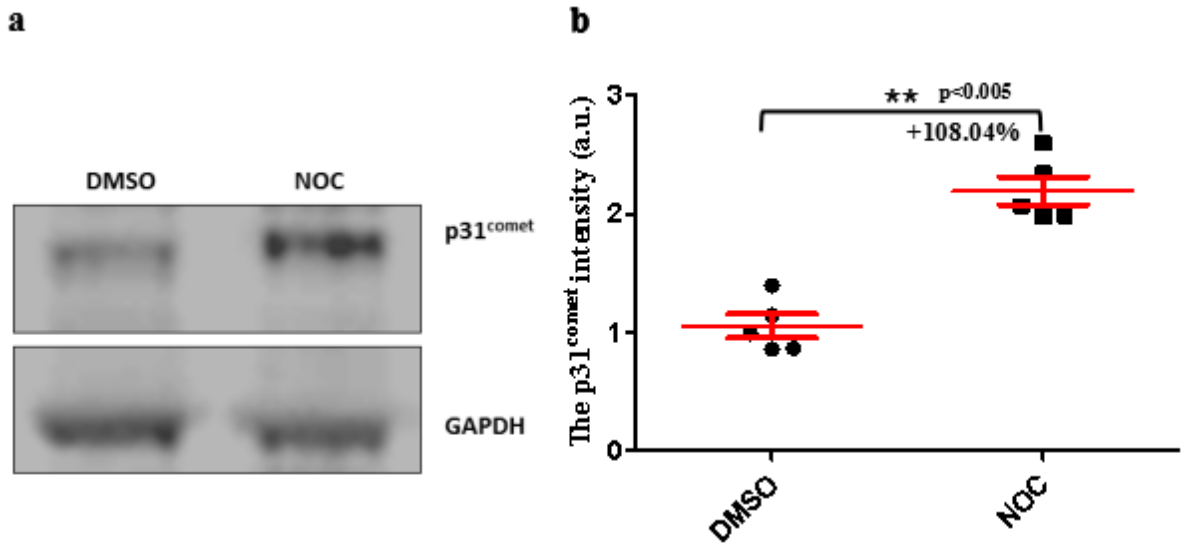

Figure 4.3: The level of p31^{comet} is elevated in HeLa cells after treatment with nocodazole.

Cell extracts were prepared from HeLa cells after treatment with 0.5% DMSO (control) and 60ng/ml nocodazole in 0.5% DMSO (v/v) for 16 hours respectively. (a) The samples of the cell extracts were run on a 10% precast Bis-Tris protein gel and the western blot membrane was probed with a specific anti-rabbit p31^{comet} antibody (Ab150363, Abcam) and an anti-GADPH antibody respectively. The bands of GAPDH were used as the loading control; (b) Quantitative comparison of the levels of p31^{comet} was produced from five independent experiments. Standard deviation bars are in red. The statistical analysis assigned the significance as: **p<0.005. +108.04% indicated that the increased level of p31^{comet} in nocodazole treating cells comparing to DMSO treating cells.

To verify whether the accumulation of p31^{comet} in response to nocodazole treatment is a common phenomenon of cancer cell lines, we then examined p31^{comet} in MCF-7, A549, HT29 and U2OS cancer lines using the same nocodazole treatment as described. Results indicated that the levels of p31^{comet} significantly increased in all cell lines after treatment with nocodazole (Figure 4.4). Thus, indicating that the increase in p31^{comet} in response to nocodazole treatment is a common phenomenon of cancer cell lines. Therefore, our immunofluorescent staining data showing high levels of p31^{comet} in unperturbed mitosis agreed with the biochemical results that the level of p31^{comet} will increase when the SAC is activated by nocodazole to arrest cells at prometaphase.

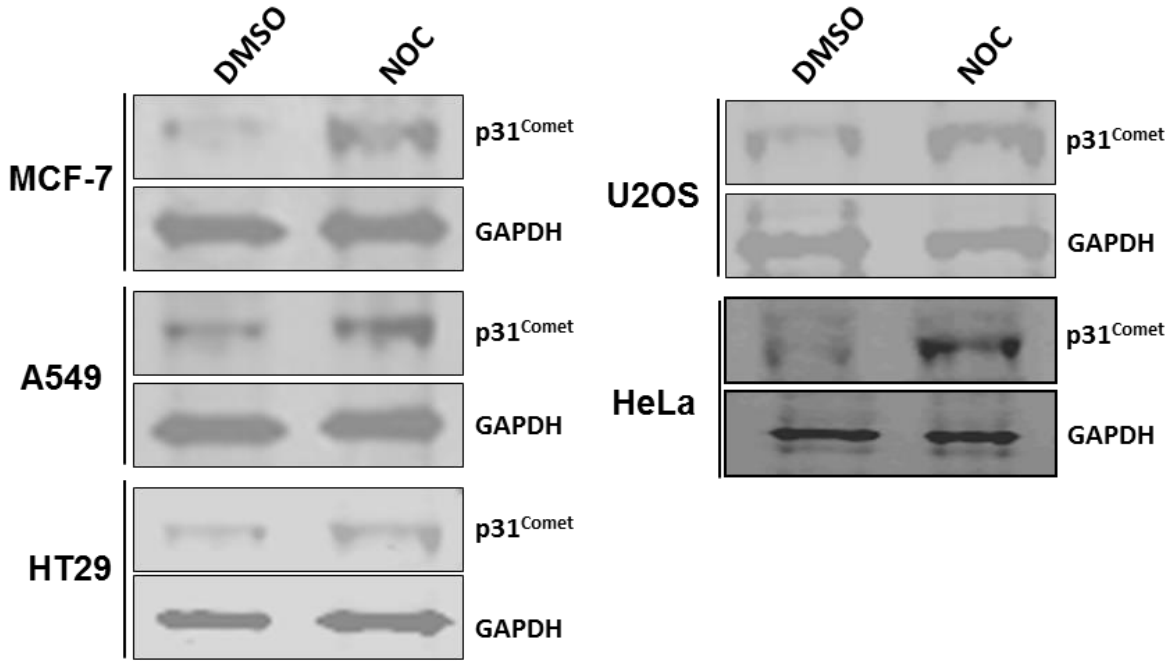

Figure 4.4: The elevated level of p31^{comet} in response to nocodazole treatment is a common phenomenon for different cancer cell lines under examination.

The cell extracts prepared from different cancer cell lines as indicated after treatment with 0.5% DMSO (control) and 60ng/ml nocodazole in 0.5% DMSO (v/v) for 16 hours. Samples were subject to western blot analysis. The western blot membrane was probed with anti-p31^{comet} antibody. GAPDH protein bands act as the loading control.

4.3.4 The accumulation of p31^{comet} in response to nocodazole treatment mainly resulted from its protein synthesis

Increasing protein synthesis or the blocking of protein degradation will both result in accumulation of protein at a particular stage in the cell cycle. To determine which of these causes the elevated p31^{comet} after nocodazole treatment, HeLa cells were treated with nocodazole, MG132 and cycloheximide under the conditions indicated (Figure 4.5). Cycloheximide is a protein synthesis inhibitor (Baliga et al., 1969, Ennis and Lubin, 1964, Dai et al., 2013, Schneider-Poetsch et al., 2010). Results showed that the cycloheximide blocked the accumulations of p31^{comet} in the presence of nocodazole (Figure 4.5, lane2), while the addition of MG132 could not restore p31^{comet} in the presence of cycloheximide (Figure 4.5, lane 3). Therefore, this suggests that protein synthesis is the main contributor to the accumulation of p31^{comet} in response to nocodazole treatment.

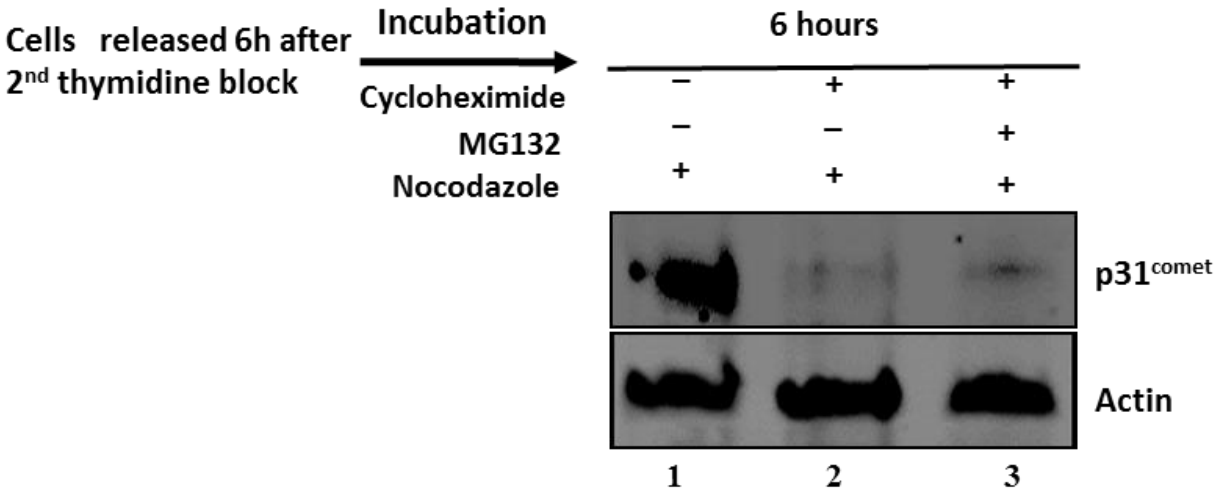

Figure 4.5: Cycloheximide can prevent the accumulation of p31^{comet} in mitotic arrested cells in the presence of nocodazole and MG132 respectively or both.

HeLa cells were released for 6 hours from a second thymidine block and were then treated with nocodazole, MG132, and Cycloheximide for another 6 hours in the combinations indicated. The cell extracts were prepared and subject to western blot analysis using a 10%

bis-tris SDS-PAGE gel and the western blot membrane was probed with an anti-p31^{comet} antibody. The actin bands acted as the loading control.

4.3.5 The elevated p31^{comet} in response to nocodazole caused arrest declined after cells exited from mitosis

Previous publications indicated that p31^{comet} was possibly destroyed after mitosis (Habu et al., 2002). In agreement with this, our preliminary immunofluorescent staining results also indicated that the p31^{comet} level in interphase is significantly lower than it is in other cell cycle stages (Figure 4.2). However, the interpretation of the immunofluorescent staining results was complicated by the antibody against p31^{comet} (Ab150363, Abcam) also recognizing a non-specific band at around 25KD. To further investigate this, nocodazole arrested HeLa cells were prepared, washed twice in fresh media and then incubated in fresh culture media without nocodazole, samples were then collected, and cell extracts were prepared at the time intervals indicated (Figure 4.6a). The samples were analyzed by western blotting, with the phospho-histone H3 (S-10) being used as the mitotic status maker. The results showed that the majority of the cells exited from mitosis 3 hours after being released from nocodazole-arrested mitosis as confirmed by the reduction of the intensity of the phosphor-histone H3 S-10 band. The levels of p31^{comet} were clearly reduced from the same sample (Figure 4.6a). The quantitative data showed that the level of p31^{comet} reduced 66.1% after 3 hours released from nocodazole (Figure 4.6b). This confirmed that the level of p31^{comet} will decline after exit from mitosis and remained low in interphase.

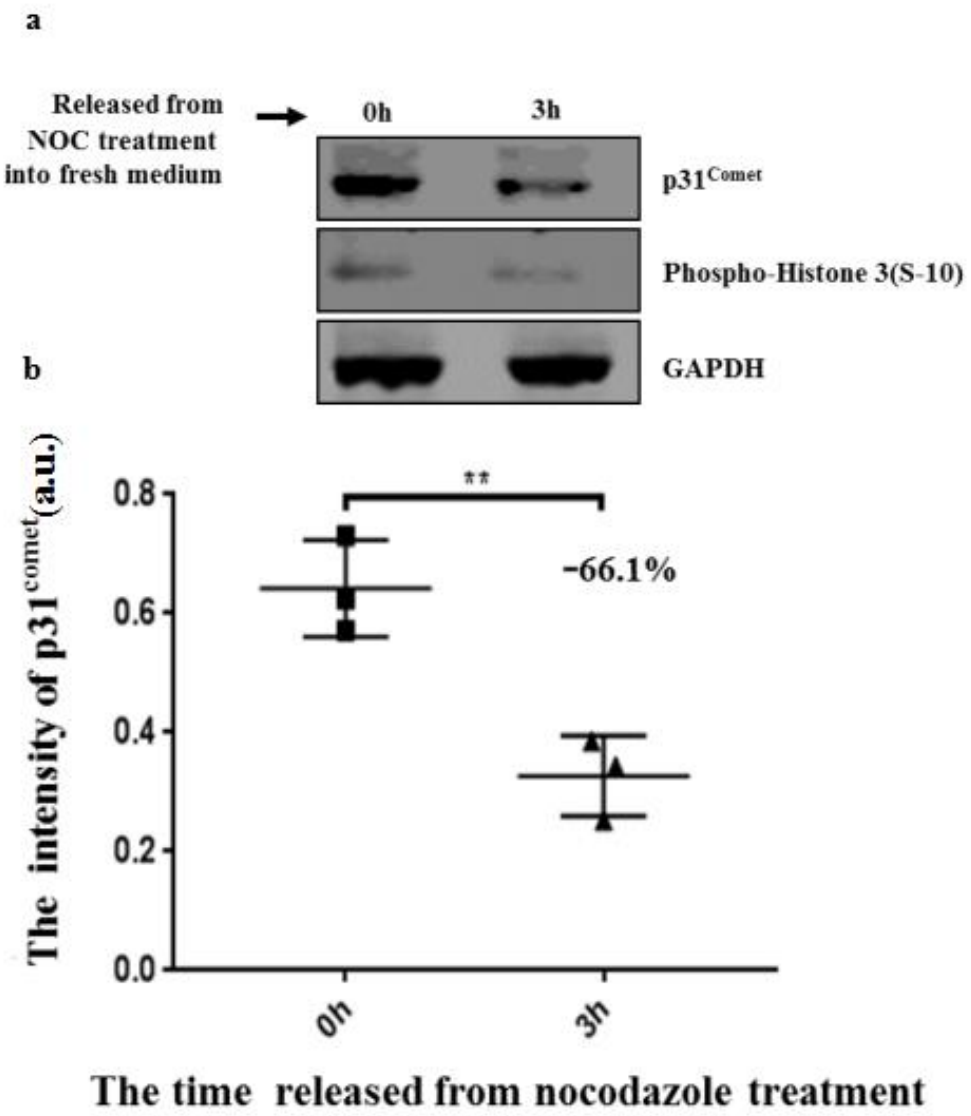

Figure 4.6: The dynamic profile of p31^{comet} in HeLa cells after being released from nocodazole treatment.

The nocodazole arrested mitotic HeLa cells were shaken off from flasks, washed briefly twice andthen incubated in fresh medium without nocodazole, and the cell extracts prepared from the samples collected at the time points indicated. (a) The samples were subject to western blot analysis using a 10% tri-bis SDS-PAGE gel, and the western blot membrane was probed with anti-p31^{comet}, anti-phospho-histone 3 (S-10) and anti-GAPDH antibodies respectively. The phospho-H3 (S-10) bands were used to illustrate the mitotic status and GAPDH bands were used as the loading control. (b) The quantitative comparison of the average intensities of the p31^{comet} western blot bands after being calibrated with the loading control. Three independent experimental results were used for quantifications. A two-tailed unpaired t-test was used to assess the significance between two groups as indicated. Statistical significance of **$p<0.005$.

4.3.6 The degradation of p31^{comet}is proteasome-dependent

Our results have supported the idea that p31^{comet} is most likely to be degraded after cells have exited mitosis, perhaps in interphase. There are two major proteolytic systems, which contribute to the degradation of intracellular proteins: the lysosomal system and the ubiquitin-proteasome system (Ciechanover, 2005, Martinez-Vicente et al., 2005, Goldberg, 2003). To determine which pathway is responsible for p31^{comet} degradation during the cell cycle, we introduced two inhibitors: MG132 and leupeptin (N- Acetyl-L- leucyl-L- leucyl- L-argininal), a known lysosome inhibitor (Grinde and Seglen, 1980, Han et al., 2014), to observe the expression of p31^{comet} after cells were released from nocodazole treatment. We expected that MG132 would block the p31^{comet} degradation if it was degraded via the ubiquitylation proteasome pathway, and that leupeptin would prevent p31^{comet} decline if it was degraded via the lysosomal pathway. Our results showed consistently that p31^{comet} significantly decreased 3 hours after the cells were released from nocodazole treatment (Figure 4.7 lane 2 compared with lane 1); and that this decline was prevented by the addition of MG132 (Figure 4.7, lane 3), but not by the addition of leupeptin (Figure 4.7, lane 4). This behavior of p31^{comet} was very similar to the decline of cyclin B1 under the same conditions (Figure 4.7). Which suggests that p31^{comet} is most likely degraded via the ubiquitylation pathway.

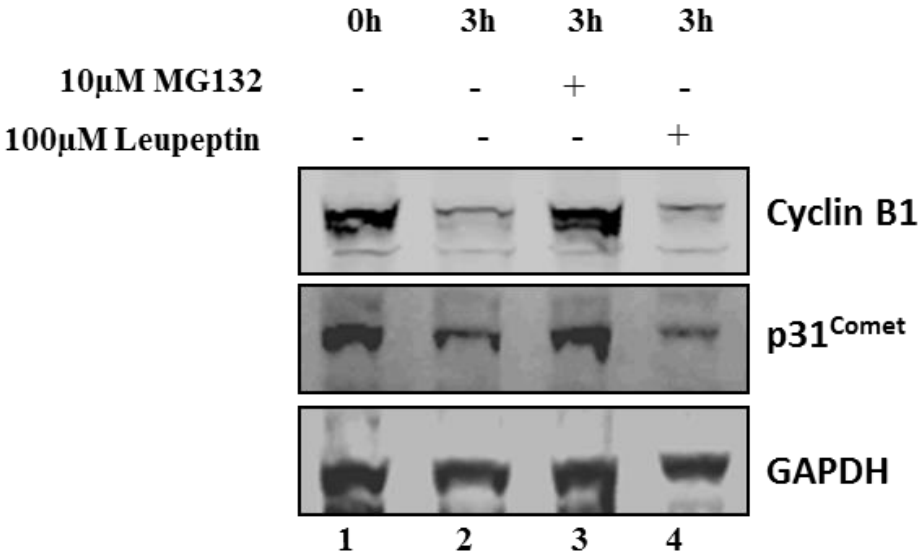

Figure 4.7: The proteolytic pathway that contributes to the degradation of p31$^{comet.}$

HeLa cells were briefly washed twice prior to being incubated in fresh media containing 10μM MG132 or 100μM leupeptin after treated with 60mg/ml nocodazole in 0.5% DMSO (v/v) for 18 hours. The cell extracts prepared from the cells were treated at the time intervals as indicated. The samples were subject to western blot analysis using a 10% tri-bis SDS-PAGE gel, and the western blot membrane was probed with anti-p31^{comet}, anti-cyclin B1 and anti-GAPDH antibodies respectively. The cyclin B1 bands were used to determine the mitotic status and GAPDH bands were used as the loading control.

4.3.7 The APC/C possibly contributes to p31^{comet} degradation

The p31^{comet} sequence contains three potential degron motifs (D-box and KEN-box) (Figure 1.7) recognized by APC/C and also a number of putative ubiquitylation sites (Udeshi et al., 2013, Wagner et al., 2011). As MG132 can prevent its decline after release from nocodazole treatment (Figure 4.7), it would be targeted by the APC/C-dependent ubiquitin-mediated proteolysis. We have examined the level of p31^{comet} after knockdown of the APC3 gene, one core subunit of the APC/C, using siRNA. We expected that p31^{comet} would increase after

depletion of APC3 if APC/C contributed to its degradation. However, the results were inconsistent and contradicted each other from experiment to experiment as so we have seen increased, unchanged and decreased levels of p31^{comet} after treatment with APC3 siRNA (Figure 4.8 a and b), Consequently it is difficult to reach a conclusion based on these preliminary results as to whether or not the APC/C contributes to the degradation of p31^{comet}.

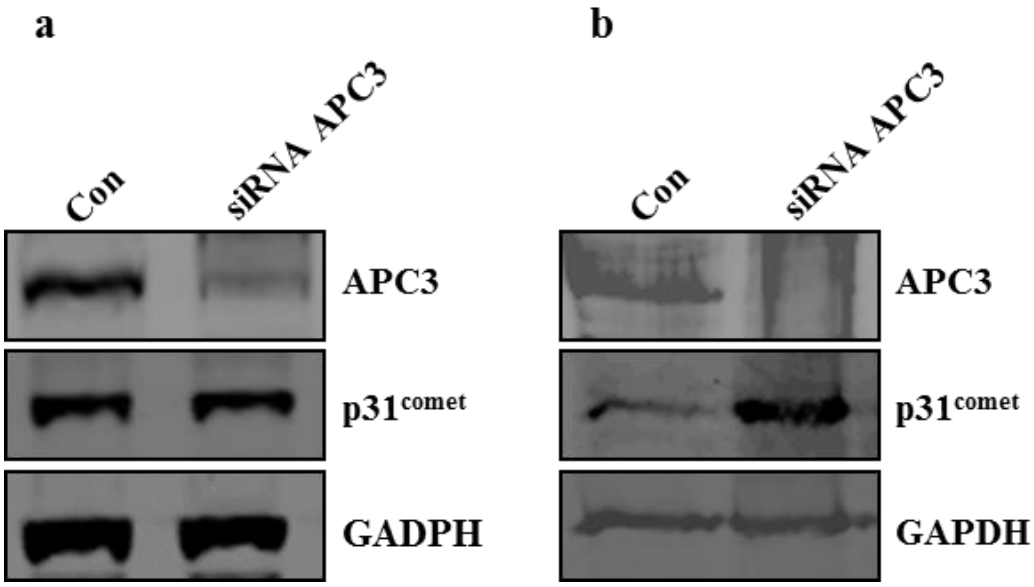

Figure 4.8: The expression of p31^{comet} after depletion of APC3.

HeLa cells were incubated either alone as a control or with APC3 siRNA (25nM final concentration) for 72 hours, the cell extracts were prepared for western blot analysis. The level of APC3 and p31^{comet} were examined by probing with relevant antibodies as indicated. GAPDH protein bands were used as the loading control.

4.3.8 SCF E3 ubiquitin-mediated proteolysis possibly contributes to the degradation of p31^{comet}

We have shown above that the degradation of p31^{comet} probably occurs by the proteasome-mediated proteolytic pathway so that the p31^{comet} level remained low in

interphase, and that the APC/C might not be a direct contributor to this process. We therefore examined the potential involvement of the Skp1-Cul1-F-box-protein (SCF) E3 ligase in the degradation of p31^{comet}. SCF ubiquitin ligase contains Skp-1, Cullins, F-Box and RBX/ROC RING finger proteins, and is mainly targets its substrates for degradation during G1 & S phases (Deshaies, 1999, Sun et al., 2001, Soucy et al., 2009). Cullin-1 is a scaffold protein and one of the core components of the SCF (Zheng et al., 2002, Goldenberg et al., 2004, Wu et al., 2000). The cullin-1 was depleted by siRNA and the level of p31^{comet} was examined. As the preliminary results shown in Figure 4.9 indicate, there was a 50-60% reduction of Cullin-1 protein after 72 hours siRNA treatment compared to that in the control and the level of p31^{comet} seems to have increased (Figure 4.9). This preliminary result suggests that the SCF E3 ligase system might be involved in the degradation of p31^{comet}; however, this has yet to be repeated and confirmed.

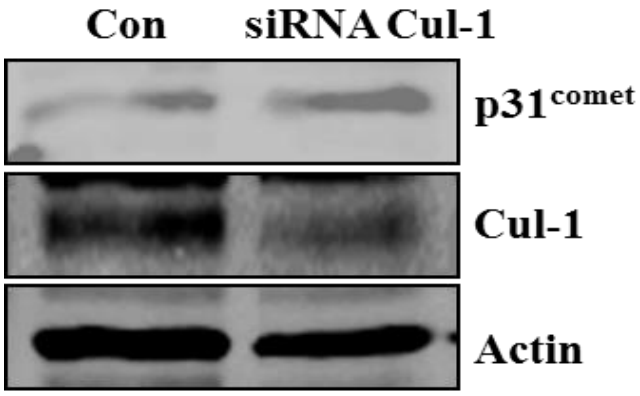

Figure 4.9: The expression of p31^{comet} after treatment with cullin-1 siRNA.

After HeLa cells were incubated either alone as a control or with cullin-1 siRNA for 72 hours, the cell extracts were prepared subject to western blot analysis. The protein levels of p31^{comet} and cullin-1 (cul-1) were probed with the relevant specific antibodies as indicated. GAPDH bands were used as the loading control.

4.4 Discussion

We have shown by immunofluorescent staining that the profile of p31^{comet} remains low in interphase, starts to increase in prophase and peaks at prometaphase and metaphase, and that this high level of p31^{comet} is sustained until telophase. Based on the antibody distribution (Abcam, Ab150363) p31^{comet} is unevenly distributed in the nucleus and partly localized around of the nuclear envelope at prophase. After nuclear envelope breakdown during prometaphase, it is distributed across the entire cell. It has been suggested that expression of p31^{comet} is cell cycle regulated (Habu et al., 2002), and we show that a high level of p31^{comet} remained during anaphase and telophase, although at a slightly lower level compared with that seen in prometaphase and metaphase. However, the level of p31^{comet} is very low in interphase, and the increase of p31^{comet} in mitosis and decrease after release from mitosis were confirmed by western blot results (Figure 4.3＆4.6). This suggests that the levels of p31^{comet} are cell cycle regulated, and it is down-regulated in interphase.

Consistent with these results from the unperturbed cell cycle, a high level of p31^{comet} was also detected when cells were arrested in a prometaphase-like stage by nocodazole treatment. The high level of accumulation of p31comet in response to nocodazole is a phenomenon common to all the cancer cell lines tested in this project. Accumulation of protein in some cell cycle stages could either be the result of protein synthesis or of the prevention of protein degradation. As the increased level of p31^{comet} in response to nocodazole treatment could be prevented by treating the cells with cycloheximide, we have confirmed that the accumulation is caused by new protein synthesis.

We have also shown that the level of p31^{comet} declined after cells were released from nocodazole treatment, and that this reduction can be prevented by MG132 but not leupeptin. Thus p31^{comet} degradation after mitosis is most likely to be mediated by the ubiquitin-proteasome pathway. The protein sequence of p31^{comet} contains three potential degron motifs (D-box and KEN-box), which are signatures motifs that would normally be targeted by the APC/C E3 ligase dependent proteolysis pathway. This suggests that the APC/C might be involved in the degradation of p31^{comet} and we anticipated that the level of p31^{comet} would be

significantly increased if the function of the APC/C was disrupted. However, treatment of the cells with APC3 siRNA, a core subunit of the APC/C, gave inconclusive results with the level of $p31^{comet}$ elevated in some cases and lowered in others. This might be due to the number of cells arrested in mitosis by APC3 siRNA being different in each experiments, and the regulation of the level of $p31^{comet}$ not being directly relevant to the APC/C. Thus, more work needs to be done to see if and how the APC/C contributes to $p31^{comet}$ degradation as the decline in the level of $p31^{comet}$ after release from nocodazole treatment, suggests that this might occur in S/G1 phase, and preliminary results indicate that there is an increased level of $p31^{comet}$ after cullin-1 siRNA treatment, it is possible that SCF E3 ligase-ubiquitin-mediated proteolysis might contribute to the degradation of $p31^{comet}$ as Cullin-1 is the essential core protein of SCF E3 ligase. Thus, the molecular basis of $p31^{comet}$ degradation needs to be further investigated.

Chapter Five: Inducing apoptosis in cancer cell lines using a small-molecule M2I-1 that disrupts the interaction between CDC20 and MAD2

5.1 Introduction

To induce cell death after prolonged mitosis under a constitutively activated SAC is a promising strategy for developing an anti-cancer therapy (Visconti et al., 2016b). Many traditional anti-mitotic drugs such as taxanes and epothilones are widely used in the clinic (McGrogan et al., 2008, Schmidt and Bastians, 2007). It has been suggested that the delayed degradation of cyclin B1 and the dynamic activity of MCL-1 jointly decide the cell fate in response to prolonged mitosis (Sloss et al., 2016, Holland and Cleveland, 2008).

As stated in the previous chapter, M2I-1 is a small molecule that can disrupt the interactions between CDC20 and MAD2 *in vitro* and causes a weakened SAC *in vivo* (Kastl et al., 2015). We have confirmed that M2I-1 can disrupt the interaction of CDC20 and MAD2 in *vivo* (Figure 3.1 ＆3.2); and shown that it also causes premature cyclin B1 degradation in HeLa cells (Figure 3.5). As a traditional microtubule poison, nocodazole causes depolymerisation of the microtubules to activate the SAC and arrests the cell at prometaphase (Rieder and Maiato, 2004), and HeLa cells can tolerate nocodazole treatment with concentration ranges between 40-400ng/ml for up to 24 hours with no significant DNA damage and cell death (Harper, 2005, Matsui et al., 2012), but interestingly, in data shown in the first chapter, we have found that significant cell death occurred when cells were treated with only 60ng/ml nocodazole combined with 50μM M2I-1 compared to cells treated with nocodazole alone (Figure 5.1a). There was no visible difference in the cell morphology when cells were treated with DMSO and M2I-1 alone (Figure 5.1a), but in contrast, some cells displayed typical apoptotic morphologies such as blebbing, shrinking and fragmentation (Vermeulen et al., 2005, Zamzami and Kroemer, 1999), when treated with the nocodazole and M2I-1 combination (Figure 5.1a). Quantitative analysis showed that there is a significant increase in cell death in cells treated with nocodazole combined with M2I-1 compared to cells from the other

treatments (Figure 5.1b). Consistent with how M2I-1 functions, the mitotic index from the cells treated with nocodazole combined with M2I-1 is lower than from those that were treated with nocodazole alone but is significantly higher than from cells treated with DMSO or M2I-1 alone (Figure 5.1c). Our explanation of this phenomenon contrasts with the previous theory that prolonged mitosis under a constitutively activated SAC and stabilized cyclinB1 result in cell death, whereas a weak SAC and normal cyclin B1 degradation results in cell survival (Sloss et al., 2016, Holland and Cleveland, 2008), and has lead us to study the mechanism which leads to cell death caused by M2I-1 combined with nocodazole.

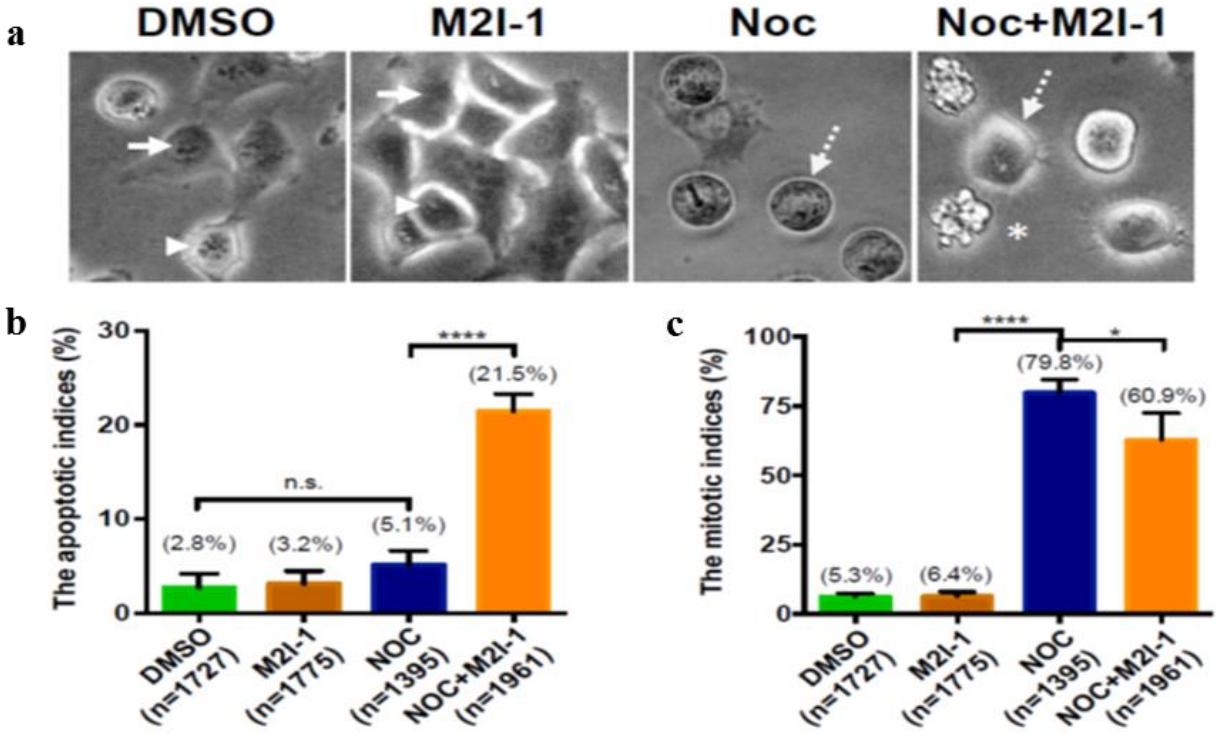

Figure 5.1: M2I-1 promotes the sensitivity of HeLa cells to nocodazole.

HeLa cells were treated with M2I-1 (50µM), nocodazole (60ng/ml), nocodazole (60ng/ml) combined with M2I-1 (50µM), and DMSO (0.5% in v/v) respectively for 16 hours. (a) Digital images were taken using a digital camera mounted on a tissue culture microscope with a 20x objective lens, and the non-mitotic cells, normal mitotic cells, mitotically arrested cells and apoptotic cells were marked with the arrows, arrowheads, dash line arrows and asterisk respectively. (b) Apoptotic indices were quantified by counting the cells with typical apoptotic morphologies after the various treatments. The total numbers of cells counted were 1727, 1775, 1395 and 1961 respectively (indicated as n) from eight independent experiments. The

statistical significance of the comparisons was assigned with a p value<0.0001(****). (c) The mitotic indices were quantified from mitotically arrested cells and the total cells counted in each group were 1727, 1775, 1395 and 1961 respectively (indicated as n). The statistical significance of the comparisons was assigned with p value: *p< 0.05, and ****p <0.0001 respectively.

5.2 Objectives

5.2.1. To confirm that cell death is induced by M2I-1 in the presence of anti-mitotic drugs.

As discussed above, an increased cell death has been observed when HeLa cells were treated by with M2I-1 in the presence of nocodazole but not by M2I-1 alone. To further verify and confirm this, we will quantitatively examine the mitotic index and cell apoptotic index of HeLa and other cancer cell lines under various drug treatments.

5.2.2. To determine the stage of the cell cycle in which cell death is induced by M2I-1 in the presence of Nocodazole.

As discussed in the introduction, the cell death induced by anti-mitotic drugs could occur either after prolonged arrest in the present mitosis or after the cell has escaped from mitosis and entered the next cell cycle. To verify this, we will use a GFP-Histone 2 B HeLa cell line treated as previously described, and record live images of the cells for 24 hours using a Nikon A1R fully automated high-speed confocal imaging system. The histone 2B-GFP signals revealing the chromosomal morphologies will be used to determine the cell cycle stages and chromosomal status. The DIC images will be used to reveal the morphological changes in the cytoplasmic membrane. The individual cells throughout the cell cycle will be tracked to determine whether cell death occurred after cell slippage from prolonged mitotic arrest or within the mitotic arrest itself.

5.2.3. To investigate the molecular basis of the cell death which is induced by M2I-1 in the presence of Nocodazole.

It is well know that cells in prolonged mitosis can enter cell death under a provoked SAC induced by anti-mitotic drugs such as Nocodazole and Taxol, and this cell death undergo either through an intrinsic apoptotic pathway (Diaz-Martinez et al., 2014, Topham and Taylor, 2013, Salmela and Kallio, 2013) (Allan and Clarke, 2007, Gascoigne and Taylor, 2008, Diaz-Martinez et al., 2014) or through independent caspase activity (Niikura et al., 2007). We will first examine the connection of this cell death induced by M2I-1 in the presence of nocodazole with the intrinsic caspase-3-dependent apoptotic pathway by western blot analysis of the levels of the caspase-3 cleavage products, and the expression profiles of a pro-survival protein MCL-1, and the pro-apoptotic proteins BIM, BID, PUMA, NOXA and MCL-1s (an alternative splicing variant of MCL-1). We will also determine whether the DNA damage pathway contributes to this cell death or not.

5.3 Results

5.3.1 M2I-1 promotes the sensitivity of the cancer cell lines to anti-mitotic drugs

To verify that the cell death that occurred was specifically induced by the combination of nocodazole and M2I-1, we have also examined and compared the results of treating cells with Taxol combined with M2I-1. Taxol is another anti-mitotic drug that can stabilize the microtubules and activates the SAC (Lopes et al., 1993, Horwitz, 1994). As for nocodazole or nocodazole combined with M2I-1, there is an increased apoptotic index and a slightly decreased mitotic index was observed in cells treated with Taxol combined with M2I-1 as compared with those treated with Taxol alone (Figure 5.1.1b & c). As shown in Figure 5.2a, the apoptotic indices are 0.5%, 2.9%, 5.1% and 18.9% for DMSO, M2I-1, Taxol and Taxol combined with M2I-1 respectively; and the mitotic indices for each group are 5.7%, 5.5%, 73.2% and 55.1% respectively. Thus, it appears that M2I-1 can potentiate the sensitivity of HeLa cells to anti-mitotic drugs like nocodazole and Taxol.

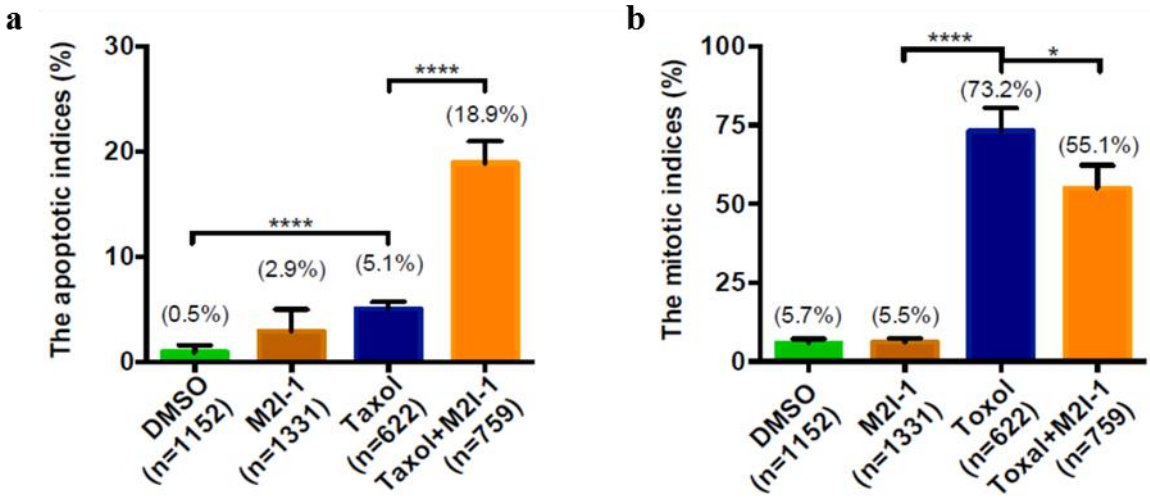

Figure 5.2: M2I-1 promotes the sensitivity of HeLa cells to Taxol.

HeLa cells were treated with M2I-1 (50µM), Taxol (30nM), Taxol (30nM) combined with M2I-1 (50µM), and DMSO (0.5% in v/v) respectively for 16 hours. (a) Apoptotic indices were quantified by counting the cells with typical apoptotic morphologies for each treatment. The total number of cells counted was 1152, 1331, 622 and 759 respectively (indicated as n). The statistical significance of comparisons was assigned with a p value<0.0001 (****). (b) The mitotic indices were quantified with mitotically arrested cells and the total cells counted from each group was 1152, 1331, 622 and 759 respectively (indicated as n). The statistical significance of comparisons was assigned with p values: *p<0.05), ****p<0.0001 respectively.

To test whether the cell death induced by the treatment with the combined drugs (nocodazole + M2I-1 or Taxol + M2I-1) is unique to HeLa cells, three other cancer cell lines were chosen and treated as described above (Figure 5.3a). The results confirmed that the observed cell deaths in the three cell lines are significant higher when they are treated with nocodazole combined with M2I-1 than when treated with nocodazole alone (Figure 5.3b).

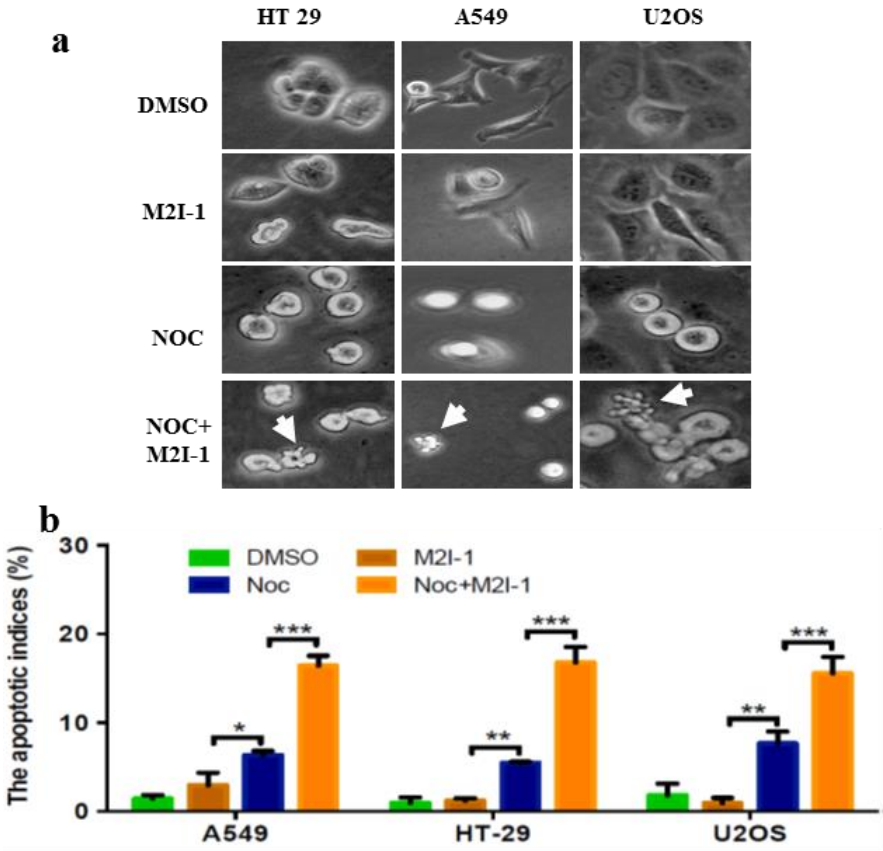

Figure 5.3: M2I-1 promotes the sensitivity of A549, HT29 and U2OS cell lines to nocodazole.

A549, HT29 and U2OS cells were treated with M2I-1 (50μM), nocodazole (60ng/ml), nocodazole (60ng/ml) combined with M2I-1 (50μM), and DMSO (0.5% in v/v) respectively for 16 hours. (a) Digital images were taken using a digital camera mounted on a tissue culture microscope using a 20x objective lens. The apoptotic cells were marked with arrowheads. (b) The statistical significance of comparisons was assigned with p values: **p< 0.01, ***p< 0.001, and ****p <0.0001 respectively.

5.3.2 Cell death mainly occurred after prolonged mitosis

In response to a prolonged mitosis, a cell might either die in mitosis, slip out of mitosis or die in the next round of the cell cycle (Rieder and Maiato, 2004, Gascoigne and Taylor, 2008, Topham and Taylor, 2013). We have previous confirmed that in HeLa cells M2I-1 can disrupt the interaction of CDC20-MAD2 *in vivo*, preventing the CDC20-MAD2 complex formation, and the premature degradation of cyclin B1 (Figure 3.1, 3.2＆3.5). Taken together with the

reduced mitotic index (Figure 5.1c), we suspected that the cell death induced by the combined drug treatment might occur in the next cell cycle after slippage. This seemed to be supported by the reduction in the level of histone H3 S-10 phosphorylation (Figure. 5.4a), one biological marker of mitosis (Hans and Dimitrov, 2001, Wang et al., 2001, Hendzel et al., 1997, Van Hooser et al., 1998). The quantitative data showed that there is about 14.8% reduction of the level of histone H3 S-10 phosphorylation (Figure 5.4b).

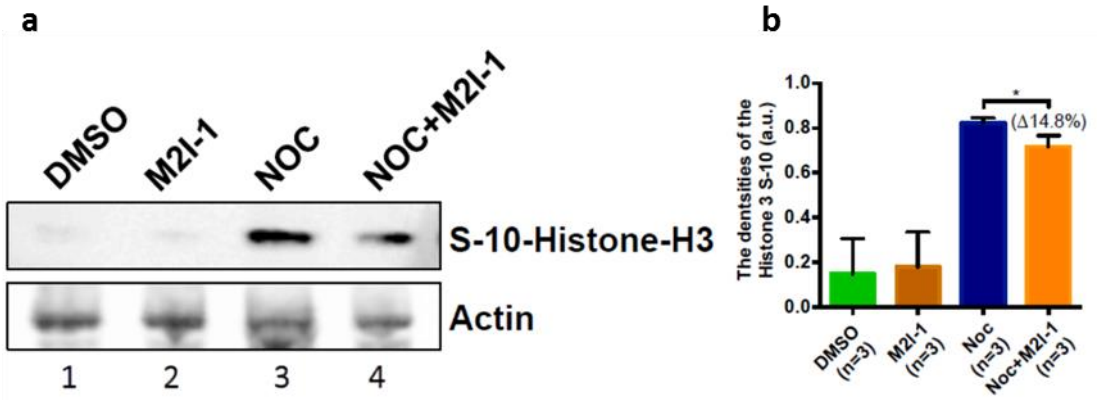

Figure 5.4: The level of the histone H3 S-10 phosphorylation in response to the different treatments.

Cell extracts were prepared after HeLa cells were treated with M2I-1(50µM), nocodazole (60ng/ml), nocodazole (60ng/ml) combined with M2I-1(50µM), and DMSO (0.5% in v/v) respectively for 16 hours. (a) The samples were subjected to SDS-PAGE and western blot analysis. The membranes were probed with a rabbit polyclonal anti-phospho-histone H3 (S-10) antibody and a mouse anti-actin antibody respectively. The actin protein bands acted as the loading control. (b) The intensity of the phosphorylated histone H3 S-10 from the different treatments revealed by the western blot was analysed by ImageJ. The results were produced from three independent experiments. The statistical significance of comparisons was assigned with a p value< 0.05 (*).

However, the reduced mitotic index could also be due to the cells dying in mitosis, because the increased cell death index is similar to the reduction in level of the mitotic index (Figure 5.1c). To test this, a HeLa cell line which over-expressed a histone 2B-GFP fusion protein was treated as above. The live images of the cells were recorded for 24 hours using a Nikon A1R

fully automated high-speed confocal imaging system for single cell analysis. The histone 2B-GFP signals revealing the chromosomal morphologies were used to determine the cell cycle stages and chromosomal status (Figure 5.5 a, b, c, d). The DIC images were used to reveal the morphological changes in the cytoplasmic membrane (Figure 5.5 a, b, c, d). The distribution, timing of the condensation, segregation and decondensation of chromosomes revealed by the histone 2B-GFP signals from the normal cells (DMSO treated cells) are consistent with previous reports(Rodrigue et al., 2013, Kanda et al., 1998) (Figure 5.5a). In responded to nocodazole treatment, the cell started to round up with condensed chromosomes and eventually arrested at a prometaphase-like stage as shown with arrowheads (Figure 5.5b). In cells treated with nocodazole combined with M2I-1. There are many cells that presented the typical apoptotic phenotypes: blebbing of the cytoplasmic membrane or shrinking of the cell body (Figure 5.5b, black arrowheads), accompanied by highly condensed chromosomes (Figure 5.5b, white dash line arrows), and broken chromosomes (Figure 5.5b, white solid arrows), and which eventually formed the typical apoptotic body (Figure 5.5b, white asterisk). There was very small proportion of cells that began the cell death program with a prophase-like morphology (Figure 5.5c). These cells seemed to begin the process of dying with chromosomal degeneration or fragmentation (Figure 5.5c, white dash line arrows) but the cytoplasmic membrane remains intact, and the typical apoptotic body was not formed until a very late stage (Figure 5.5c, white asterisk). In contrast, only a very small number of dying cells can be found from cells treated with nocodazole alone (Figure 5.5b). The quantitative results show that there was no big difference in the cell death and mitotic indices between the cells treated by DMSO and M2I-1 alone at different time points (Figure 5.5 e&f), and cell death begins at 16 hours after treatment. The cell death index is significantly higher from the group of the cells treated with nocodazole combined with M2I-1 than that treated with nocodazole alone (Figure 5.5e), and was 6% and 13.2% higher at 16 and 24 hours respectively (Figure 5.5e). In contrast to the cell death index and consistent with previous observations, the mitotic index was significant higher from the group of the cells treated with nocodazole alone than that treated with nocodazole combined with M2I-1, these were 6.9% and 15.2% at 16 and 24 hours respectively (Figure 5.5f). The proportion of cells that died in a

prophase-like stage was only about 5% after cells were treated with nocodazole combined with M2I-1 (Figure 5.5h).

To determine whether the cell death occurred after cell slippage from prolonged treatment with nocodazole or nocodazole combined M2I-1, we have tracked and examined the individual cells throughout their cell cycle (Figure 5.5d). We found that only a few cells underwent slippage after treatment with nocodazole or nocodazole combined M2I-1 (Figure 5.5g). The quantitative data suggests that the proportion of cells that underwent slippage was less than 1% from cells treated with either nocodazole or nocodazole combined with M2I-1 (Figure 5.5g). Thus, the live imaging also confirmed that nocodazole combined with M2I-1 can induce cell death, and that this cell death occurred within the first cell cycle after the drug treatment rather than in the next cell cycle after escaping from mitotic arrest. Therefore, the reduced mitotic index or the level of phosphorylation of histone H3 S-10 from the cells treated with nocodazole combined with M2I-1 compared to the cells treated with nocodazole alone, was more likely to result from the increased cell death and the decreased number of cells arrested in mitosis.

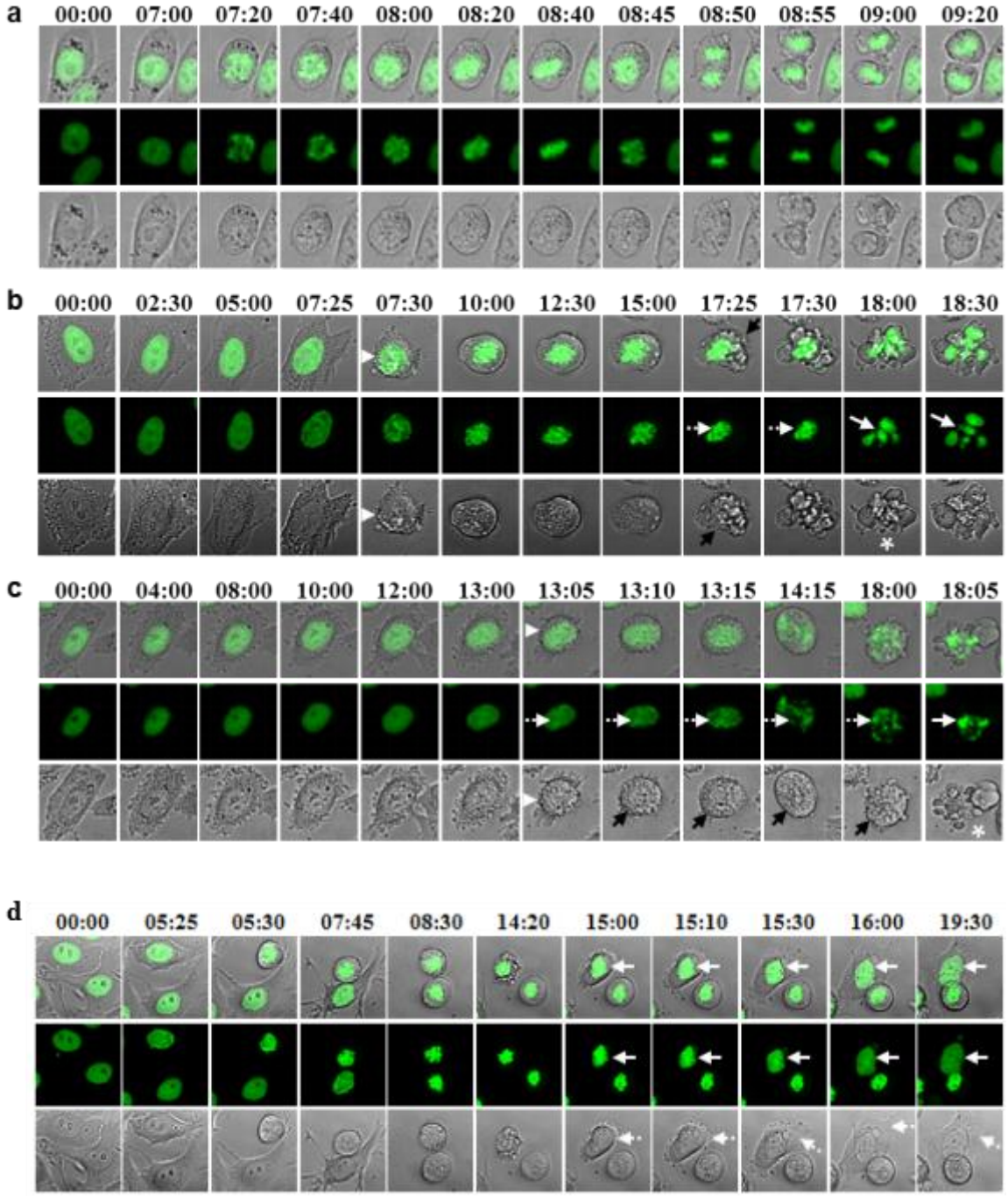
a
00:00
07:00
07:20
07:40
08:00
08:20
08:40
08:45
08:50
08:55
09:00
09:20
b
00:00
02:30
05:00
07:25
07:30
10:00
12:30
15:00
17:25
17:30
18:00
18:30
c
00:00
04:00
08:00
10:00
12:00
13:00
13:05
13:10
13:15
14:15
18:00
18:05
d
00:00
05:25
05:30
07:45
08:30
14:20
15:00
15:10
15:30
16:00
19:30

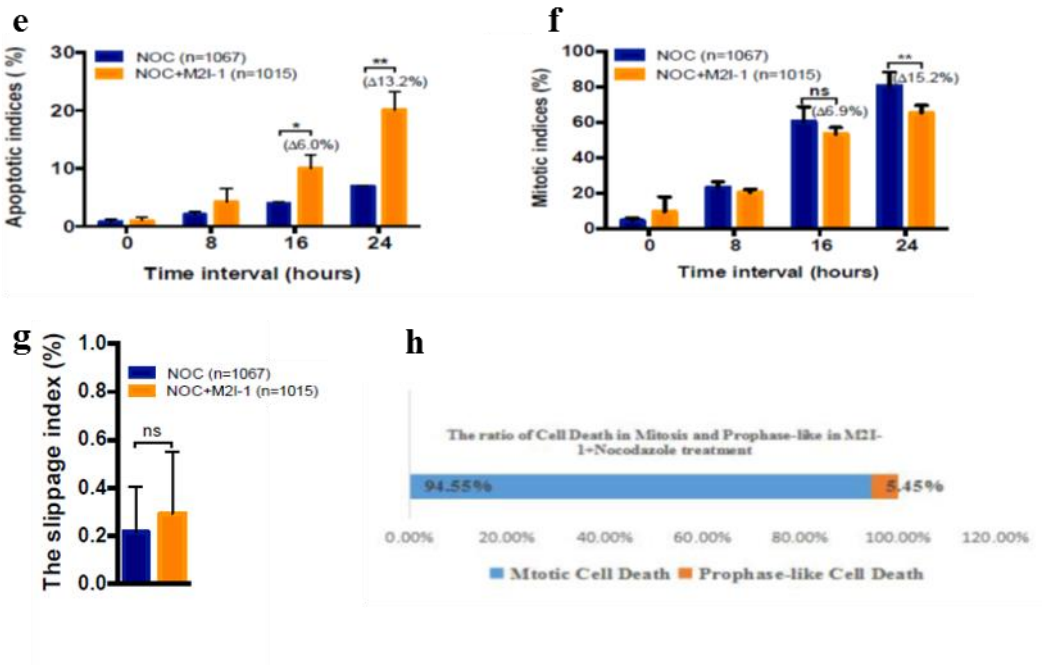

Figure 5.5: The majority of cell death occurred in the same cell cycle after the prolonged mitotic arrest under the drug treatment.

HeLa cells which over-expressed a Histone 2B-GFP fusion protein were treated with M2I-1(50µm), nocodazole (60ng/ml), nocodazole (60ng/ml) combined with M2I-1(50µm), and DMSO (0.1% in v/v) respectively for 24 hours, and time-lapse images of the live cells were recorded using a Nikon A1R fully automated high-speed confocal imaging system at 37^{o}C and supplied with 5% CO_2. The Histone 2B-GFP signals were used to reveal the chromosomal morphology and thus the cell cycle stage and chromosomal status; DIC images were used to reveal the morphological changes in the cytoplasmic membranes. (a) An example of a normal/unperturbed HeLa cell with Histone 2B-GFP (green) during the cell cycle. (b) An example of a HeLa cell with Histone 2B-GFP (green) undergoing apoptosis after prolonged mitotic arrest due to treatment with 60ng/ml nocodazole or 60ng/ml nocodazole combined with M2I-1. (c) An example of the cell death that occurred in prophase-like stages after treatment with nocodazole combined with M2I-1. (d) An example of the slippage that occurred when a cell escaped from prolonged mitotic arrest. (e) & (f) The quantitative cell death or mitotic indices at various time points after treatment. (g) The comparison of the slippage indices between the groups of cells treated with nocodazole and nocodazole combined with M2I-1. (h) The ratio of the cells that died in a prophase-like stage and in mitosis induced by the treatment of nocodazole combined with M2I-1. The statistical significance of comparisons was assigned with p values: *p< 0.05, and **p<0.01 respectively.

5.3.3 The cell death induced by M2I-1 in the presence of nocodazole is associated with the caspase-3 dependent apoptotic pathway

As the majority of the cells that died after prolonged mitotic arrest had the typical apoptotic morphology as described previously (Diaz-Martinez et al., 2014, Salmela and Kallio, 2013), we tested to see if caspase-3 activity was the contributory factorto the cell death observed above. Cell extracts were prepared from HeLa cells after treatment with DMSO, M2I-1, nocodazole, and nocodazole combined with M2I-1 under the same conditions described above. The samples were subjected to the western blot analysis using an anti-caspase-3 antibody to test the cleavage of caspase-3 (Figure 5.6a). The results showed that the cleavage of caspase-3 was undetectable in samples from cells treated with DMSO and M2I-1 alone (Figure 5.6a, lane 1and 2). The sample prepared from cells treated with nocodazole alone had a low level of cleaved caspase-3 (Figure 5.6a, lane 3), but at a significantly lower level than the signal detected from the sample treated with nocodazole combined with M2I-1 (Figure 5.6a, lane 4). The quantitative data showing the intensities of the cleaved caspase-3 under the different conditions is shown in figure 5.6b. There were no significant differences between the groups treated with nocodazole, DMSO, and M2I-1 alone (Figure 5.6b). Therefore, the cell death induced by nocodazole combined with M2I-1 is caspase-3 activity dependent. This also suggests that M2I-1 can promote the sensitivities of cancer cell lines to anti-mitotic drugs.

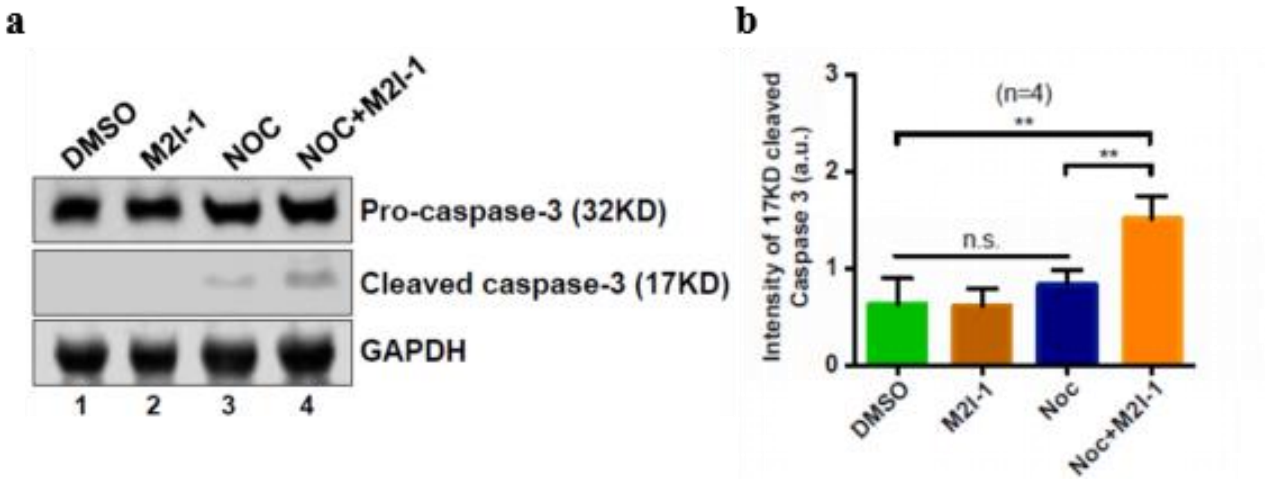

Figure 5.6: The cleavages of caspase-3 under different treatment conditions.

After cells were treated with M2I-1 (50μM), nocodazole (60ng/ml), nocodazole (60ng/ml) combined with M2I-1 (50μM), and DMSO (0.5% in v/v) respectively for 16 hours. Cell extracts were prepared for western blot analysis with an anti-caspase-3 antibody and an anti-GAPDH antibody. (a) The full-length caspase-3 (32KD) and the cleaved caspase-3 (17KD) were highlighted. GAPDH was examined as the loading control. (b) The intensities of the protein bands were quantified using ImageJ software from four independent western blotting results. The two-tailed unpaired t-test was used to assess the quantitative comparison between two groups as indicated. The statistical significance of comparisons was assigned with a p value< 0.01 (**).

5.3.4 The DNA damage checkpoint is not likely to contribute to this cell death

To examine if the cell death could be caused by DNA damage, we analysed the formation of γ-H2AX foci (phosphorylated histone 2AX, a variant of histone 2A), a typical indicator of DNA double-strand break (Khanna and Jackson, 2001), and using VP16 (etoposide), a reagent known to induce DNA damage (Duca et al., 2006) as the positive control. The percentage of cells containing more than five γ-H2AX foci found in un-arrested cells at the cell cycle stage similar to cells treated with VP16, was used to represent the DNA damage level at each time point as indicated (Tu et al., 2013). As most of the cells started to enter mitosis 16 hours after treatment with nocodazole alone or nocodazole combined with M2I-1 (Figure 5.1c and 5.5f), there were insufficient numbers of un-arrested cells at 16 hours for quantification, we

therefore quantified the average fluorescent intensities of cells containing γ-H2AX foci from the mitotic arrested cells at 16 hours intervals. Results showed that VP16 treatment leads to DNA damage occurred in most of the cells in contrast to no DNA damages caused by the treatment with DMSO alone (Figure 5.7a). Both nocodazole alone and nocodazole combined with M2I-1 gradually caused slight increases in the numbers of γ-H2AX foci at time intervals before 16 hours compared to the control treated by DMSO, but there were no significant differences between these two groups. Similarly, there was no difference in the intensities of the γ-H2AX foci at 16 hours between the groups of cells treated with nocodazole and those treated with nocodazole combined with M2I-1 although the overall levels of the γ-H2AX foci increased (Figure 5.7 a and b). DNA-PKcs/CHK2 can increase the level of γ-H2AX foci in mitotically arrested cells independent of DNA damage (Tu et al., 2013), so the significantly increased overall intensities of the γ-H2AX foci observed at 16 hours interval was probably not caused by DNA damage. All of these results suggest that the DNA damage pathway does not contribute to the cell death induced by M2I-1 in the presence of nocodazole.

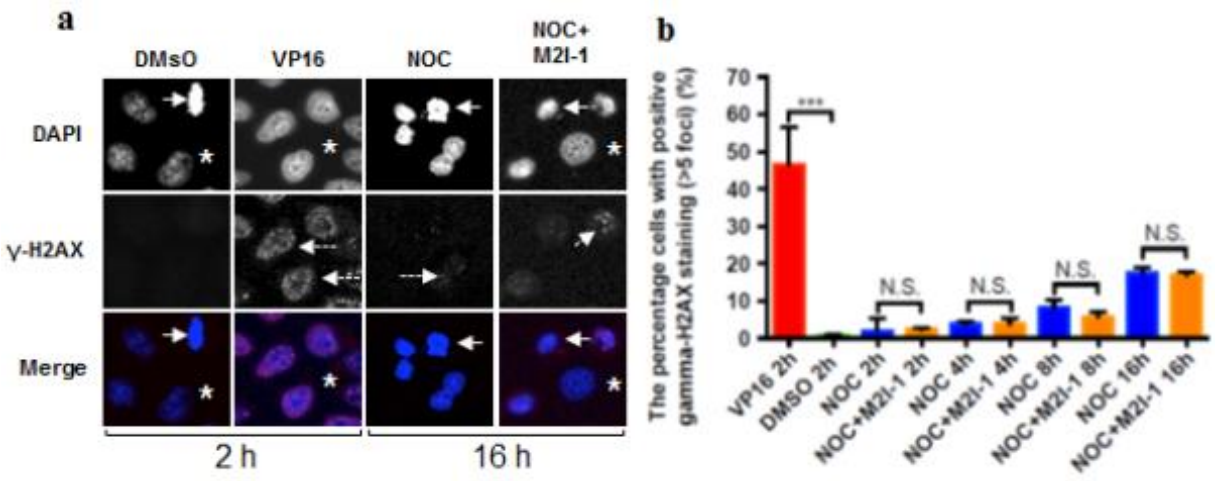

Figure 5.7: A comparison of the formation of γ-H2AX foci induced by the different drug treatments.

HeLa cells were treated with nocodazole (60ng/ml) and nocodazole (ng/ml) combined with M2I-1(50μm) for 2, 4, 8, 16 hours respectively. HeLa cells treated with DMSO (0.5%, v/v) and VP16 (10mM) for 2 hours were used as the negative and positive controls respectively. The cells were fixed with 4% formamide-PBS for immunofluorescent staining with a specific

anti-γ-H2AX antibody. DNA morphologies stained by DAPI were used to distinguish the mitotic cells. (a) Representative confocal images showed DNA staining (blue in merged images, and grey in the first row) and the immunofluorescent staining signal of γ-H2AX foci (red in merged images, and grey in the second row) at different cell cycle stages. Arrows highlight a metaphase cell treated with DMSO for 2 hours; a prometaphase-like cell from the cells treated with nocodazole (NOC) alone, and NOC + M2I-1 for 16 hours respectively. Asterisks highlight the un-arrested cells after DMSO, VP16 and NOC+M2I-1 treatments. The dash line arrows from the second row highlight the cells with positive signals of γ-H2AX foci. (b) The quantitative results comparing the DNA damage levels indicated by the percentage of cells having more than 5 γ-H2AX foci from the cell population under treatment at different time intervals as indicated. Under a 40x oil objective lens, the cells from four or five random areas of the confocal images were taken to give the quantitative results. Three independent experiments were conducted to produce the data. P value, ***<0.003. N.S.: No significant.

5.3.5 The "competing-networks" model cannot be used to explain the cell death induced by M2I-1 in the presence of nocodazole

According to the competing-networks model, the rate of cyclin B1 degradation and a yet undefined cell death signal coordinate to control the cell fate in response to the prolonged mitotic arrest (Gascoigne and Taylor, 2008). MCL-1, one of the anti-apoptotic proteins, is regarded as a critical player in prolonged mitosis as its degradation contributes to cause cell death (Harley et al., 2010, Wertz et al., 2011). While cyclin B1-dependent CDK1 kinase can phosphorylate the MCL-1 and is essential for facilitating MCL-1 degradation (Harley et al., 2010, Miniowitz-Shemtov et al., 2012), the balance between the activity of cyclin B1-dependent CDK1 kinase and the level of MCL-1 has been suggested to determine the cell death or slippage in response to the prolonged mitosis (Mocciaro and Rape, 2012). Our previous results have indicated that cell death induced by M2I-1 combined with nocodazole occurred in the same cell cycle as the arrest in mitosis (Figure 5.5). To test if cyclin B1 and MCL-1 played any roles in this cell death, we examined their levels by western blot analysis using the same treatments as previously described. The Results indicated that cyclin B1 was stabilized in the sample of the cells treated with nocodazole alone but significantly decreased in the samples of the cells treated with M2I-1 or M2I-1 combined with nocodazole (Figure 5.8). These results are consistent with the observations in chapter three (Figure 3.5), and

agreed with the property of M2I-1 weakening the SAC by disrupting the CDC20-MAD2 interaction, leading to the premature degradation of cyclin B1 by the APC/C, we also found that the MCL-1 level was significantly reduced in cells treated with nocodazole compared to cells treated with DMSO alone (Figure 5.8, lane 1 and 3), which agrees with previous reports that MCL-1 was degraded after prolonged mitotic arrest (Sanchez-Perez et al., 2010, Sloss et al., 2016, Di Cesare et al., 2017). In contrast, the treatment by M2I-1 combined with nocodazole stabilized MCL-1, and it is significantly increased when compared to the levels seen in cells treated with nocodazole alone (Figure 5.8, lane 3 and 4). According to the competing-networks model, after the combined drug treatment, the deceased cyclin B1 and increased MCL-1 should lead to more cells slipping out of mitosis, but this contradicts our results shown above. Thus the competing-networking model cannot be applied to explain the cell death induced by M2I-1 in the presence of nocodazole, and some other unknown mechanism or factors must be involved in this process.

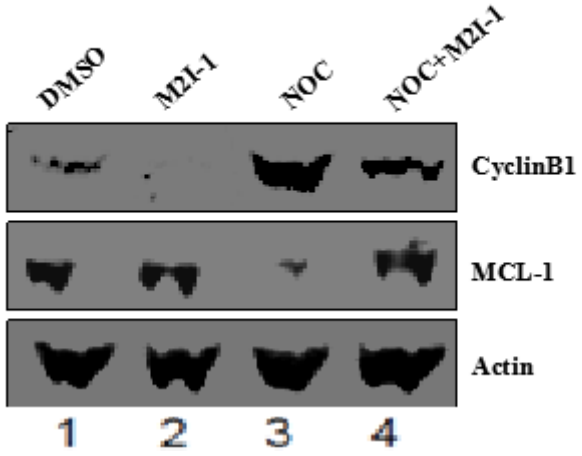

Figure 5.8:The expression profiles of cyclin B1 and MCL-1 under different drug treatments

After HeLa cells were treated by M2I-1(50μM), nocodazole (60ng/ml), nocodazole (60ng/ml) combined with M2I-1(50μM), and DMSO (0.5% in v/v) respectively for 16 hours, the cell extracts were prepared for western blot analysis using the anti-cyclin B1, anti-MCL-1, and anti-actin antibodies respectively.The profiles of cyclin B1 and MCL-1 under different drug conditions as indicated. The actin bands were used as the loading control.

5.3.6 MCL-1s is a potential culprit causing the cell death induced by M2I-1 combined with nocodazole

The MCL-1s level increased in cells treated with nocodazole combined with M2I-1 but not with nocodazole alone

Our results have shown that the cell death induced by M2I-1 combined with nocodazole is accompanied by an increased cleavage of caspase-3 (Figure 5.6), this suggests that the cell death undergoes the intrinsic apoptotic pathway, and other evidences have been shown previously (Diaz-Martinez et al., 2014, Topham and Taylor, 2013, Salmela and Kallio, 2013). To further explore the potential mechanism of the cell death induced by M2I-1 combined with nocodazole, we compared the expression profiles of the pro-apoptotic proteins of Bim, Bid, Puma, Noxa and MCL-1s in HeLa cells after the treatments described before. Results showed that Bim, Bid, and Puma remained at similar levels or even slightly decreased in cells treated with M2I-1 combined with nocodazole compared to the samples of the cells treated with nocodazole alone (Figure 5.9 a, b, c), and the level of Noxa has increased marginally (Figure 5.9d). However, we found that MCL-1s, a short form variant of the full length MCL-1, clearly increased in cells treated with the combined drugs compared to cells treated with nocodazole alone (Figure 5.9e). As a pro-apoptotic BH3 only protein, MCL-1s can act to sequester the anti-apoptotic function of the full-length MCL-1. Thus, the significant increase in MCL-1s could be the culprit causing the cell death while the slightly increased Noxa probably also exerted an auxiliary pro-apoptotic role.

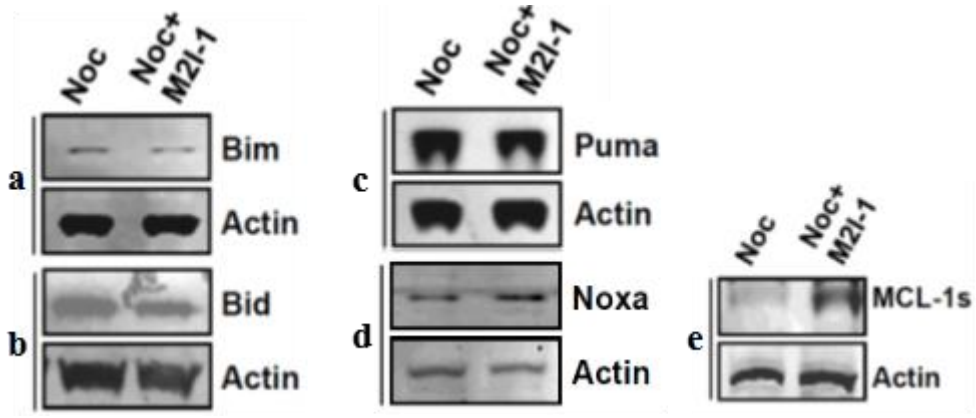

Figure 5.9: The western blot results showing the profiles of Bim, Bid, Puma, Noxa and MCL-1s under different drug treatments.

After HeLa cells were treated with nocodazole (60ng/ml), nocodazole (60ng/ml) combined with M2I-1 (50μM) respectively for 16 hours, the cell extracts were prepared for western blot analysis with the specific antibodies against Bim, Bid, Puma, Noxa and MCL-1s as well as actin.

M2I-1 in the presence of nocodazole could not induce cell death in the MCF-7 cell line, which is lacking the expression of MCL-1s

To verify if MCL-1s played an essential role in causing cell death induced by M2I-1 combined with nocodazole, we originally intended to directly examine cell death after the depletion of MCL-1s from HeLa cells by siRNA. However, as MCL1-s is an alternative splicing variant of MCL-1, it is spliced out of the exon 2 of MCL-1 during mRNA processing, it is impossible to design a specific siRNA that targets MCL-1s alone. Consequentlywe decided to study the cell death using the MCF-7 cell line, a cell line lacking the MCL-1s expression (Gautrey and Tyson-Capper, 2012). We anticipated that cell death would not occur after treated with M2I-1 combined with nocodazole in MCF-7 cells if MCL-1s played the central role in causing this cell death.

The Results showed that the changes in the morphology of MCF-7 cells are similar to those seen in HeLa cells in response to DMSO, M2I-1, and nocodazole treatment, and they have similar mitotic and apoptotic indices, but there was a significant difference of these from

MCF-7 cells treated with M2I-1 combined with nocodazole compared to HeLa cells, as for MCF-7 cells, M2I-1 failed to induce the cell death in the presence of nocodazole compared to the treatment with nocodazole alone. This result supports the idea that MCL-1s contributes to the cell death in HeLa cells induced by M2I-1 combined with nocodazole (Figure 5.10 a &b).

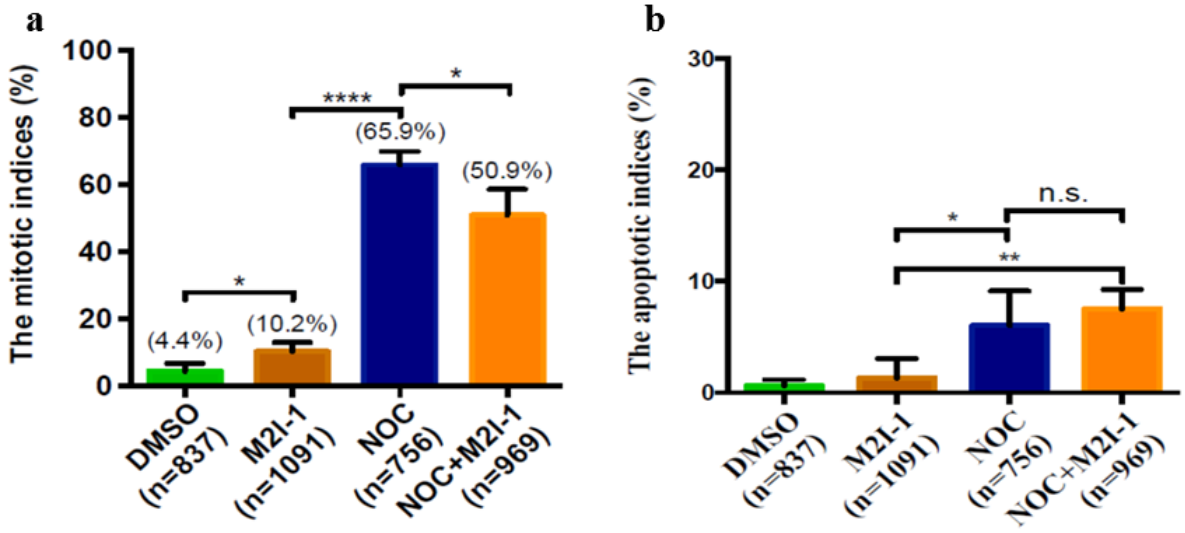

Figure 5.10: M2I-1 cannot induce cell death of MCF-7 cells in the presence of nocodazole.

MCF-7 cells were treated with 0.5% DMSO, 50µM M2I-1, 60ng/ml nocodazole, and 60ng/ml nocodazole+50µM M2I-1 respectively for 16 hours. (a) Digital images were taken using a digital camera mounted on a tissue culture microscope using a 20x objective lens, The mitotic indices were quantified from cells undergoing the different drug treatments as indicated. The number of cells counted for groups of DMSO, M2I-1, nocodazole and nocodazole combined M2I-1 are 837, 1091, 756 and 969 from 4 independent experiments respectively (indicated as n). The statistical significance of comparisons was assigned with a p value <0.05 (*), p<0.0001(****) respectively. (b) Apoptotic indices were quantified with the typical apoptotic phenotype as indicated from different groups. The number of cells counted for the groups of DMSO, M2I-1, nocodazole and nocodazole combined M2I-1 are 837, 1091, 756 and 969 respectively (indicated as n). The statistical significance of comparisons was assigned with a p value< 0.05 (*), p <0.01(**).

MCF-7 cells overexpressed with a GFP-MCL-1s fusion protein can be induced to undergo cell death by M2I-1 in the presence of nocodazole

To further confirm the role of MCL-1s in causing cell death, we have transfected 1μg of an exogenous pCMV6-AN-mGFP-MCL-1s plasmid DNA into MCF-7 cells. The GFP fluorescent signals were used as the positive marker to estimate the ratio of transfection. The MCF-7 cells were split into two groups after 24 hours transfection and were treated with nocodazole alone or M2I-1 combined with nocodazole respectively as described for the HeLa cells. As caspase-3 is absent from the MCF-7 cell line (Janicke et al., 1998, Janicke, 2009, Turner et al., 2003), the polymerase-1 (PARP-1), a nuclear protein whose cleavage fragments are a unique biomarker in cell death (Wen et al., 2012, Chaitanya et al., 2010, Fischer et al., 2003, Kaufmann et al., 1993), was used to evaluate the levels of cell death. The cell extracts from normal MCF-7 cells and pCMV6-AN-mGFP-MCL-1s transfected MCF-7 cells under the same treatment conditions were prepared after 16 hours for western blot analysis using a specific anti-PARP-1 antibody. There is no increased cleavage of PARP-1 after the normal MCF-7 cells were treated with M2I-1 combined with nocodazole compared to the sample of the cells that were treated with nocodazole alone (Figure 5.11a). However, there was a noticeable increase in the level of the cleaved PARP-1 after the transfected MCF-7 cells were treated with drugs under the same conditions (Figure 5.11b). We also noticed that the expression of this mGFP-MCL-1s fusion protein is slightly higher in cells treated with M2I-1 combined with nocodazole than in cells treated with nocodazole alone, so more controlled experiments will be required to ensure the equal expression of the fusion protein of GFP-MCL-1s and to make this a definite conclusion. However, the preliminary results indicated that more cell death could be induced in MCF-7 cells transiently expressing a GFP-MCL-1s fusion protein after treated with M2I-1 combined with nocodazole compared to nocodazole alone.

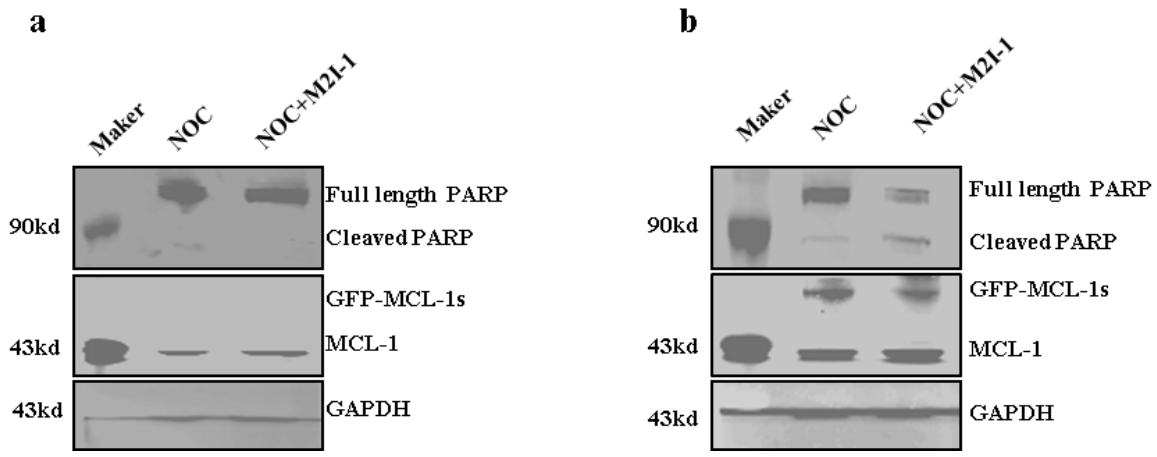

Figure 5.11: The comparison of the cleavage of PARP in MCF-7 cells and pCMV6-AN-mGFP-MCL-1s transfected MCF-7 cells after treated by nocodazole and nocodazole+M2I-1 respectively.

The normal MCF-7 cells and pCMV6-AN-mGFP-MCL-1s transfected MCF-7 cells were treated with nocodazole and nocodazole +M2I-1 for 16 hours respectively. The cell extracts were prepared and analyzed by western blotting. The PARP, MCL-1 and GFP-MCL-1s were examined with specific antibodies, and the GAPDH was tested as the loading control.

5.4 Disussion

Our results indicated that the small molecule, MAD2 inhibitor-1 (M2I-1) promotes the sensitivity of cancer cells to the anti-mitotic drugs nocodazole and Taxol. The cell death induced by M2I-1 in the presence of nocodazole cannot be explained using the 'competing-networks' model for mitotic cell death. Accompanying the cell death induced by M2I-1 combined with nocodazole, the levels of cyclin B1 was reduced and MCL-1 elevated, which contradicts the conditions described by the "competing-networks" model as the decreased cyclin B1 and increased MCL-1 should support the cell to escape the mitotic arrest and survive. We verified that this death occurred in mitosis of the first cycle via the caspase-3 pathway (accompanied with an increase in the cleavage of caspase-3). We have provided the evidence that the level of MCL-1s, the splicing variant of MCL-1, also significantly increased

in response to the same treatment. As a pro-apoptotic BH3 only protein, it is known that MCL-1s can antagonise MCL-1 to induce cell death; this suggests that MCL-1s potentially contributes to the cell death induced by M2I-1 combined with nocodazole. To support this, M2I-1 in the presence of nocodazole cannot induce cell death from MCF-7 cells, a cell line lacking the expression of MCL-1s. Furthermore, more cell death can be induced from MCF-7 cells transiently expressing a GFP-MCL-1s fusion protein when treated with M2I-1 combined with nocodazole compared to nocodazole alone.

Chapter Six: General discussion

The spindle assembly checkpoint (SAC) monitors the chromosomal alignment and microtubule attachment via the kinetochores. It prevents anaphase onset and premature chromosome segregation by inhibiting the APC/C via its effector MCC (Musacchio, 2015). The MCC consists of two sub-complexes CDC20-MAD2 and BUBR1-BUB3, however, exactly how the MCC forms is still controversial. The "MAD2 template" model describes the mechanism as the kinetochore-dependent dynamic recruitment of the SAC proteins and their facilitation on the formation of the CDC20-MAD2 complex. Somehow this CDC20-MAD2 subcomplex binds to the BUB3-BUBR1 complex to form the MCC (Lara-Gonzalez et al., 2012, Yu, 2006, De Antoni et al., 2005). Therefore, the kinetochores are the catalytic platform for the SAC signaling (Howell et al., 2000, Vink et al., 2006, Musacchio and Hardwick, 2002). Targeting of MAD2 and BUBR1 to the kinetochores is sufficient to maintain checkpoint arrest regulated by Aurora and Mps1 kinases (Kruse et al., 2014, Maldonado and Kapoor, 2011). BUBR1 accumulation and phosphorylation at unattached kinetochores plays an important role in association with other SAC components to maintain the SAC function (Chen, 2002). The MCC components are released from the kinetochores upon microtubule attachment after mitosis (Musacchio and Salmon, 2007, Shah et al., 2004). The "stripping" of MAD2, MAD1 and other SAC proteins from the kinetochores is the key process of SAC inactivation (Howell et al., 2001). Therefore, it has been widely accepted that the MCC is assembled in response to the unattached kinetochores (Yu, 2006, Lara-Gonzalez et al., 2012, Musacchio and Salmon, 2007). However, the mechanism of the kinetochore-dependent MCC formation has been challenged by many existing observations, for instance, the MCC can be isolated from cell extracts of interphase HeLa cells (Sudakin and Yen, 2004, Chan et al., 1999), the CDC20-MAD2 and MCC complexes were still detectable in the absence of a functional kinetochore in the Ndc10 mutant of budding yeast (Poddar et al., 2005, Fraschini et al., 2001). Thus, exactly how and where the CDC20-MAD2 complex or the MCC was formed remains unknown.

Previous approaches that have been used to examine the CDC20 and MAD2 interaction or MCC complex were mainly based on the co-immunoprecipitation of the interacting proteins, with cell extracts biochemically prepared from the synchronized cells to determine the cell cycle phases. However, the biochemical preparation of interphase extracts would often still contain a substantial population of prophase cells. Additionally, the drugs used for synchronisation of the cell populations may have impacted on the cell cycle organization and the information seen from the cellular compartments in comparison with the non-perturbed cell. The Duolink based proximity ligation assay (PLA) can detect the protein-protein interaction in individual cells in their native state, thus avoiding biochemical extraction or the creation of exogenous over-expressed fusion proteins and can also be used to assign signals to specific subcellular locations such as the cytoplasm or the nucleus. By using PLA with specific CDC20 and MAD2 antibodies, the lab has previously demonstrated that the formation of CDC20-MAD2 complex is dynamically regulated in a bell-shaped manner during the unperturbed HeLa cell cycle. And this project has demonstrated that the PLA signals of CDC20-MAD2 reflect the genuine interaction profile of CDC20 and MAD2. As shown in Figure 1.11, the CDC20-MAD2 complex accumulates from prophase onwards and peaks at prometaphase. Another colleague in the lab has demonstrated that the CDC20-MAD2 complex formed during prophase is not dependent on unattached kinetochores but its formation is facilitated by Tpr, one component of the nuclear pore complex (Li et al., 2017). This project has confirmed that this CDC20-MAD2 complex is functional and prevents the premature degradation of cyclin B1, which seems to indicate that this specific complex might be playing a part in the SAC signaling pathway. However, the traditional concept of the SAC is that its inhibitory cascading pathway is exclusively dependent on unattached kinetochores in late prophase and anaphase. To resolve this problem we should see if the MCC can be formed by binding this specific CDC20-MAD2 complex with the other subcomplex of BUBR1-BUB3 before prometaphase, and if the premature degradation of cyclinB1 was prevented by the sub-complex or requires the MCC after the integration of the CDC20-MAD2.

The SAC monitors the faithful segregation of the sister chromatids in mitosis by detecting kinetochore attachment. After all the kinetochores are correctly attached to microtubules and are generating tension, the SAC has to be inactivated to allow the APC/C activation to facilitate chromosome segregation and exit mitosis (Liu and Zhang, 2016, Jia et al., 2011). $p31^{comet}$ has been shown to be an important silencer that contributes to SAC inactivation either on its own (Miniowitz-Shemtov et al., 2012, Eytan et al., 2014) or jointly with a protein called Trip13 (Eytan et al., 2014). The expression profile of $p31^{comet}$ has been suggested to be cell cycle regulated and it is thought to be associated with the nuclear membrane (Habu et al., 2002), and sequence analysis has suggested that it contains several putative destruction motifs (Habu et al., 2002), which would make it a target for APC/C-dependent ubiquitin-mediated proteolysis. However, it has also been contradictorily suggested that $p31^{comet}$ levels remain constant throughout the cell cycle (Xia et al., 2004). Thus, the molecular basis of the degradation of $p31^{comet}$ needs to be studied further.

We have confirmed, by immunofluorescent staining with an antibody against $p31^{comet}$ (Abcam, Ab150363), that the expression profile of $p31^{comet}$ is indeed cell cycle regulated (Figure 4.2) though this antibody also recognizes a non-specific band at around 25KD (Figure4.1). The results showed that the level of $p31^{comet}$ is low in interphase, starts to increase from prophase and peaks at pro-metaphase or metaphase, the high level of $p31^{comet}$remaining into telophase (Figure 4.2). In prophase, the localization of $p31^{comet}$ was found around the nuclear envelope and was unevenly distributed in the nucleus, which also agrees with previous publications (Westhorpe et al., 2011, Yang et al., 2007). After NEBD, it is distributed across the entire cytosol (Habu et al., 2002). These results indicated that $p31^{comet}$ is present at a high level even before the metaphase-anaphase transition in mitosis and only declined in G1/S or interphase. The 25KD non-specific band complicated the interpretation of the localization and expression of $p31^{comet}$ but the idea that there is a high level of $p31^{comet}$ in mitosis was partly supported by the observations that higher levels of $p31^{comet}$ accumulated in prometaphase arrested HeLa cells after nocodazole treatment (Figure4.3). This accumulation of $p31^{comet}$ in response to the

nocodazole treatment is a common phenomenon seen from several other cancer cell lines we tested (Figure 4.4).

The increase in the level of p31^{comet} starting in prophase and peaking at prometaphase, suggests that protein synthesis might be involved and this was confirmed by showing that cyclonheximide can prevent the accumulation of p31^{comet} in the presence of nocodazole and even in the presence of MG132 (Figure 4.5). Thus, protein synthesis contributes to the accumulation of p31^{comet} both in response to nocodazole treatment and in the normal progression of mitosis.

The interpretation of whether p31^{comet} is or is not degraded in the late stages of mitosis was complicated by the non-specific binding of the antibody (Figure 4.1) and the contradictory findings from previous publications (Xia et al., 2004, Habu et al., 2002). To further test this, HeLa cells were released from nocodazole-arrested mitosis, samples were collected at various time intervals and analysed by western blotting (Figure 4.6). The results showed that p31^{comet} significantly decreased in the three hours after being released from nocodazole- arrested mitosis (Figure 4.6). This confirmed the findings that p31^{comet} is a cell cycle regulated protein and is probably degraded during interphase. This has been further confirmed by Nanmao Dang, a colleague in the lab, using live images of a GFP-p31^{comet} expressed in HeLa cells (data not shown). Furthermore, the decline of p31^{comet} in cells released from nocodazole treatment can be restored by MG132, a known inhibitor of 20s proteasome activity which blocks protein degradation via the ubiquitylation pathway (Zhang et al., 2013, Kisselev and Goldberg, 2001, Genschik et al., 1998, Steinhilb et al., 2001). In contrast, the decline of p31^{comet} cannot be prevented by leupeptin, a known lysosome inhibitor (Grinde and Seglen, 1980, Han et al., 2014) (Figure 4.7). This suggests that the degradation of p31^{comet} occurred through the ubiquitin-mediated proteolysis pathway.

The protein sequence of p31^{comet} contains 3 potential D-box or KEN-box degron motifs (Figure 1.7) and it has been speculated that it is a substrate of the APC/C (Habu et al., 2002).

To test this, we compared the levels of p31^{comet} in normal HeLa cells and in HeLa cells after APC3 knockdown using siRNA, APC3 is a core protein of the APC/C complex (Izawa and Pines, 2011, Yamaguchi et al., 2015). Our results are equivocal as sometimes we have observed the level of p31^{comet} increases after APC3 depletion (Figure 4.8b), but in other experiments this was not the case (Figure 4.8a). We speculate that the different changes in the p31^{comet} level after siRNA APC3 could be caused by the different number of cells arrested in mitosis in different experiments. What is more, even in the situation where the level of p31^{comet} increased in response to the depletion of APC3, it would still be difficult to say that the high level of p31^{comet} resulted from the prevention of its proteolysis because of the increased number of mitotic cells naturally expressing a higher level of p31^{comet}. Thus, based on the preliminary results obtained so far, it is difficult to draw a conclusion about whether the APC/C contributed to the degradation of p31^{comet} or not. To further test this, would require the synchronization of the cells before depletion of APC3 or other components of the APC/C using siRNA. Alternatively, it might be better to inhibit the APC/C activity either by chemical means or using siRNA and quantify the levels of p31^{comet} after the cells exit from mitosis.

Our immunofluorescent staining results and the fact that the level of p31^{comet} declined after the cells were released from mitotic arrest, all indicated that the degradation of p31^{comet} might have occurred in late mitosis or in S phase. Therefore, we have also examined the potential involvement of the SCF, the other E3 ligase in controlling the degradation of p31^{comet} in G1/S phase. This was done by examining the levels of p31^{comet} after the depletion of Cullin-1 using siRNA. Cullin-1 is a core scaffold protein of the SCF complex (Zheng et al., 2002, Goldenberg et al., 2004, Wu et al., 2000). The preliminary data showed that the levels of p31^{comet} increased after the depletion of cullin-1 (Figure 4.9). This preliminary result implies that the SCF might contribute to the degradation of p31^{comet}; though more controlled experiments need to be done to confirm this.

It has been shown *in vivo* that p31^{comet} can regulate insulin signaling by blocking the interaction of MAD2-BUBR1 with the insulin receptor on the plasma membrane (Choi et al.,

2016), and hence the regulation of blood glucose concentration. In the clinic, disorders in the regulation of blood glucose link up with the progression of critical illness (Hermanides et al., 2010, Marik, 2016, Krinsley, 2008a, Ingels et al., 2018), particularly in sepsis patients (Preechasuk et al., 2017, Krinsley, 2008b). However, how the levels of $p31^{comet}$ could be used to predict the development of critical illness of patients is still unknown.

M2I-1 (MAD2 inhibitor-1) is the first small molecule that has been identified which disrupts the CDC20-MAD2 interaction (Kastl et al., 2015). We have shown in the first result chapter that M2I-1 can prevent the CDC20-MAD2 complex formation both at prophase, before NEBD (nuclear envelope breakdown), and at prometaphase and metaphase (Figure 3.2). The disruption of the interaction between CDC20 and MAD2 induced by M2I-1 accompanied by the premature degradation of cyclin B1 at both stages (Figure 3.5).Intriguingly, we found that M2I-1 in the presence of nocodazole or Taxol can significantly increase cell death in several cancer cell lines (Figure 5.1, 5.2 & 5.3). This cell death occurred in the same cell cycle (Figure 5.4 &5.5), and the terminal morphologies that these dying cells displayed were similar to those of typical apoptotic cells (Figure 5.1&5.5).

It has been believed that under prolonged mitotic arrest, a gradually decline in the level of cyclin B1 and a stabilized level of MCL-1 serve as a survival signal which competes with an as yet undefined death signal to determine whether the cell would die in mitosis or would exit from mitosis and enter the next cell cycle (Gascoigne and Taylor, 2008, Gascoigne and Taylor, 2009, Mocciaro and Rape, 2012). This was summarized as a "competing-networks" model and explained how the cell fate was determined in prolonged mitosis (Gascoigne and Taylor, 2008, Gascoigne and Taylor, 2009). Our results, however, show that in HeLa cells, M2I-1 in the presence of nocodazole or Taxol could induce cell death in cells with a low level of cyclin B1, a stabilized MCL-1 and a weakened SAC (Figure 5.8). The elevated MCL-1 and reduced cyclin B1 did not directly trigger the slippage within our 24 hours observation period, and this phenomenon cannot be explained by the "competing-networks" model (Gascoigne and Taylor, 2009, Gascoigne and Taylor, 2008). It is likely that the premature degradation of cyclin B1

caused by M2I-1 combined with the disruption of the microtubule network caused by nocodazole or Taxol reduced the cells fitness and triggered cell death via mitotic catastrophe as the evidence shows that the DNA damage pathway was not involved in the cell death (Figure 5.7). The higher level of cleavage capspase-3 induced by M2I-1, in the presence of nocodazole confirmed the involvement of the caspase-3 dependent apoptotic pathway.

To understand the molecular basis of how the apoptotic pathway causes cell death, we have examined the pro- and anti-apoptotic proteins from the Bcl-2 super family. Results showed that the levels of the pro-apoptotic proteins Bim, Bid, and Puma remained relatively unchanged or were even slightly reduced (Figure 5.9a, b & c), but Noxa (Figure 5.9d) increased marginally. However, the levels of an anti-survival protein, MCL-1s (a short form variant of the full-length MCL-1 which acts to sequester the function of MCL-1) clearly increased when the cells were treated with the combination of M2I-1 and nocodazole compared to nocodazole alone (Figure 5.9e). Therefore, the increased levels of the pro-apoptotic protein MCL-1s might play an important role in antagonizing the function of the increased level of MCL-1 in stopping the cells from entering apoptosis. This was supported by the observations that M2I-1 in the presence of nocodazole failed to induce cells death in MCF-7 cells, a cell line lacking the expression of MCL-1s (Gautrey and Tyson-Capper, 2012) (Figure 5.10).

We would want to observe this cell death phenomenon connection with MCL-1s by directly depletion of MCL-1s using siRNA in HeLa cells. However, MCL-1s is the consequence of the alternative pre-mRNA splicing events of the full length of MCL-1 (Bae et al., 2000, Bingle et al., 2000). It is impossible to design siRNA experiments directly and specifically for targeting MCL-1s for depletion. To further confirm that MCL-1s is the cause of the cell death induced by M2I-1 in the presence of nocodazole in HeLa cells, we have observed the cell death in MCF-7 cells after transfection and expression of an exogenous GFP-MCL-1s fusion protein in the presence of M2I-1 and nocodazole. Due to caspase-3 also being absent from the MCF-7 cell line (Janicke et al., 1998, Janicke, 2009, Turner et al., 2003), we examined the cleavage

levels of polymerase-1 (PARP-1) protein to evaluate the cell death. PARP-1 is a nuclear protein involved in the apoptotic pathway and its cleavage is a well-established biomarker of cell death via the apoptotic pathway (Wen et al., 2012, Chaitanya et al., 2010, Fischer et al., 2003, Kaufmann et al., 1993). The preliminary results suggest that the MCF-7 cells transfected with a GFP-MCL-1s after treated with M2I-1 combined with nocodazole show an increased level of the cleaved PARP-1 (Figure 5.11) compared to the control samples where MCF-7 cells were not transfected with the GFP-MCL-1s. Although the experiment has yet to be repeated with more controlled conditions, the preliminary results, suggest that MCL-1s directly contributes to the cell death induced by M2I-1 in the presence of nocodazole.

We have shown that as a single agent M2I-1 cannot cause cell death in several cancer cell lines, but it can significantly induce cell death within the same cell cycle in the presence of anti-mitotic drugs, such as nocodazole and Taxol. This might prove to be significant, as it would increase the clinical efficacies of current anti-mitotic drugs such as taxanes, epothilones, and vinca alkaloids in killing cancer cells and so potentially reduce the length of treatment as well as the dose used. It might also reduce the development of resistance and the potential relapse or new tumorigenesis after chemotherapy using current anti-mitotic drugs, though this has yet to be tested.

Reference

ABRIEU, A., KAHANA, J. A., WOOD, K. W. & CLEVELAND, D. W. 2000. CENP-E as an essential component of the mitotic checkpoint in vitro. *Cell,* 102**,** 817-26.

ABRIEU, A., MAGNAGHI-JAULIN, L., KAHANA, J. A., PETER, M., CASTRO, A., VIGNERON, S., LORCA, T., CLEVELAND, D. W. & LABBE, J. C. 2001. Mps1 is a kinetochore-associated kinase essential for the vertebrate mitotic checkpoint. *Cell,* 106**,** 83-93.

ALBERTS, B. J., ALEXANDER; LEWIS, JULIAN; MORGAN, DAVID; RAFF, MARTIN; ROBERTS, KEITH; WALTER, PETER. 2015. *Molecular Biology of the Cell (6th ed.)*, Garland Science.

ALLAN, L. A. & CLARKE, P. R. 2007. Phosphorylation of caspase-9 by CDK1/cyclin B1 protects mitotic cells against apoptosis. *Mol Cell,* 26**,** 301-10.

BAE, J., LEO, C. P., HSU, S. Y. & HSUEH, A. J. 2000. MCL-1S, a splicing variant of the antiapoptotic BCL-2 family member MCL-1, encodes a proapoptotic protein possessing only the BH3 domain. *J Biol Chem,* 275**,** 25255-61.

BAKHOUM, S. F., KABECHE, L., COMPTON, D. A., POWELL, S. N. & BASTIANS, H. 2017. Mitotic DNA Damage Response: At the Crossroads of Structural and Numerical Cancer Chromosome Instabilities. *Trends Cancer,* 3**,** 225-234.

BALIGA, B. S., PRONCZUK, A. W. & MUNRO, H. N. 1969. Mechanism of cycloheximide inhibition of protein synthesis in a cell-free system prepared from rat liver. *J Biol Chem,* 244**,** 4480-9.

BARFORD, D. 2011. Structural insights into anaphase-promoting complex function and mechanism. *Philos Trans R Soc Lond B Biol Sci,* 366**,** 3605-24.

BARISIC, M. & GELEY, S. 2011. Spindly switch controls anaphase: spindly and RZZ functions in chromosome attachment and mitotic checkpoint control. *Cell Cycle,* 10**,** 449-56.

BARISIC, M., SOHM, B., MIKOLCEVIC, P., WANDKE, C., RAUCH, V., RINGER, T., HESS, M., BONN, G. & GELEY, S. 2010. Spindly/CCDC99 is required for efficient chromosome congression and mitotic checkpoint regulation. *Mol Biol Cell,* 21**,** 1968-81.

BERTOLI, C., SKOTHEIM, J. M. & DE BRUIN, R. A. 2013. Control of cell cycle transcription during G1 and S phases. *Nat Rev Mol Cell Biol,* 14**,** 518-28.

BINGLE, C. D., CRAIG, R. W., SWALES, B. M., SINGLETON, V., ZHOU, P. & WHYTE, M. K. 2000. Exon skipping in Mcl-1 results in a bcl-2 homology domain 3 only gene product that promotes cell death. *J Biol Chem,* 275**,** 22136-46.

BOEKHOUT, M. & WOLTHUIS, R. 2015. Nek2A destruction marks APC/C activation at the prophase-to-prometaphase transition by spindle-checkpoint-restricted Cdc20. *J Cell Sci,* 128**,** 1639-53.

BRAUNSTEIN, I., MINIOWITZ, S., MOSHE, Y. & HERSHKO, A. 2007. Inhibitory factors associated with anaphase-promoting complex/cylosome in mitotic checkpoint. *Proc Natl Acad Sci U S A,* 104**,** 4870-5.

BRITO, D. A. & RIEDER, C. L. 2006. Mitotic checkpoint slippage in humans occurs via cyclin B destruction in the presence of an active checkpoint. *Curr Biol,* 16**,** 1194-200.

BROWN, N. G., VANDERLINDEN, R., WATSON, E. R., QIAO, R., GRACE, C. R., YAMAGUCHI, M., WEISSMANN, F., FRYE, J. J., DUBE, P., EI CHO, S., ACTIS, M. L., RODRIGUES, P., FUJII, N., PETERS, J. M., STARK, H. & SCHULMAN, B. A. 2015. RING E3 mechanism for ubiquitin ligation to a

disordered substrate visualized for human anaphase-promoting complex. *Proc Natl Acad Sci U S A,* 112**,** 5272-9.

BROWN, N. G., WATSON, E. R., WEISSMANN, F., JARVIS, M. A., VANDERLINDEN, R., GRACE, C. R. R., FRYE, J. J., QIAO, R., DUBE, P., PETZOLD, G., CHO, S. E., ALSHARIF, O., BAO, J., DAVIDSON, I. F., ZHENG, J. J., NOURSE, A., KURINOV, I., PETERS, J. M., STARK, H. & SCHULMAN, B. A. 2014. Mechanism of polyubiquitination by human anaphase-promoting complex: RING repurposing for ubiquitin chain assembly. *Mol Cell,* 56**,** 246-260.

BRUCE ALBERTS, A. J., JULIAN LEWIS ,MARTIN RAFF, KEITH ROBERTSPETER WALTER. 2008. *Molecular Biology Of The Cell , Fifth Edition,* Biochemistry and molecular biology education.

BRULOTTE, M. L., JEONG, B. C., LI, F., LI, B., YU, E. B., WU, Q., BRAUTIGAM, C. A., YU, H. & LUO, X. 2017. Mechanistic insight into TRIP13-catalyzed Mad2 structural transition and spindle checkpoint silencing. *Nat Commun,* 8**,** 1956.

BUFFIN, E., LEFEBVRE, C., HUANG, J., GAGOU, M. E. & KARESS, R. E. 2005. Recruitment of Mad2 to the kinetochore requires the Rod/Zw10 complex. *Curr Biol,* 15**,** 856-61.

BURGESS, R. C., BURMAN, B., KRUHLAK, M. J. & MISTELI, T. 2014. Activation of DNA damage response signaling by condensed chromatin. *Cell Rep,* 9**,** 1703-1717.

BURTON, J. L. & SOLOMON, M. J. 2001. D box and KEN box motifs in budding yeast Hsl1p are required for APC-mediated degradation and direct binding to Cdc20p and Cdh1p. *Genes Dev,* 15**,** 2381-95.

BURTON, J. L. & SOLOMON, M. J. 2007. Mad3p, a pseudosubstrate inhibitor of APCCdc20 in the spindle assembly checkpoint. *Genes Dev,* 21**,** 655-67.

BUSCHHORN, B. A., PETZOLD, G., GALOVA, M., DUBE, P., KRAFT, C., HERZOG, F., STARK, H. & PETERS, J. M. 2011. Substrate binding on the APC/C occurs between the coactivator Cdh1 and the processivity factor Doc1. *Nat Struct Mol Biol,* 18**,** 6-13.

CAMPBELL, M. S., CHAN, G. K. & YEN, T. J. 2001. Mitotic checkpoint proteins HsMAD1 and HsMAD2 are associated with nuclear pore complexes in interphase. *J Cell Sci,* 114**,** 953-63.

CASTRO, A., BERNIS, C., VIGNERON, S., LABBE, J. C. & LORCA, T. 2005. The anaphase-promoting complex: a key factor in the regulation of cell cycle. *Oncogene,* 24**,** 314-25.

CHAITANYA, G. V., STEVEN, A. J. & BABU, P. P. 2010. PARP-1 cleavage fragments: signatures of cell-death proteases in neurodegeneration. *Cell Commun Signal,* 8**,** 31.

CHAN, G. K., JABLONSKI, S. A., SUDAKIN, V., HITTLE, J. C. & YEN, T. J. 1999. Human BUBR1 is a mitotic checkpoint kinase that monitors CENP-E functions at kinetochores and binds the cyclosome/APC. *J Cell Biol,* 146**,** 941-54.

CHAN, Y. W., FAVA, L. L., ULDSCHMID, A., SCHMITZ, M. H., GERLICH, D. W., NIGG, E. A. & SANTAMARIA, A. 2009. Mitotic control of kinetochore-associated dynein and spindle orientation by human Spindly. *J Cell Biol,* 185**,** 859-74.

CHAN, Y. W., MA, H. T., WONG, W., HO, C. C., ON, K. F. & POON, R. Y. 2008. CDK1 inhibitors antagonize the immediate apoptosis triggered by spindle disruption but promote apoptosis following the subsequent rereplication and abnormal mitosis. *Cell Cycle,* 7**,** 1449-61.

CHANG, D. C., XU, N. & LUO, K. Q. 2003. Degradation of cyclin B is required for the onset of anaphase in Mammalian cells. *J Biol Chem,* 278**,** 37865-73.

CHANG, L. & BARFORD, D. 2014. Insights into the anaphase-promoting complex: a molecular machine that regulates mitosis. *Curr Opin Struct Biol,* 29**,** 1-9.

CHANG, L. F., ZHANG, Z., YANG, J., MCLAUGHLIN, S. H. & BARFORD, D. 2014. Molecular architecture and mechanism of the anaphase-promoting complex. *Nature,* 513**,** 388-393.

CHEESEMAN, I. M., CHAPPIE, J. S., WILSON-KUBALEK, E. M. & DESAI, A. 2006. The conserved KMN network constitutes the core microtubule-binding site of the kinetochore. *Cell,* 127**,** 983-97.

CHEN, Q., ZHANG, X. Y., JIANG, Q., CLARKE, P. R. & ZHANG, C. N. 2008. Cyclin B1 is localized to unattached kinetochores and contributes to efficient microtubule attachment and proper chromosome alignment during mitosis. *Cell Research,* 18**,** 268-280.

CHEN, R. H. 2002. BubR1 is essential for kinetochore localization of other spindle checkpoint proteins and its phosphorylation requires Mad1. *J Cell Biol,* 158**,** 487-96.

CHEN, R. H., WATERS, J. C., SALMON, E. D. & MURRAY, A. W. 1996. Association of spindle assembly checkpoint component XMAD2 with unattached kinetochores. *Science,* 274**,** 242-6.

CHIBAZAKURA, T., MCGREW, S. G., COOPER, J. A., YOSHIKAWA, H. & ROBERTS, J. M. 2004. Regulation of cyclin-dependent kinase activity during mitotic exit and maintenance of genome stability by p21, p27, and p107. *Proc Natl Acad Sci U S A,* 101**,** 4465-70.

CHOI, E., ZHANG, X. L., XING, C. & YU, H. T. 2016. Mitotic Checkpoint Regulators Control Insulin Signaling and Metabolic Homeostasis. *Cell,* 166**,** 567-581.

CHOUDHURY, R., BONACCI, T., ARCECI, A., LAHIRI, D., MILLS, C. A., KERNAN, J. L., BRANIGAN, T. B., DECAPRIO, J. A., BURKE, D. J. & EMANUELE, M. J. 2016. APC/C and SCFcyclin F constitute a reciprocal feedback circuit controlling S-phase entry. *Cell reports,* 16**,** 3359-3372.

CHU, R., TERRANO, D. T. & CHAMBERS, T. C. 2012. Cdk1/cyclin B plays a key role in mitotic arrest-induced apoptosis by phosphorylation of Mcl-1, promoting its degradation and freeing Bak from sequestration. *Biochem Pharmacol,* 83**,** 199-206.

CIECHANOVER, A. 2005. Proteolysis: from the lysosome to ubiquitin and the proteasome. *Nat Rev Mol Cell Biol,* 6**,** 79-87.

CILIBERTO, A. & SHAH, J. V. 2009. A quantitative systems view of the spindle assembly checkpoint. *EMBO J,* 28**,** 2162-73.

CLUTE, P. & PINES, J. 1999. Temporal and spatial control of cyclin B1 destruction in metaphase. *Nat Cell Biol,* 1**,** 82-7.

COHEN-FIX, O., PETERS, J. M., KIRSCHNER, M. W. & KOSHLAND, D. 1996. Anaphase initiation in Saccharomyces cerevisiae is controlled by the APC-dependent degradation of the anaphase inhibitor Pds1p. *Genes Dev,* 10**,** 3081-93.

COLLIN, P., NASHCHEKINA, O., WALKER, R. & PINES, J. 2013. The spindle assembly checkpoint works like a rheostat rather than a toggle switch. *Nat Cell Biol,* 15**,** 1378-85.

COOPER, G. M. 2000. *The Cell: A Molecular Approach.,* Sunderland (MA), Sinauer Associates.

COOPER, S. 2004. Is whole-culture synchronization biology's 'perpetual-motion machine'? *Trends Biotechnol,* 22**,** 266-9.

COQUELLE, A., MOUHAMAD, S., PEQUIGNOT, M. O., BRAUN, T., CARVALHO, G., VIVET, S., METIVIER, D., CASTEDO, M. & KROEMER, G. 2006. Enrichment of non-synchronized cells in the G1, S and G2 phases of the cell cycle for the study of apoptosis. *Biochem Pharmacol,* 72**,** 1396-404.

CRASTA, K., HUANG, P., MORGAN, G., WINEY, M. & SURANA, U. 2006. Cdk1 regulates centrosome separation by restraining proteolysis of microtubule-associated proteins. *EMBO J,* 25**,** 2551-63.

DA FONSECA, P. C., KONG, E. H., ZHANG, Z., SCHREIBER, A., WILLIAMS, M. A., MORRIS, E. P. & BARFORD, D. 2011. Structures of APC/C(Cdh1) with substrates identify Cdh1 and Apc10 as the D-box co-receptor. *Nature,* 470**,** 274-8.

DAI, C. L., SHI, J., CHEN, Y., IQBAL, K., LIU, F. & GONG, C. X. 2013. Inhibition of protein synthesis alters protein degradation through activation of protein kinase B (AKT). *J Biol Chem,* 288**,** 23875-83.

DATE, D. A., BURROWS, A. C. & SUMMERS, M. K. 2014. Phosphorylation regulates the p31Comet-mitotic arrest-deficient 2 (Mad2) interaction to promote spindle assembly checkpoint (SAC) activity. *J Biol Chem,* 289**,** 11367-73.

DE ANTONI, A., PEARSON, C. G., CIMINI, D., CANMAN, J. C., SALA, V., NEZI, L., MAPELLI, M., SIRONI, L., FARETTA, M., SALMON, E. D. & MUSACCHIO, A. 2005. The Mad1/Mad2 complex as a template for Mad2 activation in the spindle assembly checkpoint. *Curr Biol,* 15**,** 214-25.

DELANNOY, A., WILHELM, E., EILEBRECHT, S., ALVARADO-CUEVAS, E. M., BENECKE, A. G. & BELL, B. 2018. BIM and NOXA are mitochondrial effectors of TAF6 delta-driven apoptosis. *Cell Death & Disease,* 9.

DESHAIES, R. J. 1999. SCF and Cullin/Ring H2-based ubiquitin ligases. *Annu Rev Cell Dev Biol,* 15**,** 435-67.

DI CESARE, E., VERRICO, A., MIELE, A., GIUBETTINI, M., ROVELLA, P., COLUCCIA, A., FAMIGLINI, V., LA REGINA, G., CUNDARI, E., SILVESTRI, R. & LAVIA, P. 2017. Mitotic cell death induction by targeting the mitotic spindle with tubulin-inhibitory indole derivative molecules. *Oncotarget,* 8**,** 19738-19759.

DIAZ-MARTINEZ, L. A., KARAMYSHEVA, Z. N., WARRINGTON, R., LI, B., WEI, S., XIE, X. J., ROTH, M. G. & YU, H. 2014. Genome-wide siRNA screen reveals coupling between mitotic apoptosis and adaptation. *EMBO J,* 33**,** 1960-76.

DILWORTH, D., GUDAVICIUS, G., XU, X., BOYCE, A. K. J., O'SULLIVAN, C., SERPA, J. J., BILENKY, M., PETROCHENKO, E. V., BORCHERS, C. H., HIRST, M., SWAYNE, L. A., HOWARD, P. & NELSON, C. J. 2018. The prolyl isomerase FKBP25 regulates microtubule polymerization impacting cell cycle progression and genomic stability. *Nucleic Acids Res,* 46**,** 2459-2478.

DOBLES, M. & SORGER, P. K. 2000. Mitotic checkpoints, genetic instability, and cancer. *Cold Spring Harb Symp Quant Biol,* 65**,** 361-8.

DUCA, M., GUIANVARC'H, D., OUSSEDIK, K., HALBY, L., GARBESI, A., DAUZONNE, D., MONNERET, C., OSHEROFF, N., GIOVANNANGELI, C. & ARIMONDO, P. B. 2006. Molecular basis of the targeting of topoisomerase II-mediated DNA cleavage by VP16 derivatives conjugated to triplex-forming oligonucleotides. *Nucleic Acids Res,* 34**,** 1900-11.

DULLA, K. & SANTAMARIA, A. 2011. Large-scale mitotic cell synchronization. *Methods Mol Biol,* 761**,** 65-74.

ELMORE, S. 2007. Apoptosis: a review of programmed cell death. *Toxicol Pathol,* 35**,** 495-516.

EME, L., TRILLES, A., MOREIRA, D. & BROCHIER-ARMANET, C. 2011. The phylogenomic analysis of the anaphase promoting complex and its targets points to complex and modern-like control of the cell cycle in the last common ancestor of eukaryotes. *BMC Evol Biol,* 11**,** 265.

ENNIS, H. L. & LUBIN, M. 1964. Cycloheximide: Aspects of Inhibition of Protein Synthesis in Mammalian Cells. *Science,* 146**,** 1474-6.

EYTAN, E., WANG, K., MINIOWITZ-SHEMTOV, S., SITRY-SHEVAH, D., KAISARI, S., YEN, T. J., LIU, S. T. & HERSHKO, A. 2014. Disassembly of mitotic checkpoint complexes by the joint action of the AAA-ATPase TRIP13 and p31(comet). *Proc Natl Acad Sci U S A,* 111**,** 12019-24.

FANG, G. 2002. Checkpoint protein BubR1 acts synergistically with Mad2 to inhibit anaphase-promoting complex. *Mol Biol Cell,* 13**,** 755-66.

FANG, G., YU, H. & KIRSCHNER, M. W. 1998. The checkpoint protein MAD2 and the mitotic regulator CDC20 form a ternary complex with the anaphase-promoting complex to control anaphase initiation. *Genes Dev,* 12**,** 1871-83.

FISCHER, U., JANICKE, R. U. & SCHULZE-OSTHOFF, K. 2003. Many cuts to ruin: a comprehensive update of caspase substrates. *Cell Death Differ,* 10**,** 76-100.

FITZHARRIS, G. 2012. Anaphase B precedes anaphase A in the mouse egg. *Curr Biol,* 22**,** 437-44.

FOLEY, E. A. & KAPOOR, T. M. 2013. Microtubule attachment and spindle assembly checkpoint signalling at the kinetochore. *Nat Rev Mol Cell Biol,* 14**,** 25-37.

FOSTER, S. A. & MORGAN, D. O. 2012. The APC/C subunit Mnd2/Apc15 promotes Cdc20 autoubiquitination and spindle assembly checkpoint inactivation. *Mol Cell,* 47**,** 921-32.

FRASCHINI, R., BERETTA, A., SIRONI, L., MUSACCHIO, A., LUCCHINI, G. & PIATTI, S. 2001. Bub3 interaction with Mad2, Mad3 and Cdc20 is mediated by WD40 repeats and does not require intact kinetochores. *EMBO J,* 20**,** 6648-59.

FRY, A. M. & YAMANO, H. 2006. APC/C-mediated degradation in early mitosis: how to avoid spindle assembly checkpoint inhibition. *Cell Cycle,* 5**,** 1487-91.

FUNG, T. K. & POON, R. Y. 2005. A roller coaster ride with the mitotic cyclins. *Semin Cell Dev Biol,* 16**,** 335-42.

GASCOIGNE, K. E. & TAYLOR, S. S. 2008. Cancer cells display profound intra- and interline variation following prolonged exposure to antimitotic drugs. *Cancer Cell,* 14**,** 111-22.

GASCOIGNE, K. E. & TAYLOR, S. S. 2009. How do anti-mitotic drugs kill cancer cells? *J Cell Sci,* 122**,** 2579-85.

GASSMANN, R., HOLLAND, A. J., VARMA, D., WAN, X., CIVRIL, F., CLEVELAND, D. W., OEGEMA, K., SALMON, E. D. & DESAI, A. 2010. Removal of Spindly from microtubule-attached kinetochores controls spindle checkpoint silencing in human cells. *Genes Dev,* 24**,** 957-71.

GAUTREY, H. L. & TYSON-CAPPER, A. J. 2012. Regulation of Mcl-1 by SRSF1 and SRSF5 in cancer cells. *PLoS One,* 7**,** e51497.

GENSCHIK, P., CRIQUI, M. C., PARMENTIER, Y., DEREVIER, A. & FLECK, J. 1998. Cell cycle -dependent proteolysis in plants. Identification Of the destruction box pathway and metaphase arrest produced by the proteasome inhibitor mg132. *Plant Cell,* 10**,** 2063-76.

GLOTZER, M., MURRAY, A. W. & KIRSCHNER, M. W. 1991. Cyclin is degraded by the ubiquitin pathway. *Nature,* 349**,** 132-8.

GOLDBERG, A. L. 2003. Protein degradation and protection against misfolded or damaged proteins. *Nature,* 426**,** 895-9.

GOLDENBERG, S. J., CASCIO, T. C., SHUMWAY, S. D., GARBUTT, K. C., LIU, J., XIONG, Y. & ZHENG, N. 2004. Structure of the Cand1-Cul1-Roc1 complex reveals regulatory mechanisms for the assembly of the multisubunit cullin-dependent ubiquitin ligases. *Cell,* 119**,** 517-28.

GOTTESFELD, J. M. & FORBES, D. J. 1997. Mitotic repression of the transcriptional machinery. *Trends Biochem Sci,* 22**,** 197-202.

GOULDING, S. E. & EARNSHAW, W. C. 2005. Shugoshin: a centromeric guardian senses tension. *Bioessays,* 27**,** 588-91.

GRINDE, B. & SEGLEN, P. O. 1980. Differential effects of proteinase inhibitors and amines on the lysosomal and non-lysosomal pathways of protein degradation in isolated rat hepatocytes. *Biochim Biophys Acta,* 632**,** 73-86.

GUARDAVACCARO, D. & PAGANO, M. 2006. Stabilizers and destabilizers controlling cell cycle oscillators. *Mol Cell,* 22**,** 1-4.

GULLBERG, M., GUSTAFSDOTTIR, S. M., SCHALLMEINER, E., JARVIUS, J., BJARNEGARD, M., BETSHOLTZ, C., LANDEGREN, U. & FREDRIKSSON, S. 2004. Cytokine detection by antibody-based proximity ligation. *Proc Natl Acad Sci U S A,* 101**,** 8420-4.

GURLEY, L. R., D'ANNA, J. A., BARHAM, S. S., DEAVEN, L. L. & TOBEY, R. A. 1978. Histone phosphorylation and chromatin structure during mitosis in Chinese hamster cells. *Eur J Biochem,* 84**,** 1-15.

HAASE, J., STEPHENS, A., VERDAASDONK, J., YEH, E. & BLOOM, K. 2012. Bub1 kinase and Sgo1 modulate pericentric chromatin in response to altered microtubule dynamics. *Curr Biol,* 22**,** 471-81.

HABU, T., KIM, S. H., WEINSTEIN, J. & MATSUMOTO, T. 2002. Identification of a MAD2-binding protein, CMT2, and its role in mitosis. *EMBO J,* 21**,** 6419-28.

HABU, T. & MATSUMOTO, T. 2013. p31(comet) inactivates the chemically induced Mad2-dependent spindle assembly checkpoint and leads to resistance to anti-mitotic drugs. *Springerplus,* 2**,** 562.

HAGAN, R. S., MANAK, M. S., BUCH, H. K., MEIER, M. G., MERALDI, P., SHAH, J. V. & SORGER, P. K. 2011. p31(comet) acts to ensure timely spindle checkpoint silencing subsequent to kinetochore attachment. *Mol Biol Cell,* 22**,** 4236-46.

HAGTING, A., JACKMAN, M., SIMPSON, K. & PINES, J. 1999. Translocation of cyclin B1 to the nucleus at prophase requires a phosphorylation-dependent nuclear import signal. *Current Biology,* 9**,** 680-689.

HAN, K. Y., CHANG, J. H., DUGAS-FORD, J., ALEXANDER, J. S. & AZAR, D. T. 2014. Involvement of lysosomal degradation in VEGF-C-induced down-regulation of VEGFR-3. *FEBS Lett,* 588**,** 4357-63.

HANS, F. & DIMITROV, S. 2001. Histone H3 phosphorylation and cell division. *Oncogene,* 20**,** 3021-7.

HARAGUCHI, T., KANEDA, T. & HIRAOKA, Y. 1997. Dynamics of chromosomes and microtubules visualized by multiple-wavelength fluorescence imaging in living mammalian cells: effects of mitotic inhibitors on cell cycle progression. *Genes Cells,* 2**,** 369-80.

HARASHIMA, H., DISSMEYER, N. & SCHNITTGER, A. 2013. Cell cycle control across the eukaryotic kingdom. *Trends Cell Biol,* 23**,** 345-56.

HARDWICK, K. G., JOHNSTON, R. C., SMITH, D. L. & MURRAY, A. W. 2000. MAD3 encodes a novel component of the spindle checkpoint which interacts with Bub3p, Cdc20p, and Mad2p. *J Cell Biol,* 148**,** 871-82.

HARDWICK, K. G., WEISS, E., LUCA, F. C., WINEY, M. & MURRAY, A. W. 1996. Activation of the budding yeast spindle assembly checkpoint without mitotic spindle disruption. *Science,* 273**,** 953-6.

HARLEY, M. E., ALLAN, L. A., SANDERSON, H. S. & CLARKE, P. R. 2010. Phosphorylation of Mcl-1 by CDK1-cyclin B1 initiates its Cdc20-dependent destruction during mitotic arrest. *EMBO J,* 29**,** 2407-20.

HARPER, J. V. 2005. Synchronization of cell populations in G1/S and G2/M phases of the cell cycle. *Methods Mol Biol,* 296**,** 157-66.

HASCHKA, M. D., SORATROI, C., KIRSCHNEK, S., HACKER, G., HILBE, R., GELEY, S., VILLUNGER, A. & FAVA, L. L. 2015. The NOXA-MCL1-BIM axis defines lifespan on extended mitotic arrest. *Nat Commun,* 6**,** 6891.

HAUF, S., COLE, R. W., LATERRA, S., ZIMMER, C., SCHNAPP, G., WALTER, R., HECKEL, A., VAN MEEL, J., RIEDER, C. L. & PETERS, J. M. 2003. The small molecule Hesperadin reveals a role for Aurora B in correcting kinetochore-microtubule attachment and in maintaining the spindle assembly checkpoint. *J Cell Biol,* 161**,** 281-94.

HENDZEL, M. J., WEI, Y., MANCINI, M. A., VAN HOOSER, A., RANALLI, T., BRINKLEY, B. R., BAZETT-JONES, D. P. & ALLIS, C. D. 1997. Mitosis-specific phosphorylation of histone H3 initiates primarily within pericentromeric heterochromatin during G2 and spreads in an ordered fashion coincident with mitotic chromosome condensation. *Chromosoma,* 106**,** 348-60.

HERMANIDES, J., VRIESENDORP, T. M., BOSMAN, R. J., ZANDSTRA, D. F., HOEKSTRA, J. B. & DEVRIES, J. H. 2010. Glucose variability is associated with intensive care unit mortality. *Crit Care Med,* 38**,** 838-42.

HERZOG, F., PRIMORAC, I., DUBE, P., LENART, P., SANDER, B., MECHTLER, K., STARK, H. & PETERS, J. M. 2009. Structure of the anaphase-promoting complex/cyclosome interacting with a mitotic checkpoint complex. *Science,* 323**,** 1477-81.

HEWITT, L., TIGHE, A., SANTAGUIDA, S., WHITE, A. M., JONES, C. D., MUSACCHIO, A., GREEN, S. & TAYLOR, S. S. 2010. Sustained Mps1 activity is required in mitosis to recruit O-Mad2 to the Mad1-C-Mad2 core complex. *J Cell Biol,* 190**,** 25-34.

HOFFMAN, D. B., PEARSON, C. G., YEN, T. J., HOWELL, B. J. & SALMON, E. D. 2001. Microtubule-dependent changes in assembly of microtubule motor proteins and mitotic spindle checkpoint proteins at PtK1 kinetochores. *Mol Biol Cell,* 12**,** 1995-2009.

HOLLAND, A. J. & CLEVELAND, D. W. 2008. Beyond genetics: surprising determinants of cell fate in antitumor drugs. *Cancer Cell,* 14**,** 103-5.

HORWITZ, S. B. 1994. Taxol (paclitaxel): mechanisms of action. *Ann Oncol,* 5 Suppl 6**,** S3-6.

HOWELL, B. J., HOFFMAN, D. B., FANG, G., MURRAY, A. W. & SALMON, E. D. 2000. Visualization of Mad2 dynamics at kinetochores, along spindle fibers, and at spindle poles in living cells. *J Cell Biol,* 150**,** 1233-50.

HOWELL, B. J., MCEWEN, B. F., CANMAN, J. C., HOFFMAN, D. B., FARRAR, E. M., RIEDER, C. L. & SALMON, E. D. 2001. Cytoplasmic dynein/dynactin drives kinetochore protein transport to the spindle poles and has a role in mitotic spindle checkpoint inactivation. *J Cell Biol,* 155**,** 1159-72.

HOWELL, B. J., MOREE, B., FARRAR, E. M., STEWART, S., FANG, G. & SALMON, E. D. 2004. Spindle checkpoint protein dynamics at kinetochores in living cells. *Curr Biol,* 14**,** 953-64.

HOYT, M. A., TOTIS, L. & ROBERTS, B. T. 1991. S. cerevisiae genes required for cell cycle arrest in response to loss of microtubule function. *Cell,* 66**,** 507-17.

HU, H., TAN, C., LIU, X., LUO, F. & LI, K. 2015. Upregulation of the MCL-1S protein variant following dihydroartemisinin treatment induces apoptosis in cholangiocarcinoma cells. *Oncol Lett,* 10**,** 3545-3550.

HUANG, J. & RAFF, J. W. 1999. The disappearance of cyclin B at the end of mitosis is regulated spatially in Drosophila cells. *EMBO J,* 18**,** 2184-95.

HWANG, L. H., LAU, L. F., SMITH, D. L., MISTROT, C. A., HARDWICK, K. G., HWANG, E. S., AMON, A. & MURRAY, A. W. 1998. Budding yeast Cdc20: a target of the spindle checkpoint. *Science,* 279**,** 1041-4.

INGELS, C., VANHOREBEEK, I. & VAN DEN BERGHE, G. 2018. Glucose homeostasis, nutrition and infections during critical illness. *Clin Microbiol Infect,* 24**,** 10-15.

INUZUKA, H., FUKUSHIMA, H., SHAIK, S., LIU, P., LAU, A. W. & WEI, W. 2011a. Mcl-1 ubiquitination and destruction. *Oncotarget,* 2**,** 239-44.

INUZUKA, H., SHAIK, S., ONOYAMA, I., GAO, D. M., TSENG, A., MASER, R. S., ZHAI, B., WAN, L. X., GUTIERREZ, A., LAU, A. W., XIAO, Y. H., CHRISTIE, A. L., ASTER, J., SETTLEMAN, J., GYGI, S. P., KUNG, A. L., LOOK, T., NAKAYAMA, K. I., DEPINHO, R. A. & WEI, W. Y. 2011b. SCFFBW7 regulates cellular apoptosis by targeting MCL1 for ubiquitylation and destruction. *Nature,* 471**,** 104-U128.

ITO, M. 2000. Factors controlling cyclin B expression. *Plant Mol Biol,* 43**,** 677-90.

IZAWA, D. & PINES, J. 2011. How APC/C-Cdc20 changes its substrate specificity in mitosis. *Nat Cell Biol,* 13**,** 223-33.

IZAWA, D. & PINES, J. 2012. Mad2 and the APC/C compete for the same site on Cdc20 to ensure proper chromosome segregation. *J Cell Biol,* 199**,** 27-37.

IZAWA, D. & PINES, J. 2015. The mitotic checkpoint complex binds a second CDC20 to inhibit active APC/C. *Nature,* 517**,** 631-4.

JACKMAN, M., LINDON, C., NIGG, E. A. & PINES, J. 2003. Active cyclin B1-Cdk1 first appears on centrosomes in prophase. *Nat Cell Biol,* 5**,** 143-8.

JANG, J. K., MESSINA, L., ERDMAN, M. B., ARBEL, T. & HAWLEY, R. S. 1995. Induction of metaphase arrest in Drosophila oocytes by chiasma-based kinetochore tension. *Science,* 268**,** 1917-9.

JANICKE, R. U. 2009. MCF-7 breast carcinoma cells do not express caspase-3. *Breast Cancer Res Treat,* 117**,** 219-21.

JANICKE, R. U., NG, P., SPRENGART, M. L. & PORTER, A. G. 1998. Caspase-3 is required for alpha-fodrin cleavage but dispensable for cleavage of other death substrates in apoptosis. *J Biol Chem,* 273**,** 15540-5.

JANSSEN, A., KOPS, G. J. & MEDEMA, R. H. 2011. Targeting the mitotic checkpoint to kill tumor cells. *Horm Cancer,* 2**,** 113-6.

JANSSEN, A. & MEDEMA, R. H. 2011. Mitosis as an anti-cancer target. *Oncogene,* 30**,** 2799-809.

JARVIUS, M., PAULSSON, J., WEIBRECHT, I., LEUCHOWIUS, K. J., ANDERSSON, A. C., WAHLBY, C., GULLBERG, M., BOTLING, J., SJOBLOM, T., MARKOVA, B., OSTMAN, A., LANDEGREN, U. & SODERBERG, O. 2007. In situ detection of phosphorylated platelet-derived growth factor receptor beta using a generalized proximity ligation method. *Mol Cell Proteomics,* 6**,** 1500-9.

JIA, L., KIM, S. & YU, H. 2013. Tracking spindle checkpoint signals from kinetochores to APC/C. *Trends Biochem Sci,* 38**,** 302-11.

JIA, L., LI, B., WARRINGTON, R. T., HAO, X., WANG, S. & YU, H. 2011. Defining pathways of spindle checkpoint silencing: functional redundancy between Cdc20 ubiquitination and p31(comet). *Mol Biol Cell,* 22**,** 4227-35.

JIN, F. Z. & WANG, Y. C. 2013. The signaling network that silences the spindle assembly checkpoint upon the establishment of chromosome bipolar attachment. *Proceedings of the National Academy of Sciences of the United States of America,* 110**,** 21036-21041.

JOHNSON, D. G. & WALKER, C. L. 1999. Cyclins and cell cycle checkpoints. *Annu Rev Pharmacol Toxicol,* 39**,** 295-312.

JOHNSON, V. L., SCOTT, M. I., HOLT, S. V., HUSSEIN, D. & TAYLOR, S. S. 2004. Bub1 is required for kinetochore localization of BubR1, Cenp-E, Cenp-F and Mad2, and chromosome congression. *J Cell Sci,* 117**,** 1577-89.

JORDAN, M. A., THROWER, D. & WILSON, L. 1992. Effects of vinblastine, podophyllotoxin and nocodazole on mitotic spindles. Implications for the role of microtubule dynamics in mitosis. *J Cell Sci,* 102 (Pt 3)**,** 401-16.

JORDAN, M. A. & WILSON, L. 2004. Microtubules as a target for anticancer drugs. *Nat Rev Cancer,* 4**,** 253-65.

KALITSIS, P., EARLE, E., FOWLER, K. J. & CHOO, K. H. 2000. Bub3 gene disruption in mice reveals essential mitotic spindle checkpoint function during early embryogenesis. *Genes Dev,* 14**,** 2277-82.

KALLIO, M. J., BEARDMORE, V. A., WEINSTEIN, J. & GORBSKY, G. J. 2002. Rapid microtubule-independent dynamics of Cdc20 at kinetochores and centrosomes in mammalian cells. *J Cell Biol,* 158**,** 841-7.

KANDA, T., SULLIVAN, K. F. & WAHL, G. M. 1998. Histone-GFP fusion protein enables sensitive analysis of chromosome dynamics in living mammalian cells. *Curr Biol,* 8**,** 377-85.

KANG, J., CHEN, Y., ZHAO, Y. & YU, H. 2007. Autophosphorylation-dependent activation of human Mps1 is required for the spindle checkpoint. *Proc Natl Acad Sci U S A,* 104**,** 20232-7.

KARESS, R. 2005. Rod-Zw10-Zwilch: a key player in the spindle checkpoint. *Trends Cell Biol,* 15**,** 386-92.

KARESS, R. E. & GLOVER, D. M. 1989. rough deal: a gene required for proper mitotic segregation in Drosophila. *J Cell Biol,* 109**,** 2951-61.

KASTL, J., BRAUN, J., PRESTEL, A., MOLLER, H. M., HUHN, T. & MAYER, T. U. 2015. Mad2 Inhibitor-1 (M2I-1): A Small Molecule Protein-Protein Interaction Inhibitor Targeting the Mitotic Spindle Assembly Checkpoint. *ACS Chem Biol,* 10**,** 1661-6.

KASUBOSKI, J. M., BADER, J. R., VAUGHAN, P. S., TAUHATA, S. B., WINDING, M., MORRISSEY, M. A., JOYCE, M. V., BOGGESS, W., VOS, L., CHAN, G. K., HINCHCLIFFE, E. H. & VAUGHAN, K. T. 2011. Zwint-1 is a novel Aurora B substrate required for the assembly of a dynein-binding platform on kinetochores. *Mol Biol Cell,* 22**,** 3318-30.

KAUFMANN, S. H., DESNOYERS, S., OTTAVIANO, Y., DAVIDSON, N. E. & POIRIER, G. G. 1993. Specific proteolytic cleavage of poly(ADP-ribose) polymerase: an early marker of chemotherapy-induced apoptosis. *Cancer Res,* 53**,** 3976-85.

KAWABATA, T., TANIMURA, S., ASAI, K., KAWASAKI, R., MATSUMARU, Y. & KOHNO, M. 2012. Up-regulation of pro-apoptotic protein Bim and down-regulation of anti-apoptotic protein Mcl-1 cooperatively mediate enhanced tumor cell death induced by the combination of ERK kinase (MEK) inhibitor and microtubule inhibitor. *J Biol Chem,* 287**,** 10289-300.

KERR, J. F., WYLLIE, A. H. & CURRIE, A. R. 1972. Apoptosis: a basic biological phenomenon with wide-ranging implications in tissue kinetics. *Br J Cancer,* 26**,** 239-57.

KHANNA, K. K. & JACKSON, S. P. 2001. DNA double-strand breaks: signaling, repair and the cancer connection. *Nat Genet,* 27**,** 247-54.

KIMATA, Y., BAXTER, J. E., FRY, A. M. & YAMANO, H. 2008. A role for the Fizzy/Cdc20 family of proteins in activation of the APC/C distinct from substrate recruitment. *Mol Cell,* 32**,** 576-83.

KING, J. M. & NICKLAS, R. B. 2000. Tension on chromosomes increases the number of kinetochore microtubules but only within limits. *J Cell Sci,* 113 Pt 21**,** 3815-23.

KISSELEV, A. F. & GOLDBERG, A. L. 2001. Proteasome inhibitors: from research tools to drug candidates. *Chem Biol,* 8**,** 739-58.

KITAGAWA, R. 2009. The spindle assembly checkpoint in Caenorhabditis elegans: one who lacks Mad1 becomes mad one. *Cell Cycle,* 8**,** 338-44.

KLEBIG, C., KORINTH, D. & MERALDI, P. 2009. Bub1 regulates chromosome segregation in a kinetochore-independent manner. *J Cell Biol,* 185**,** 841-58.

KOFF, A., GIORDANO, A., DESAI, D., YAMASHITA, K., HARPER, J. W., ELLEDGE, S., NISHIMOTO, T., MORGAN, D. O., FRANZA, B. R. & ROBERTS, J. M. 1992. Formation and activation of a cyclin E-cdk2 complex during the G1 phase of the human cell cycle. *Science,* 257**,** 1689-94.

KOPS, G. J., WEAVER, B. A. & CLEVELAND, D. W. 2005. On the road to cancer: aneuploidy and the mitotic checkpoint. *Nat Rev Cancer,* 5**,** 773-85.

KRINSLEY, J. S. 2008a. Glycemic variability: a strong independent predictor of mortality in critically ill patients. *Crit Care Med,* 36**,** 3008-13.

KRINSLEY, J. S. 2008b. The severity of sepsis: yet another factor influencing glycemic control. *Crit Care,* 12**,** 194.

KRUSE, T., LARSEN, M. S., SEDGWICK, G. G., SIGURDSSON, J. O., STREICHER, W., OLSEN, J. V. & NILSSON, J. 2014. A direct role of Mad1 in the spindle assembly checkpoint beyond Mad2 kinetochore recruitment. *EMBO Rep,* 15**,** 282-90.

KUILMAN, T., MICHALOGLOU, C., MOOI, W. J. & PEEPER, D. S. 2010. The essence of senescence. *Genes Dev,* 24**,** 2463-79.

KULUKIAN, A., HAN, J. S. & CLEVELAND, D. W. 2009. Unattached kinetochores catalyze production of an anaphase inhibitor that requires a Mad2 template to prime Cdc20 for BubR1 binding. *Dev Cell,* 16**,** 105-17.

LARA-GONZALEZ, P., SCOTT, M. I., DIEZ, M., SEN, O. & TAYLOR, S. S. 2011. BubR1 blocks substrate recruitment to the APC/C in a KEN-box-dependent manner. *J Cell Sci,* 124**,** 4332-45.

LARA-GONZALEZ, P., WESTHORPE, F. G. & TAYLOR, S. S. 2012. The spindle assembly checkpoint. *Curr Biol,* 22**,** R966-80.

LARSEN, N. A., AL-BASSAM, J., WEI, R. R. & HARRISON, S. C. 2007. Structural analysis of Bub3 interactions in the mitotic spindle checkpoint. *Proc Natl Acad Sci U S A,* 104**,** 1201-6.

LARSEN, N. A. & HARRISON, S. C. 2004. Crystal structure of the spindle assembly checkpoint protein Bub3. *J Mol Biol,* 344**,** 885-92.

LEE, S. H., STERLING, H., BURLINGAME, A. & MCCORMICK, F. 2008. Tpr directly binds to Mad1 and Mad2 and is important for the Mad1-Mad2-mediated mitotic spindle checkpoint. *Genes Dev,* 22**,** 2926-31.

LENS, S. M., WOLTHUIS, R. M., KLOMPMAKER, R., KAUW, J., AGAMI, R., BRUMMELKAMP, T., KOPS, G. & MEDEMA, R. H. 2003. Survivin is required for a sustained spindle checkpoint arrest in response to lack of tension. *EMBO J,* 22**,** 2934-47.

LEW, D. J. & BURKE, D. J. 2003. The spindle assembly and spindle position checkpoints. *Annu Rev Genet,* 37**,** 251-82.

LI, D., MORLEY, G., WHITAKER, M. & HUANG, J. Y. 2010. Recruitment of Cdc20 to the kinetochore requires BubR1 but not Mad2 in Drosophila melanogaster. *Mol Cell Biol,* 30**,** 3384-95.

LI, J., DANG, N., WOOD, D. J. & HUANG, J. Y. 2017. The kinetochore-dependent and -independent formation of the CDC20-MAD2 complex and its functions in HeLa cells. *Sci Rep,* 7**,** 41072.

LI, R. & MURRAY, A. W. 1991. Feedback control of mitosis in budding yeast. *Cell,* 66**,** 519-31.

LI, X. & NICKLAS, R. B. 1995. Mitotic forces control a cell-cycle checkpoint. *Nature,* 373**,** 630-2.

LI, Y. & BENEZRA, R. 1996. Identification of a human mitotic checkpoint gene: hsMAD2. *Science,* 274**,** 246-8.

LINDQVIST, A., VAN ZON, W., KARLSSON ROSENTHAL, C. & WOLTHUIS, R. M. 2007. Cyclin B1-Cdk1 activation continues after centrosome separation to control mitotic progression. *PLoS Biol,* 5**,** e123.

LIU, S. T. & ZHANG, H. 2016. The mitotic checkpoint complex (MCC): looking back and forth after 15 years. *AIMS Mol Sci,* 3**,** 597-634.

LIU, X. & WINEY, M. 2012. The MPS1 family of protein kinases. *Annual review of biochemistry,* 81**,** 561-585.

LODISH H, B. A., ZIPURSKY SL, ET AL 2000. *Molecular Cell Biology. 4th edition,* New York, W. H. Freeman.

LOGARINHO, E., BOUSBAA, H., DIAS, J. M., LOPES, C., AMORIM, I., ANTUNES-MARTINS, A. & SUNKEL, C. E. 2004. Different spindle checkpoint proteins monitor microtubule attachment and tension at kinetochores in Drosophila cells. *J Cell Sci,* 117**,** 1757-71.

LOHKA, M. J., HAYES, M. K. & MALLER, J. L. 1988. Purification of maturation-promoting factor, an intracellular regulator of early mitotic events. *Proc Natl Acad Sci U S A,* 85**,** 3009-13.

LOMONOSOVA, E., RYERSE, J. & CHINNADURAI, G. 2009. BAX/BAK-independent mitoptosis during cell death induced by proteasome inhibition? *Mol Cancer Res,* 7**,** 1268-84.

LONDON, N., CETO, S., RANISH, J. A. & BIGGINS, S. 2012. Phosphoregulation of Spc105 by Mps1 and PP1 regulates Bub1 localization to kinetochores. *Curr Biol,* 22**,** 900-6.

LOPES, N. M., ADAMS, E. G., PITTS, T. W. & BHUYAN, B. K. 1993. Cell kill kinetics and cell cycle effects of taxol on human and hamster ovarian cell lines. *Cancer Chemother Pharmacol,* 32**,** 235-42.

LUO, X., FANG, G., COLDIRON, M., LIN, Y., YU, H., KIRSCHNER, M. W. & WAGNER, G. 2000. Structure of the Mad2 spindle assembly checkpoint protein and its interaction with Cdc20. *Nat Struct Biol,* 7**,** 224-9.

LUO, X., TANG, Z., RIZO, J. & YU, H. 2002. The Mad2 spindle checkpoint protein undergoes similar major conformational changes upon binding to either Mad1 or Cdc20. *Mol Cell,* 9**,** 59-71.

LUO, X., TANG, Z., XIA, G., WASSMANN, K., MATSUMOTO, T., RIZO, J. & YU, H. 2004. The Mad2 spindle checkpoint protein has two distinct natively folded states. *Nat Struct Mol Biol,* 11**,** 338-45.

LUO, X. & YU, H. 2008. Protein metamorphosis: the two-state behavior of Mad2. *Structure,* 16**,** 1616-25.

MA, H. T., CHAN, Y. Y., CHEN, X., ON, K. F. & POON, R. Y. 2012. Depletion of p31comet protein promotes sensitivity to antimitotic drugs. *J Biol Chem,* 287**,** 21561-9.

MA, H. T. & POON, R. Y. C. 2016. TRIP13 Regulates Both the Activation and Inactivation of the Spindle-Assembly Checkpoint. *Cell Rep,* 14**,** 1086-1099.

MACIEJOWSKI, J., GEORGE, K. A., TERRET, M. E., ZHANG, C., SHOKAT, K. M. & JALLEPALLI, P. V. 2010. Mps1 directs the assembly of Cdc20 inhibitory complexes during interphase and mitosis to control M phase timing and spindle checkpoint signaling. *J Cell Biol,* 190**,** 89-100.

MAGIDSON, V., HE, J., AULT, J. G., O'CONNELL, C. B., YANG, N., TIKHONENKO, I., MCEWEN, B. F., SUI, H. & KHODJAKOV, A. 2016. Unattached kinetochores rather than intrakinetochore tension arrest mitosis in taxol-treated cells. *J Cell Biol,* 212**,** 307-19.

MAIATO, H., DELUCA, J., SALMON, E. D. & EARNSHAW, W. C. 2004. The dynamic kinetochore-microtubule interface. *J Cell Sci,* 117**,** 5461-77.

MAIATO, H. & LINCE-FARIA, M. 2010. The perpetual movements of anaphase. *Cell Mol Life Sci,* 67**,** 2251-69.

MAIATO, H. & SUNKEL, C. E. 2004. Kinetochore-microtubule interactions during cell division. *Chromosome Res,* 12**,** 585-97.

MALDONADO, M. & KAPOOR, T. M. 2011. Constitutive Mad1 targeting to kinetochores uncouples checkpoint signalling from chromosome biorientation. *Nat Cell Biol,* 13**,** 475-82.

MALUREANU, L. A., JEGANATHAN, K. B., HAMADA, M., WASILEWSKI, L., DAVENPORT, J. & VAN DEURSEN, J. M. 2009. BubR1 N terminus acts as a soluble inhibitor of cyclin B degradation by APC/C(Cdc20) in interphase. *Dev Cell,* 16**,** 118-31.

MANIC, G., CORRADI, F., SISTIGU, A., SITENI, S. & VITALE, I. 2017. Molecular Regulation of the Spindle Assembly Checkpoint by Kinases and Phosphatases. *Int Rev Cell Mol Biol,* 328**,** 105-161.

MAO, Y., ABRIEU, A. & CLEVELAND, D. W. 2003. Activating and silencing the mitotic checkpoint through CENP-E-dependent activation/inactivation of BubR1. *Cell,* 114**,** 87-98.

MAPELLI, M., FILIPP, F. V., RANCATI, G., MASSIMILIANO, L., NEZI, L., STIER, G., HAGAN, R. S., CONFALONIERI, S., PIATTI, S., SATTLER, M. & MUSACCHIO, A. 2006. Determinants of conformational dimerization of Mad2 and its inhibition by p31comet. *EMBO J,* 25**,** 1273-84.

MAPELLI, M., MASSIMILIANO, L., SANTAGUIDA, S. & MUSACCHIO, A. 2007. The Mad2 conformational dimer: structure and implications for the spindle assembly checkpoint. *Cell,* 131**,** 730-43.

MAPELLI, M. & MUSACCHIO, A. 2007. MAD contortions: conformational dimerization boosts spindle checkpoint signaling. *Curr Opin Struct Biol,* 17**,** 716-25.

MARESCA, T. J. & SALMON, E. D. 2010. Welcome to a new kind of tension: translating kinetochore mechanics into a wait-anaphase signal. *J Cell Sci,* 123**,** 825-35.

MARIK, P. E. 2016. Tight glycemic control in acutely ill patients: low evidence of benefit, high evidence of harm! *Intensive Care Med,* 42**,** 1475-7.

MARTINEZ-VICENTE, M., SOVAK, G. & CUERVO, A. M. 2005. Protein degradation and aging. *Exp Gerontol,* 40**,** 622-33.

MASUI, Y. 2001. From oocyte maturation to the in vitro cell cycle: the history of discoveries of Maturation-Promoting Factor (MPF) and Cytostatic Factor (CSF). *Differentiation,* 69**,** 1-17.

MATSON, D. R. & STUKENBERG, P. T. 2011. Spindle poisons and cell fate: a tale of two pathways. *Mol Interv,* 11**,** 141-50.

MATSUI, Y., NAKAYAMA, Y., OKAMOTO, M., FUKUMOTO, Y. & YAMAGUCHI, N. 2012. Enrichment of cell populations in metaphase, anaphase, and telophase by synchronization using nocodazole and blebbistatin: a novel method suitable for examining dynamic changes in proteins during mitotic progression. *Eur J Cell Biol,* 91**,** 413-9.

MCGROGAN, B. T., GILMARTIN, B., CARNEY, D. N. & MCCANN, A. 2008. Taxanes, microtubules and chemoresistant breast cancer. *Biochim Biophys Acta,* 1785**,** 96-132.

MCKINLEY, K. L. & CHEESEMAN, I. M. 2017. Large-Scale Analysis of CRISPR/Cas9 Cell-Cycle Knockouts Reveals the Diversity of p53-Dependent Responses to Cell-Cycle Defects. *Dev Cell,* 40**,** 405-420 e2.

MERALDI, P., DRAVIAM, V. M. & SORGER, P. K. 2004. Timing and checkpoints in the regulation of mitotic progression. *Dev Cell,* 7**,** 45-60.

MILLBAND, D. N. & HARDWICK, K. G. 2002. Fission yeast Mad3p is required for Mad2p to inhibit the anaphase-promoting complex and localizes to kinetochores in a Bub1p-, Bub3p-, and Mph1p-dependent manner. *Mol Cell Biol,* 22**,** 2728-42.

MINIOWITZ-SHEMTOV, S., EYTAN, E., GANOTH, D., SITRY-SHEVAH, D., DUMIN, E. & HERSHKO, A. 2012. Role of phosphorylation of Cdc20 in p31(comet)-stimulated disassembly of the mitotic checkpoint complex. *Proc Natl Acad Sci U S A,* 109**,** 8056-60.

MINIOWITZ-SHEMTOV, S., TEICHNER, A., SITRY-SHEVAH, D. & HERSHKO, A. 2010. ATP is required for the release of the anaphase-promoting complex/cyclosome from inhibition by the mitotic checkpoint. *Proc Natl Acad Sci U S A,* 107**,** 5351-6.

MISCHE, S., HE, Y., MA, L., LI, M., SERR, M. & HAYS, T. S. 2008. Dynein light intermediate chain: an essential subunit that contributes to spindle checkpoint inactivation. *Mol Biol Cell,* 19**,** 4918-29.

MOCCIARO, A. & RAPE, M. 2012. Emerging regulatory mechanisms in ubiquitin-dependent cell cycle control. *J Cell Sci,* 125**,** 255-63.

MODRIANSKY, M. & DVORAK, Z. 2005. Microtubule disruptors and their interaction with biotransformation enzymes. *Biomed Pap Med Fac Univ Palacky Olomouc Czech Repub,* 149**,** 213-5.

MOLLINEDO, F. & GAJATE, C. 2003. Microtubules, microtubule-interfering agents and apoptosis. *Apoptosis,* 8**,** 413-50.

MORROW, C. J., TIGHE, A., JOHNSON, V. L., SCOTT, M. I., DITCHFIELD, C. & TAYLOR, S. S. 2005. Bub1 and aurora B cooperate to maintain BubR1-mediated inhibition of APC/CCdc20. *J Cell Sci,* 118**,** 3639-52.

MURRAY, A. 1994. Cell cycle checkpoints. *Curr Opin Cell Biol,* 6**,** 872-6.

MUSACCHIO, A. 2015. The Molecular Biology of Spindle Assembly Checkpoint Signaling Dynamics. *Curr Biol,* 25**,** R1002-18.

MUSACCHIO, A. & HARDWICK, K. G. 2002. The spindle checkpoint: structural insights into dynamic signalling. *Nat Rev Mol Cell Biol,* 3**,** 731-41.

MUSACCHIO, A. & SALMON, E. D. 2007. The spindle-assembly checkpoint in space and time. *Nat Rev Mol Cell Biol,* 8**,** 379-93.

NASMYTH, K. 2005. How might cohesin hold sister chromatids together? *Philos Trans R Soc Lond B Biol Sci,* 360**,** 483-96.

NASMYTH, K. & HAERING, C. H. 2009. Cohesin: its roles and mechanisms. *Annu Rev Genet,* 43**,** 525-58.

NICKLAS, R. B. & WARD, S. C. 1994. Elements of error correction in mitosis: microtubule capture, release, and tension. *J Cell Biol,* 126**,** 1241-53.

NIIKURA, Y., DIXIT, A., SCOTT, R., PERKINS, G. & KITAGAWA, K. 2007. BUB1 mediation of caspase-independent mitotic death determines cell fate. *J Cell Biol,* 178**,** 283-96.

NILSSON, J., YEKEZARE, M., MINSHULL, J. & PINES, J. 2008. The APC/C maintains the spindle assembly checkpoint by targeting Cdc20 for destruction. *Nat Cell Biol,* 10**,** 1411-20.

NOATYNSKA, A., GOTTA, M. & MERALDI, P. 2012. Mitotic spindle (DIS)orientation and DISease: cause or consequence? *J Cell Biol,* 199**,** 1025-35.

NURSE, P. 2000. A long twentieth century of the cell cycle and beyond. *Cell,* 100**,** 71-8.

ODA, E., OHKI, R., MURASAWA, H., NEMOTO, J., SHIBUE, T., YAMASHITA, T., TOKINO, T., TANIGUCHI, T. & TANAKA, N. 2000. Noxa, a BH3-only member of the Bcl-2 family and candidate mediator of p53-induced apoptosis. *Science,* 288**,** 1053-8.

PAN, J. & CHEN, R. H. 2004. Spindle checkpoint regulates Cdc20p stability in Saccharomyces cerevisiae. *Genes Dev,* 18**,** 1439-51.

PANGILINAN, F. & SPENCER, F. 1996. Abnormal kinetochore structure activates the spindle assembly checkpoint in budding yeast. *Mol Biol Cell,* 7**,** 1195-208.

PAULSON, J. R. & TAYLOR, S. S. 1982. Phosphorylation of histones 1 and 3 and nonhistone high mobility group 14 by an endogenous kinase in HeLa metaphase chromosomes. *J Biol Chem,* 257**,** 6064-72.

PEDLEY, R. & GILMORE, A. P. 2016. Mitosis and mitochondrial priming for apoptosis. *Biol Chem,* 397**,** 595-605.

PFLEGER, C. M. & KIRSCHNER, M. W. 2000. The KEN box: an APC recognition signal distinct from the D box targeted by Cdh1. *Genes Dev,* 14**,** 655-65.

PINSKY, B. A. & BIGGINS, S. 2005. The spindle checkpoint: tension versus attachment. *Trends Cell Biol,* 15**,** 486-93.

PODDAR, A., STUKENBERG, P. T. & BURKE, D. J. 2005. Two complexes of spindle checkpoint proteins containing Cdc20 and Mad2 assemble during mitosis independently of the kinetochore in Saccharomyces cerevisiae. *Eukaryot Cell,* 4**,** 867-78.

PREECHASUK, L., SUWANSAKSRI, N., IPICHART, N., VANNASAENG, S., PERMPIKUL, C. & SRIWIJITKAMOL, A. 2017. Hyperglycemia and glycemic variability are associated with the severity of sepsis in nondiabetic subjects. *J Crit Care,* 38**,** 319-323.

PRINZ, S., HWANG, E. S., VISINTIN, R. & AMON, A. 1998. The regulation of Cdc20 proteolysis reveals a role for APC components Cdc23 and Cdc27 during S phase and early mitosis. *Curr Biol,* 8**,** 750-60.

QIAO, R., WEISSMANN, F., YAMAGUCHI, M., BROWN, N. G., VANDERLINDEN, R., IMRE, R., JARVIS, M. A., BRUNNER, M. R., DAVIDSON, I. F., LITOS, G., HASELBACH, D., MECHTLER, K., STARK, H., SCHULMAN, B. A. & PETERS, J. M. 2016. Mechanism of APC/CCDC20 activation by mitotic phosphorylation. *Proc Natl Acad Sci U S A,* 113**,** E2570-8.

RAFF, J. W., JEFFERS, K. & HUANG, J. Y. 2002. The roles of Fzy/Cdc20 and Fzr/Cdh1 in regulating the destruction of cyclin B in space and time. *J Cell Biol,* 157**,** 1139-49.

REDDY, S. K., RAPE, M., MARGANSKY, W. A. & KIRSCHNER, M. W. 2007. Ubiquitination by the anaphase-promoting complex drives spindle checkpoint inactivation. *Nature,* 446**,** 921-5.

RIEDER, C. L., COLE, R. W., KHODJAKOV, A. & SLUDER, G. 1995. The checkpoint delaying anaphase in response to chromosome monoorientation is mediated by an inhibitory signal produced by unattached kinetochores. *J Cell Biol,* 130**,** 941-8.

RIEDER, C. L. & MAIATO, H. 2004. Stuck in division or passing through: what happens when cells cannot satisfy the spindle assembly checkpoint. *Dev Cell,* 7**,** 637-51.

RIEDER, C. L., SCHULTZ, A., COLE, R. & SLUDER, G. 1994. Anaphase onset in vertebrate somatic cells is controlled by a checkpoint that monitors sister kinetochore attachment to the spindle. *J Cell Biol,* 127**,** 1301-10.

RODRIGUE, A., COULOMBE, Y., JACQUET, K., GAGNE, J. P., ROQUES, C., GOBEIL, S., POIRIER, G. & MASSON, J. Y. 2013. The RAD51 paralogs ensure cellular protection against mitotic defects and aneuploidy. *J Cell Sci,* 126**,** 348-59.

ROSSIO, V., GALATI, E. & PIATTI, S. 2010. Adapt or die: how eukaryotic cells respond to prolonged activation of the spindle assembly checkpoint. *Biochem Soc Trans,* 38**,** 1645-9.

SAKURIKAR, N., EICHHORN, J. M. & CHAMBERS, T. C. 2012. Cyclin-dependent kinase-1 (Cdk1)/cyclin B1 dictates cell fate after mitotic arrest via phosphoregulation of antiapoptotic Bcl-2 proteins. *J Biol Chem,* 287**,** 39193-204.

SALMELA, A. L. & KALLIO, M. J. 2013. Mitosis as an anti-cancer drug target. *Chromosoma,* 122**,** 431-49.

SANCHEZ-PEREZ, T., ORTIZ-FERRON, G. & LOPEZ-RIVAS, A. 2010. Mitotic arrest and JNK-induced proteasomal degradation of FLIP and Mcl-1 are key events in the sensitization of breast tumor cells to TRAIL by antimicrotubule agents. *Cell Death Differ,* 17**,** 883-94.

SANTAGUIDA, S., TIGHE, A., D'ALISE, A. M., TAYLOR, S. S. & MUSACCHIO, A. 2010. Dissecting the role of MPS1 in chromosome biorientation and the spindle checkpoint through the small molecule inhibitor reversine. *J Cell Biol,* 190**,** 73-87.

SCAEROU, F., STARR, D. A., PIANO, F., PAPOULAS, O., KARESS, R. E. & GOLDBERG, M. L. 2001. The ZW10 and Rough Deal checkpoint proteins function together in a large, evolutionarily conserved complex targeted to the kinetochore. *J Cell Sci,* 114**,** 3103-14.

SCHMIDT, M. & BASTIANS, H. 2007. Mitotic drug targets and the development of novel anti-mitotic anticancer drugs. *Drug Resist Updat,* 10**,** 162-81.

SCHNEIDER-POETSCH, T., JU, J., EYLER, D. E., DANG, Y., BHAT, S., MERRICK, W. C., GREEN, R., SHEN, B. & LIU, J. O. 2010. Inhibition of eukaryotic translation elongation by cycloheximide and lactimidomycin. *Nat Chem Biol,* 6**,** 209-217.

SCHWEIZER, N., FERRAS, C., KERN, D. M., LOGARINHO, E., CHEESEMAN, I. M. & MAIATO, H. 2013. Spindle assembly checkpoint robustness requires Tpr-mediated regulation of Mad1/Mad2 proteostasis. *J Cell Biol,* 203**,** 883-93.

SCZANIECKA, M., FEOKTISTOVA, A., MAY, K. M., CHEN, J. S., BLYTH, J., GOULD, K. L. & HARDWICK, K. G. 2008. The spindle checkpoint functions of Mad3 and Mad2 depend on a Mad3 KEN box-mediated interaction with Cdc20-anaphase-promoting complex (APC/C). *J Biol Chem,* 283**,** 23039-47.

SEDGWICK, G. G., HAYWARD, D. G., DI FIORE, B., PARDO, M., YU, L., PINES, J. & NILSSON, J. 2013. Mechanisms controlling the temporal degradation of Nek2A and Kif18A by the APC/C-Cdc20 complex. *EMBO J,* 32**,** 303-14.

SETHI, N., MONTEAGUDO, M. C., KOSHLAND, D., HOGAN, E. & BURKE, D. J. 1991. The CDC20 gene product of Saccharomyces cerevisiae, a beta-transducin homolog, is required for a subset of microtubule-dependent cellular processes. *Mol Cell Biol,* 11**,** 5592-602.

SHAH, J. V., BOTVINICK, E., BONDAY, Z., FURNARI, F., BERNS, M. & CLEVELAND, D. W. 2004. Dynamics of centromere and kinetochore proteins; implications for checkpoint signaling and silencing. *Curr Biol,* 14**,** 942-52.

SHANDILYA, J., MEDLER, K. F. & ROBERTS, S. G. 2016. Regulation of AURORA B function by mitotic checkpoint protein MAD2. *Cell Cycle,* 15**,** 2196-2201.

SHARP-BAKER, H. & CHEN, R. H. 2001. Spindle checkpoint protein Bub1 is required for kinetochore localization of Mad1, Mad2, Bub3, and CENP-E, independently of its kinase activity. *J Cell Biol,* 153**,** 1239-50.

SHEPPERD, L. A., MEADOWS, J. C., SOCHAJ, A. M., LANCASTER, T. C., ZOU, J., BUTTRICK, G. J., RAPPSILBER, J., HARDWICK, K. G. & MILLAR, J. B. 2012. Phosphodependent recruitment of

Bub1 and Bub3 to Spc7/KNL1 by Mph1 kinase maintains the spindle checkpoint. *Curr Biol,* 22**,** 891-9.

SHERR, C. J. 1994. G1 phase progression: cycling on cue. *Cell,* 79**,** 551-5.

SHI, J., ORTH, J. D. & MITCHISON, T. 2008. Cell type variation in responses to antimitotic drugs that target microtubules and kinesin-5. *Cancer Res,* 68**,** 3269-76.

SHIN, H. J., PARK, E. R., YUN, S. H., KIM, S. H., JUNG, W. H., WOO, S. R., JOO, H. Y., JANG, S. H., CHUNG, H. Y., HONG, S. H., CHO, M. H., PARK, J. J., YUN, M. & LEE, K. H. 2015. p31(comet)-Induced Cell Death Is Mediated by Binding and Inactivation of Mad2. *PLoS One,* 10.

SIMONETTA, M., MANZONI, R., MOSCA, R., MAPELLI, M., MASSIMILIANO, L., VINK, M., NOVAK, B., MUSACCHIO, A. & CILIBERTO, A. 2009. The influence of catalysis on mad2 activation dynamics. *PLoS Biol,* 7**,** e10.

SIRONI, L., MELIXETIAN, M., FARETTA, M., PROSPERINI, E., HELIN, K. & MUSACCHIO, A. 2001. Mad2 binding to Mad1 and Cdc20, rather than oligomerization, is required for the spindle checkpoint. *EMBO J,* 20**,** 6371-82.

SKOUFIAS, D. A., ANDREASSEN, P. R., LACROIX, F. B., WILSON, L. & MARGOLIS, R. L. 2001. Mammalian mad2 and bub1/bubR1 recognize distinct spindle-attachment and kinetochore-tension checkpoints. *Proc Natl Acad Sci U S A,* 98**,** 4492-7.

SLEE, E. A., ADRAIN, C. & MARTIN, S. J. 2001. Executioner caspase-3, -6, and -7 perform distinct, non-redundant roles during the demolition phase of apoptosis. *J Biol Chem,* 276**,** 7320-6.

SLOSS, O., TOPHAM, C., DIEZ, M. & TAYLOR, S. 2016. Mcl-1 dynamics influence mitotic slippage and death in mitosis. *Oncotarget,* 7**,** 5176-92.

SODERBERG, O., GULLBERG, M., JARVIUS, M., RIDDERSTRALE, K., LEUCHOWIUS, K. J., JARVIUS, J., WESTER, K., HYDBRING, P., BAHRAM, F., LARSSON, L. G. & LANDEGREN, U. 2006. Direct observation of individual endogenous protein complexes in situ by proximity ligation. *Nat Methods,* 3**,** 995-1000.

SOLOMON, M. J. & BURTON, J. L. 2008. Securin' M-phase entry. *Nat Cell Biol,* 10**,** 381-3.

SOUCY, T. A., SMITH, P. G., MILHOLLEN, M. A., BERGER, A. J., GAVIN, J. M., ADHIKARI, S., BROWNELL, J. E., BURKE, K. E., CARDIN, D. P., CRITCHLEY, S., CULLIS, C. A., DOUCETTE, A., GARNSEY, J. J., GAULIN, J. L., GERSHMAN, R. E., LUBLINSKY, A. R., MCDONALD, A., MIZUTANI, H., NARAYANAN, U., OLHAVA, E. J., PELUSO, S., REZAEI, M., SINTCHAK, M. D., TALREJA, T., THOMAS, M. P., TRAORE, T., VYSKOCIL, S., WEATHERHEAD, G. S., YU, J., ZHANG, J., DICK, L. R., CLAIBORNE, C. F., ROLFE, M., BOLEN, J. B. & LANGSTON, S. P. 2009. An inhibitor of NEDD8-activating enzyme as a new approach to treat cancer. *Nature,* 458**,** 732-6.

SPENCER, F. & HIETER, P. 1992. Centromere DNA mutations induce a mitotic delay in Saccharomyces cerevisiae. *Proc Natl Acad Sci U S A,* 89**,** 8908-12.

STANULIS-PRAEGER, B. M. 1987. Cellular senescence revisited: a review. *Mech Ageing Dev,* 38**,** 1-48.

STEINHILB, M. L., TURNER, R. S. & GAUT, J. R. 2001. The protease inhibitor, MG132, blocks maturation of the amyloid precursor protein Swedish mutant preventing cleavage by beta-Secretase. *J Biol Chem,* 276**,** 4476-84.

STEVENS, J. B., LIU, G., BREMER, S. W., YE, K. J., XU, W., XU, J., SUN, Y., WU, G. S., SAVASAN, S., KRAWETZ, S. A., YE, C. J. & HENG, H. H. 2007. Mitotic cell death by chromosome fragmentation. *Cancer Res,* 67**,** 7686-94.

SUDAKIN, V., CHAN, G. K. & YEN, T. J. 2001. Checkpoint inhibition of the APC/C in HeLa cells is mediated by a complex of BUBR1, BUB3, CDC20, and MAD2. *J Cell Biol,* 154**,** 925-36.

SUDAKIN, V. & YEN, T. J. 2004. Purification of the mitotic checkpoint complex, an inhibitor of the APC/C from HeLa cells. *Methods Mol Biol,* 281**,** 199-212.

SUN, Y., TAN, M., DUAN, H. & SWAROOP, M. 2001. SAG/ROC/Rbx/Hrt, a zinc RING finger gene family: molecular cloning, biochemical properties, and biological functions. *Antioxid Redox Signal,* 3**,** 635-50.

TAIT, S. W. & GREEN, D. R. 2010. Mitochondria and cell death: outer membrane permeabilization and beyond. *Nat Rev Mol Cell Biol,* 11**,** 621-32.

TANAKA, K., MUKAE, N., DEWAR, H., VAN BREUGEL, M., JAMES, E. K., PRESCOTT, A. R., ANTONY, C. & TANAKA, T. U. 2005a. Molecular mechanisms of kinetochore capture by spindle microtubules. *Nature,* 434**,** 987-94.

TANAKA, T. U., STARK, M. J. & TANAKA, K. 2005b. Kinetochore capture and bi-orientation on the mitotic spindle. *Nat Rev Mol Cell Biol,* 6**,** 929-42.

TANG, Z., BHARADWAJ, R., LI, B. & YU, H. 2001a. Mad2-Independent inhibition of APCCdc20 by the mitotic checkpoint protein BubR1. *Dev Cell,* 1**,** 227-37.

TANG, Z., LI, B., BHARADWAJ, R., ZHU, H., OZKAN, E., HAKALA, K., DEISENHOFER, J. & YU, H. 2001b. APC2 Cullin protein and APC11 RING protein comprise the minimal ubiquitin ligase module of the anaphase-promoting complex. *Mol Biol Cell,* 12**,** 3839-51.

TANG, Z., SHU, H., ONCEL, D., CHEN, S. & YU, H. 2004. Phosphorylation of Cdc20 by Bub1 provides a catalytic mechanism for APC/C inhibition by the spindle checkpoint. *Mol Cell,* 16**,** 387-97.

TANGE, Y. & NIWA, O. 2008. Schizosaccharomyces pombe Bub3 is dispensable for mitotic arrest following perturbed spindle formation. *Genetics,* 179**,** 785-92.

TAYLOR, R. C., CULLEN, S. P. & MARTIN, S. J. 2008. Apoptosis: controlled demolition at the cellular level. *Nat Rev Mol Cell Biol,* 9**,** 231-41.

TAYLOR, S. S., HA, E. & MCKEON, F. 1998. The human homologue of Bub3 is required for kinetochore localization of Bub1 and a Mad3/Bub1-related protein kinase. *J Cell Biol,* 142**,** 1-11.

TAYLOR, S. S. & MCKEON, F. 1997. Kinetochore localization of murine Bub1 is required for normal mitotic timing and checkpoint response to spindle damage. *Cell,* 89**,** 727-35.

TEICHNER, A., EYTAN, E., SITRY-SHEVAH, D., MINIOWITZ-SHEMTOV, S., DUMIN, E., GROMIS, J. & HERSHKO, A. 2011. p31comet Promotes disassembly of the mitotic checkpoint complex in an ATP-dependent process. *Proc Natl Acad Sci U S A,* 108**,** 3187-92.

THORNTON, B. R., NG, T. M., MATYSKIELA, M. E., CARROLL, C. W., MORGAN, D. O. & TOCZYSKI, D. P. 2006. An architectural map of the anaphase-promoting complex. *Genes Dev,* 20**,** 449-60.

TIPTON, A. R., JI, W., STURT-GILLESPIE, B., BEKIER, M. E., 2ND, WANG, K., TAYLOR, W. R. & LIU, S. T. 2013. Monopolar spindle 1 (MPS1) kinase promotes production of closed MAD2 (C-MAD2) conformer and assembly of the mitotic checkpoint complex. *J Biol Chem,* 288**,** 35149-58.

TIPTON, A. R., TIPTON, M., YEN, T. & LIU, S. T. 2011a. Closed MAD2 (C-MAD2) is selectively incorporated into the mitotic checkpoint complex (MCC). *Cell Cycle,* 10**,** 3740-50.

TIPTON, A. R., WANG, K., LINK, L., BELLIZZI, J. J., HUANG, H., YEN, T. & LIU, S. T. 2011b. BUBR1 and closed MAD2 (C-MAD2) interact directly to assemble a functional mitotic checkpoint complex. *J Biol Chem,* 286**,** 21173-9.

TOPHAM, C. H. & TAYLOR, S. S. 2013. Mitosis and apoptosis: how is the balance set? *Curr Opin Cell Biol,* 25**,** 780-5.

TU, W. Z., LI, B., HUANG, B., WANG, Y., LIU, X. D., GUAN, H., ZHANG, S. M., TANG, Y., RANG, W. Q. & ZHOU, P. K. 2013. gammaH2AX foci formation in the absence of DNA damage: mitotic H2AX phosphorylation is mediated by the DNA-PKcs/CHK2 pathway. *FEBS Lett,* 587**,** 3437-43.

TURNER, C., DEVITT, A., PARKER, K., MACFARLANE, M., GIULIANO, M., COHEN, G. M. & GREGORY, C. D. 2003. Macrophage-mediated clearance of cells undergoing caspase-3-independent death. *Cell Death Differ,* 10**,** 302-12.

UDESHI, N. D., SVINKINA, T., MERTINS, P., KUHN, E., MANI, D. R., QIAO, J. W. & CARR, S. A. 2013. Refined preparation and use of anti-diglycine remnant (K-epsilon-GG) antibody enables routine quantification of 10,000s of ubiquitination sites in single proteomics experiments. *Mol Cell Proteomics,* 12**,** 825-31.

UHLMANN, F., LOTTSPEICH, F. & NASMYTH, K. 1999. Sister-chromatid separation at anaphase onset is promoted by cleavage of the cohesin subunit Scc1. *Nature,* 400**,** 37-42.

UHLMANN, F., WERNIC, D., POUPART, M. A., KOONIN, E. V. & NASMYTH, K. 2000. Cleavage of cohesin by the CD clan protease separin triggers anaphase in yeast. *Cell,* 103**,** 375-86.

URBANI, L., SHERWOOD, S. W. & SCHIMKE, R. T. 1995. Dissociation of nuclear and cytoplasmic cell cycle progression by drugs employed in cell synchronization. *Exp Cell Res,* 219**,** 159-68.

UZUNOVA, K., DYE, B. T., SCHUTZ, H., LADURNER, R., PETZOLD, G., TOYODA, Y., JARVIS, M. A., BROWN, N. G., POSER, I., NOVATCHKOVA, M., MECHTLER, K., HYMAN, A. A., STARK, H., SCHULMAN, B. A. & PETERS, J. M. 2012. APC15 mediates CDC20 autoubiquitylation by APC/C(MCC) and disassembly of the mitotic checkpoint complex. *Nat Struct Mol Biol,* 19**,** 1116-23.

VAN HOOSER, A., GOODRICH, D. W., ALLIS, C. D., BRINKLEY, B. R. & MANCINI, M. A. 1998. Histone H3 phosphorylation is required for the initiation, but not maintenance, of mammalian chromosome condensation. *J Cell Sci,* 111 (Pt 23)**,** 3497-506.

VAN ZON, W. & WOLTHUIS, R. M. 2010. Cyclin A and Nek2A: APC/C-Cdc20 substrates invisible to the mitotic spindle checkpoint. *Biochem Soc Trans,* 38**,** 72-7.

VANOOSTHUYSE, V. & HARDWICK, K. G. 2009. A novel protein phosphatase 1-dependent spindle checkpoint silencing mechanism. *Curr Biol,* 19**,** 1176-81.

VANOOSTHUYSE, V., MEADOWS, J. C., VAN DER SAR, S. J., MILLAR, J. B. & HARDWICK, K. G. 2009. Bub3p facilitates spindle checkpoint silencing in fission yeast. *Mol Biol Cell,* 20**,** 5096-105.

VARETTI, G., GUIDA, C., SANTAGUIDA, S., CHIROLI, E. & MUSACCHIO, A. 2011. Homeostatic control of mitotic arrest. *Mol Cell,* 44**,** 710-20.

VERMEULEN, K., VAN BOCKSTAELE, D. R. & BERNEMAN, Z. N. 2003. The cell cycle: a review of regulation, deregulation and therapeutic targets in cancer. *Cell Prolif,* 36**,** 131-49.

VERMEULEN, K., VAN BOCKSTAELE, D. R. & BERNEMAN, Z. N. 2005. Apoptosis: mechanisms and relevance in cancer. *Ann Hematol,* 84**,** 627-39.

VIGNERON, S., PRIETO, S., BERNIS, C., LABBE, J. C., CASTRO, A. & LORCA, T. 2004. Kinetochore localization of spindle checkpoint proteins: who controls whom? *Mol Biol Cell,* 15**,** 4584-96.

VINK, M., SIMONETTA, M., TRANSIDICO, P., FERRARI, K., MAPELLI, M., DE ANTONI, A., MASSIMILIANO, L., CILIBERTO, A., FARETTA, M., SALMON, E. D. & MUSACCHIO, A. 2006. In vitro FRAP identifies the minimal requirements for Mad2 kinetochore dynamics. *Curr Biol,* 16**,** 755-66.

VISCONTI, R., DELLA MONICA, R. & GRIECO, D. 2016a. Cell cycle checkpoint in cancer: a therapeutically targetable double-edged sword. *J Exp Clin Cancer Res,* 35**,** 153.

VISCONTI, R., DELLA MONICA, R. & GRIECO, D. 2016b. Sustaining the spindle assembly checkpoint to improve cancer therapy. *Mol Cell Oncol,* 3**,** e1046583.

VITALE, I., GALLUZZI, L., CASTEDO, M. & KROEMER, G. 2011. Mitotic catastrophe: a mechanism for avoiding genomic instability. *Nat Rev Mol Cell Biol,* 12**,** 385-92.

WAGNER, S. A., BELI, P., WEINERT, B. T., NIELSEN, M. L., COX, J., MANN, M. & CHOUDHARY, C. 2011. A proteome-wide, quantitative survey of in vivo ubiquitylation sites reveals widespread regulatory roles. *Mol Cell Proteomics,* 10**,** M111 013284.

WAIZENEGGER, I., GIMENEZ-ABIAN, J. F., WERNIC, D. & PETERS, J. M. 2002. Regulation of human separase by securin binding and autocleavage. *Curr Biol,* 12**,** 1368-78.

WANG, K., STURT-GILLESPIE, B., HITTLE, J. C., MACDONALD, D., CHAN, G. K., YEN, T. J. & LIU, S. T. 2014. Thyroid hormone receptor interacting protein 13 (TRIP13) AAA-ATPase is a novel mitotic checkpoint-silencing protein. *J Biol Chem,* 289**,** 23928-37.

WANG, Y. & BURKE, D. J. 1995. Checkpoint genes required to delay cell division in response to nocodazole respond to impaired kinetochore function in the yeast Saccharomyces cerevisiae. *Mol Cell Biol,* 15**,** 6838-44.

WANG, Y., ZHANG, W., JIN, Y., JOHANSEN, J. & JOHANSEN, K. M. 2001. The JIL-1 tandem kinase mediates histone H3 phosphorylation and is required for maintenance of chromatin structure in Drosophila. *Cell,* 105**,** 433-43.

WATERS, J. C., CHEN, R. H., MURRAY, A. W. & SALMON, E. D. 1998. Localization of Mad2 to kinetochores depends on microtubule attachment, not tension. *J Cell Biol,* 141**,** 1181-91.

WEAVER, B. A. & CLEVELAND, D. W. 2005. Decoding the links between mitosis, cancer, and chemotherapy: The mitotic checkpoint, adaptation, and cell death. *Cancer Cell,* 8**,** 7-12.

WEI, M. C., ZONG, W. X., CHENG, E. H., LINDSTEN, T., PANOUTSAKOPOULOU, V., ROSS, A. J., ROTH, K. A., MACGREGOR, G. R., THOMPSON, C. B. & KORSMEYER, S. J. 2001. Proapoptotic BAX and BAK: a requisite gateway to mitochondrial dysfunction and death. *Science,* 292**,** 727-30.

WEI, Y., MIZZEN, C. A., COOK, R. G., GOROVSKY, M. A. & ALLIS, C. D. 1998. Phosphorylation of histone H3 at serine 10 is correlated with chromosome condensation during mitosis and meiosis in Tetrahymena. *Proc Natl Acad Sci U S A,* 95**,** 7480-4.

WEISS, E. & WINEY, M. 1996. The Saccharomyces cerevisiae spindle pole body duplication gene MPS1 is part of a mitotic checkpoint. *J Cell Biol,* 132**,** 111-23.

WEN, X., LIN, Z. Q., LIU, B. & WEI, Y. Q. 2012. Caspase-mediated programmed cell death pathways as potential therapeutic targets in cancer. *Cell Prolif,* 45**,** 217-24.

WERTZ, I. E., KUSAM, S., LAM, C., OKAMOTO, T., SANDOVAL, W., ANDERSON, D. J., HELGASON, E., ERNST, J. A., EBY, M., LIU, J., BELMONT, L. D., KAMINKER, J. S., O'ROURKE, K. M., PUJARA, K., KOHLI, P. B., JOHNSON, A. R., CHIU, M. L., LILL, J. R., JACKSON, P. K., FAIRBROTHER, W. J., SESHAGIRI, S., LUDLAM, M. J., LEONG, K. G., DUEBER, E. C., MAECKER, H., HUANG, D. C. & DIXIT, V. M. 2011. Sensitivity to antitubulin chemotherapeutics is regulated by MCL1 and FBW7. *Nature,* 471**,** 110-4.

WESTHORPE, F. G., TIGHE, A., LARA-GONZALEZ, P. & TAYLOR, S. S. 2011. p31comet-mediated extraction of Mad2 from the MCC promotes efficient mitotic exit. *J Cell Sci,* 124**,** 3905-16.

WIGGE, P. A. & KILMARTIN, J. V. 2001. The Ndc80p complex from Saccharomyces cerevisiae contains conserved centromere components and has a function in chromosome segregation. *J Cell Biol,* 152**,** 349-60.

WILLIAMS, B. C., KARR, T. L., MONTGOMERY, J. M. & GOLDBERG, M. L. 1992. The Drosophila l(1)zw10 gene product, required for accurate mitotic chromosome segregation, is redistributed at anaphase onset. *J Cell Biol,* 118**,** 759-73.

WILLIAMS, B. C., LI, Z., LIU, S., WILLIAMS, E. V., LEUNG, G., YEN, T. J. & GOLDBERG, M. L. 2003. Zwilch, a new component of the ZW10/ROD complex required for kinetochore functions. *Mol Biol Cell,* 14**,** 1379-91.

WU, K., CHEN, A. & PAN, Z. Q. 2000. Conjugation of Nedd8 to CUL1 enhances the ability of the ROC1-CUL1 complex to promote ubiquitin polymerization. *J Biol Chem,* 275**,** 32317-24.

XIA, G., LUO, X., HABU, T., RIZO, J., MATSUMOTO, T. & YU, H. 2004. Conformation-specific binding of p31(comet) antagonizes the function of Mad2 in the spindle checkpoint. *EMBO J,* 23**,** 3133-43.

YAMAGISHI, Y., YANG, C. H., TANNO, Y. & WATANABE, Y. 2012. MPS1/Mph1 phosphorylates the kinetochore protein KNL1/Spc7 to recruit SAC components. *Nat Cell Biol,* 14**,** 746-52.

YAMAGUCHI, M., YU, S., QIAO, R., WEISSMANN, F., MILLER, D. J., VANDERLINDEN, R., BROWN, N. G., FRYE, J. J., PETERS, J. M. & SCHULMAN, B. A. 2015. Structure of an APC3-APC16 complex: insights into assembly of the anaphase-promoting complex/cyclosome. *J Mol Biol,* 427**,** 1748-64.

YANAGIDA, M. 2005. Basic mechanism of eukaryotic chromosome segregation. *Philos Trans R Soc Lond B Biol Sci,* 360**,** 609-21.

YANG, M., LI, B., LIU, C. J., TOMCHICK, D. R., MACHIUS, M., RIZO, J., YU, H. & LUO, X. 2008. Insights into mad2 regulation in the spindle checkpoint revealed by the crystal structure of the symmetric mad2 dimer. *PLoS Biol,* 6**,** e50.

YANG, M., LI, B., TOMCHICK, D. R., MACHIUS, M., RIZO, J., YU, H. & LUO, X. 2007. p31comet blocks Mad2 activation through structural mimicry. *Cell,* 131**,** 744-55.

YAO, X., ABRIEU, A., ZHENG, Y., SULLIVAN, K. F. & CLEVELAND, D. W. 2000. CENP-E forms a link between attachment of spindle microtubules to kinetochores and the mitotic checkpoint. *Nat Cell Biol,* 2**,** 484-91.

YE, Q., ROSENBERG, S. C., MOELLER, A., SPEIR, J. A., SU, T. Y. & CORBETT, K. D. 2015. TRIP13 is a protein-remodeling AAA+ ATPase that catalyzes MAD2 conformation switching. *Elife,* 4.

YIN, M. B., GUO, B., PANADERO, A., FRANK, C., WRZOSEK, C., SLOCUM, H. K. & RUSTUM, Y. M. 1999. Cyclin E-cdk2 activation is associated with cell cycle arrest and inhibition of DNA replication induced by the thymidylate synthase inhibitor Tomudex. *Exp Cell Res,* 247**,** 189-99.

YIN, X. M. 2006. Bid, a BH3-only multi-functional molecule, is at the cross road of life and death. *Gene,* 369**,** 7-19.

YU, H. 2006. Structural activation of Mad2 in the mitotic spindle checkpoint: the two-state Mad2 model versus the Mad2 template model. *J Cell Biol,* 173**,** 153-7.

YU, H. 2007. Cdc20: a WD40 activator for a cell cycle degradation machine. *Mol Cell,* 27**,** 3-16.

YUDKOVSKY, Y., SHTEINBERG, M., LISTOVSKY, T., BRANDEIS, M. & HERSHKO, A. 2000. Phosphorylation of Cdc20/fizzy negatively regulates the mammalian cyclosome/APC in the mitotic checkpoint. *Biochem Biophys Res Commun,* 271**,** 299-304.

ZAMZAMI, N. & KROEMER, G. 1999. Condensed matter in cell death. *Nature,* 401**,** 127-8.

ZHANG, L., TANG, H., KOU, Y., LI, R., ZHENG, Y., WANG, Q., ZHOU, X. & JIN, L. 2013. MG132-mediated inhibition of the ubiquitin-proteasome pathway ameliorates cancer cachexia. *J Cancer Res Clin Oncol,* 139**,** 1105-15.

ZHANG, S., CHANG, L., ALFIERI, C., ZHANG, Z., YANG, J., MASLEN, S., SKEHEL, M. & BARFORD, D. 2016. Molecular mechanism of APC/C activation by mitotic phosphorylation. *Nature,* 533**,** 260-264.

ZHENG, L., CHEN, Y. & LEE, W. H. 1999. Hec1p, an evolutionarily conserved coiled-coil protein, modulates chromosome segregation through interaction with SMC proteins. *Mol Cell Biol,* 19**,** 5417-28.

ZHENG, N., SCHULMAN, B. A., SONG, L., MILLER, J. J., JEFFREY, P. D., WANG, P., CHU, C., KOEPP, D. M., ELLEDGE, S. J., PAGANO, M., CONAWAY, R. C., CONAWAY, J. W., HARPER, J. W. & PAVLETICH, N. P. 2002. Structure of the Cul1-Rbx1-Skp1-F boxSkp2 SCF ubiquitin ligase complex. *Nature,* 416**,** 703-9.

ZHONG, Q., GAO, W. H., DU, F. H. & WANG, X. D. 2005. Mule/ARF-BP1, a BH3-only E3 ubiquitin ligase, catalyzes the polyubiquitination of Mcl-1 and regulates apoptosis. *Cell,* 121**,** 1085-1095.

ZHOU, J., YAO, J. & JOSHI, H. C. 2002. Attachment and tension in the spindle assembly checkpoint. *J Cell Sci,* 115**,** 3547-55.